ISTANBUL TECHNICAL UNIVERSITY ★ GRADUATE SCHOOL OF SCIENCE ENGINEERING AND TECHNOLOGY

ANALYSIS OF COMPOSITE SANDWICH STRUCTURES WITH A VISCOELASTIC LAYER MODELLED WITH FRACTIONAL CALCULUS AND MULTI-PARAMETER OPTIMIZATION

Ph.D. THESIS

Aytaç ARIKOĞLU

Department of Aeronautics and Astronautics Engineering

Aeronautics and Astronautics Engineering Programme

NOVEMBER 2011

ISTANBUL TECHNICAL UNIVERSITY ★ GRADUATE SCHOOL OF SCIENCE ENGINEERING AND TECHNOLOGY

ANALYSIS OF COMPOSITE SANDWICH STRUCTURES WITH A VISCOELASTIC LAYER MODELLED WITH FRACTIONAL CALCULUS AND MULTI-PARAMETER OPTIMIZATION

Ph.D. THESIS

Aytaç ARIKOĞLU
(511032011)

Department of Aeronautics and Astronautics Engineering

Aeronautics and Astronautics Engineering Programme

Thesis Advisor: Prof. Dr. İbrahim ÖZKOL

NOVEMBER 2011

İSTANBUL TEKNİK ÜNİVERSİTESİ ★ FEN BİLİMLERİ ENSTİTÜSÜ

VİSKOELASTİK MERKEZLİ KOMPOZİT YAPILARIN KESİRLİ TÜREV İLE MODELLENMESİ VE ÇOK PARAMETRELİ OPTİMİZASYONU

DOKTORA TEZİ

Aytaç ARIKOĞLU
(511032011)

Uçak ve Uzay Mühendisliği Anabilim Dalı

Uçak ve Uzay Mühendisliği Programı

Tez Danışmanı: Prof. Dr. İbrahim ÖZKOL

KASIM 2011

Aytaç Arıkoğlu, a **Ph.D.** student of ITU **Institute of / Graduate School of Science Engineering and Technology** student ID **511032011**, successfully defended the **dissertation** entitled "**ANALYSIS OF COMPOSITE SANDWICH STRUCTURES WITH A VISCOELASTIC LAYER MODELLED WITH FRACTIONAL CALCULUS AND MULTI-PARAMETER OPTIMIZATION**", which he prepared after fulfilling the requirements specified in the associated legislations, before the jury whose signatures are below.

Thesis Advisor :	**Prof. Dr. İbrahim ÖZKOL** İstanbul Technical University	.....
Jury Members :	**Prof. Dr. Zahit MECİTOĞLU** İstanbul Technical University	.....
	Prof. Dr. Ata MUĞAN İstanbul Technical University	.....
	Prof. Dr. Metin O. KAYA İstanbul Technical University	.....
	Prof. Dr. Erol UZAL İstanbul University	.....

Date of Submission : 12 September 2011
Date of Defense : 25 November 2011

This work is dedicated to my parents
Azize and İsmail Arıkoğlu

FOREWORD

I would like to express my gratitude to my supervisor Professor İbrahim Özkol for his guidance and advice that he has given me over the past nine years. I also would like to thank my committee members Professor Ata Muğan and Professor Zahit Mecitoğlu for their valuable advice throughout all stages of this work.
My most sincere gratitude goes to my family for their love, encouragement and endless support.

November 2011

Aytaç ARIKOĞLU
Aeronautical Engineer

TABLE OF CONTENTS

Page

ABBREVIATIONS

ADF : Anelastic Displacement Fields
BEM : Boundary Element Method
Br-Ep : Boron-Epoxy
CLD : Constrained-Layer Damping
CFRP : Carbon-Fiber Reinforced Plastic
CPT : Classical Plate Theory
DQM : Differential Quadrature Method
DTM : Differential Transform Method
EA : Evolutionary Algorithm
FDM : Finite Difference Method
FE : Finite Element
FEM : Finite Element Method
FRF : Frequency Response Function
FSDT : First Order Shear Deformation Theory
GA : Genetic Algorithm
GDQM : Generalized Differential Quadrature Method
GFRP : Glass-Fiber Reinforced Plastic
GHM : Golla-Hughes-McTavish
Gl-Ep : Glass-Epoxy
Gr-Ep : Graphite-Epoxy
HSDT : High Order Shear Deformation Theory
MDoF : Multiple Degree of Freedom

LIST OF TABLES

Page

LIST OF FIGURES

Page

ANALYSIS OF COMPOSITE SANDWICH STRUCTURES WITH A VISCOELASTIC LAYER MODELLED WITH FRACTIONAL CALCULUS AND MULTIPARAMETER OPTIMIZATION

SUMMARY

In this thesis, the vibration analyses and optimization of sandwich beams and plates with composite face layers and viscoelastic core are carried out. The frequency dependency of the core layer is modeled by using the five-parameter fractional derivative Zener model and the unknown parameters that appear in this model are obtained from the experimental data that exist in literature for four commercial polymeric damping materials, which are 3M ISD-110, 3M 467, DYAD 606 and DYAD 609. A new methodology that depends on fitting the experimental data and theoretical model simultaneously is presented for the first time.

The governing equations and related boundary conditions are derived by using the principle of virtual work for the free vibrations of three-layered sandwich beams and plates. The differential transform method (DTM) and the generalized differential quadrature method (GDQM) are utilized to solve these equations for sandwich beams and plates respectively, for the first time. In order to validate both the beam and plate models together with the solution techniques, results are compared with the ones that already exist in literature and a good agreement is observed. In addition, parametric analyses are carried out for sandwich beams and plates to understand the effects of system parameters on loss factor and frequency. A two-node sandwich beam finite element with four degrees of freedom per node and a four-node sandwich plate finite element with seven degrees of freedom per node are developed for the validation of DTM and GDQM results. The results for the parametric analyses are presented in graphical form with comparison to the currently developed FEM models and a good agreement is observed.

Lastly, the multi-parameter optimization is carried out by using genetic algorithms to determine the layer thicknesses, the choice of materials used in these layers and the lamination angle of the face layers that correspond to the optimal configurations in terms of vibration damping of sandwich beams and plates. Different from the ones that exist in literature, the objective function is defined in terms of the first modal loss factor and the receptance frequency response at zero frequency. Frequency responses of the initial and optimal designs are presented graphically and a great improvement is observed.

VİSKOELASTİK MERKEZLİ KOMPOZİT YAPILARIN KESİRLİ TÜREV İLE MODELLENMESİ VE ÇOK PARAMETRELİ OPTİMİZASYONU

ÖZET

Titreşim sonucu oluşan gerilme ve yer değiştirmeler, gürültüye, yorulmaya ve söz konusu yapının yada bir parçasının aksamasına yada bozulmasına neden olabilecek ciddi problemlerdir. Bu sebeple, yapıların titreşim sönümlemesi ve azaltılması büyük önem taşımaktadır. Bu hedefe ulaşmak için viskoelastik malzemeden oluşan sönümleme katmanları sıklıkla kullanılan çözümlerdir. Bu katmanlar, incelenen probleme göre aktif yada pasif olabilecekleri gibi serbest (yapının yüzeyinde) yada zorlanmış (yapının içerisinde) da olabilmektedir. Zorlanmış katman sönümleme iyileştirmesi, ucuzluk ve verimlilik bakımından diğer titreşim sönümleme yöntemlerine nazaran sahip olduğu üstünlükler sebebiyle sıklıkla tercih edilen ve mühendislik uygulamalarında da çokça rastlanan bir titreşim sönümleme yöntemidir.

Tipik bir sandviç yapı, eğilme yükünün büyük bir bölümünü taşıyan sert dış katmanlardan ve bu katmanlar arasına yerleştirilmiş, enerji sönümleme özelliği olan, yumuşak nüve katmanından oluşur. Bu tarz yapılar mühendislikte ve özellikle de havacılıkta yük taşıyan yapısal bileşenler olarak sıklıkla kullanılırlar. Dış katmanlarda kullanılan malzemeler arasında kontraplak, sac ve özellikle de yüksek katılık/ağırlık oranları sebebiyle elyaf-takviyeli kompozit malzemeler bulunmaktadır. Nüve katmanında ise çoğunlukla bal peteği, sentaktik köpük, balsa ağacı, polimerik köpük ve filmlerin çeşitli tipleri kullanılmaktadır.

Nüve katmanında kullanılan malzemeler arasında viskoelastik polimerik sönümleme malzemeleri yüksek enerji sönümleme özellikleri sebebiyle büyük uygulama alanı bulmuştur. Bu malzemelerin elastisite modülleri ve sönüm faktörleri yüksek oranda frekans ve sıcaklığa bağlılık gösterirler. Dolayısıyla bu malzemelerin kendilerine has bu özelliklerini dikkate almadan, başarılı bir titreşim sönümlemesi gerçekleştirmek mümkün değildir. Viskoelastik davranışı modellemek üzere literatürde birçok yaklaşım mevcuttur ve bunlar arasında kesirli türev viskoelastik modeller diğer modellere kıyasla sahip oldukları avantajlar neticesinde öne çıkmaktadırlar.

Diğer bir husus ise incelenen yapının matematiksel modelini oluşturmak ve bu modeli çözmektir. Bunun için en sık kullanılan yöntem tartışmasız sonlu elemanlar yöntemidir. Bu yöntem kompleks geometri, kısıt ve yükleme durumları ile kolaylıkla başa çıkabilmektedir fakat yaklaşık bir çözüm yöntemi olması sebebiyle özünde hata barındırır. Bu nedenle, sonlu elemanlara alternatif olabilecek hassas çözüm yöntemleri, hesaplamalı mekanikte önemli bir araştırma konusudur.

Bu tezde, kompozit dış katmanlı, viskoelastik nüveli sandviç kiriş ve plakların titreşim analizi ve optimizasyonu incelenmektedir. Tezin ikinci bölümde, ilk olarak geleneksel viskoelastik modellerin sürünme, gerilme gevşemesi ve toparlanma davranışlarını taklit etmedeki başarıları tartışılmıştır. Daha sonra dört parametreli kesirli türev Zener modeli ve, bu tezde viskoelastik davranışı modellemede kullanılan, beş parametreli kesirli türev Zener modelleri incelenmiştir.

Bu modeldeki bilinmeyen parametreler, literatürde bulunan dört polimerik sönümleme malzemesi (3M ISD-110, 3M 467, DYAD 606 ve DYAD 609) için elde edilmiştir. Ayrıca, teorik modeldeki bilinmeyen parametrelerin deneysel datadan elde edilmesiyle ilgili olarak yeni bir yaklaşım ortaya konulmuştur.

Üçüncü bölümde sandviç kirişlerin titreşim ve sönüm analizi gerçekleştirilmiştir. Hareket denklemleri ve sınır şartları, virtüel iş prensibi kullanılarak elde edilmiş ve bu denklemler ilk defa diferansiyel transform yöntemi kullanılarak çözülmüştür. Taylor serisi açılımına dayanan bu yarı analitik nümerik teknik kullanılarak hareket denklemleri reküratif bağıntılara ve sınır şartları cebrik denklemlere dönüştürülür. Çözüm yönteminin ve üç katmanlı sandviç kiriş modelinin validasyonu, sonuçların literatürde bulunan sonuçlarla kıyaslanmasıyla gerçekleştirilmiştir. Katman kalınlıkları, kompozit dış katmanların oryantasyon açıları ve kiriş uzunluğu gibi parametrelerin kiriş doğal frekansı ve kayıp faktörü üzerindeki etkilerini incelemek üzere parametrik analizler gerçekleştirilmiştir. Ayrıca bu analizlerde elde edilen diferansiyel transform sonuçları, yine bu tezde geliştirilen iki nodlu ve nod başına dört serbestlik dereceli sandviç kiriş sonlu elemanlar modeli sonuçları ile kıyaslamalı olarak verilmiş ve bu iki metod arasında oldukça iyi bir uyum gözlenmiştir.

Bölüm dörtte, sandviç plakların titreşim ve sönüm analizi gerçekleştirilmiştir. Hareket denklemleri ve sınır şartları, yine virtüel iş prensibi kullanılarak, kesit kuvvet ve moment bileşenleri cinsinden elde edilmiştir. Elde edilen bu hareket denklemlerinin tanımladığı özdeğer problemi, yine ilk defa, genelleştirilmiş diferansiyel kuadratür yöntemi kullanılarak çözülmüştür. Sonuçların, basit mesnetli ve ankastre plaklar için literatürde bulunan test problemleri ile kıyaslanması ile metodun ve plak modelinin validasyonu gerçekleştirilmiştir. Daha sonra parametrik analizler gerçekleştirilerek, plak nüve malzemesinin, katman kalınlıklarının ve kompozit dış katman oryantasyon açılarının titreşim ve sönüm karekteristikleri üzerine etkileri incelenmiştir. Diferansiyel kuadratür yöntemi ile elde edilen parametrik analiz sonuçları, yine bu tezde geliştirilen dört nodlu ve nod başına yedi serbestlik dereceli sandviç plak sonlu elemanlar modeli ile kıyaslamalı olarak verilmiş ve iyi bir uyum gözlenmiştir.

Beşinci bölümde, öncelikle genetik algoritmaların temel prensipleri ayrıntılı bir şekilde anlatılmıştır. Daha sonra, izlenecek optimizasyon stratejisi ortaya konulmuş ve üç katmanlı sandviç kiriş ve plakların titreşim ve sönüm özelliklerinin optimal olduğu durumlar, izin verilen dizayn ağırlığının farklı değerleri için, elde edilmiştir. Ayrıca, ilk ve optimal dizaynlar, frekans cevapları cinsinden kıyaslamalı olarak gösterilmiş ve bu konfigürasyonlar arasında ciddi bir fark gözlenmiştir. Hedef fonksiyonu modal kayıp faktörü ve frekansın sıfır olduğu durumdaki frekans cevabı cinsinden tanımlanmış ve literatürde var olan çalışmalara nazaran daha fazla sayıda dizayn parametresi için optimal durumlar aranmıştır.

Tezde elde edilen bulgular neticesinde beş parametreli kesirli Zener modelinin viskoelastik davranışı oldukça başarılı bir şekilde ifade edebildiği anlaşılmaktadır. Nümerik sonuçlar göstermiştir ki, diferansiyel dönüşüm ve genelleştirilmiş kuadratür yöntemleri sandviç kiriş ve sandviç plakların titreşim analizlerinde kullanılabilecek, sonlu elemanlar yöntemine alternatif, güvenilir ve hassas yöntemlerdir.

Hem parametrik analizler hem de optimizasyon sonuçları, en iyi titreşim sönümlemesi için simetrik kesitlerin kullanılması gerektiğini ortaya çıkarmıştır. Kompozit dış katmanların oryantasyon açılarının 0° yada 90° olduğu durumlarda titreşim sönümlemesinin maksimum olduğu gözlenmiştir. Ayrıca, ankastre-serbest kirişler için optimal duruma karşılık gelen konfigürasyonlarda nüve katmanının dış katmanlara oranla kalın olduğu gözlenmiştir. Ankastre sandviç plaklarda ise bu oran izin verilen maksimum dizayn ağırlığına bağlı olarak değişmektedir.

Tezde elde edilen bulgulara göre, en iyi titreşim sönümlemesine karşılık gelen katman malzemeleri yine izin verilen maksimum ağırlığa göre değişim göstermektedir. Optimizasyon sonuçlarına göre, incelenen malzemeler arasında, kompozit dış katmanların Grafit-Epoksi yada Bor-Epoksi, viskoelastik nüve katmanının ise 3M ISD-110 yada GE.SMRD olduğu durumlarda en iyi titreşim sönümlemesi gerçekleşmektedir.

1. INTRODUCTION

Vibration induced stresses and displacements are major problems, which may cause unwanted noise and fatigue that may lead to the failure of a component or the structure itself. Therefore, damping and reduction of these vibrations are of great importance and damping layers that consist of viscoelastic materials are commonly used to achieve this goal. These materials can either be adapted during the design stage or added after the completion of the design process. Damping layers are applied to the structure as active or passive layers and depending on the problem considered, they may be implemented as free or constrained layers. Among the vibration control and reduction methods, the most efficient, easy and commonly used one is the constrained-layer damping (CLD) treatment. When this type of structure is subjected to cyclic bending, the damping layer is primarily subjected to shear strain due to the relative motion of the base and the constraining layers. Strong internal friction caused by this type of motion reduces the vibration amplitude for each bending cycle by dissipating the mechanical energy as heat.

A typical sandwich structure consists of two stiff face layers that carry the great portion of the bending load separated by a light inner core having energy dissipating property. These structures find application as load carrying structural members in many engineering areas and especially in the field of aerospace. The face layers are usually made of plywood or sheet metal but mostly fiber-reinforced composite laminates due to their high stiffness/weight ratio. On the other hand, the most commonly used types for cores are the honeycombs, syntactic foams, balsa wood and various types of polymeric foams and films.

Among these, viscoelastic polymeric materials have found great applications in engineering due to their high damping and energy dissipation properties. The dynamic modulus of elasticity and the loss factor of these materials show strong dependence on frequency and temperature. Therefore, it is not possible to obtain satisfying results, in terms of vibration damping, without taking proper account of the unique characteristics of these materials.

There are several approaches to model the frequency dependence of the dynamical properties of viscoelastic materials and the most commonly used ones are Golla-Hughes-McTavish (GHM) [1, 2] and anelastic displacement field (ADF) methods [3]. In both of these methods, the complex modulus of the viscoelastic material is represented in terms of series of functions, where the fitting between the theoretical and experimental results is improved by increasing the number of terms considered. The obtained material properties are not valid for wide frequency ranges; besides, they are valid inside the frequency band, which is chosen for performing the fitting of master curves. On the other hand, fractional order models of viscoelasticity obtained from the modification of conventional models such as Maxwell, Kelvin and Zener exist in literature [4, 5], which overcome the drawbacks and limitations of GHM and ADF.

In the analysis of sandwich structures, it is important to build a mathematical model, which can reflect the physical reality correctly while being feasible in terms of computation time. For this purpose, researchers have proposed various beam and plate theories. The simplest among them are the Euler beam theory and Kirchhoff plate theory, which neglect the transverse shear strain and give reasonable results for thin beams and plates. For thicker beams and plates, it may be necessary to use more advanced theories such as Timoshenko beam theory, Mindlin-Reissner plate theory, high order shear deformation theories (HSDT) and the zig-zag theory. However, one should avoid an unnecessarily detailed model if the obtained accuracy does not justify the additional computational cost.

The next stage, after building an appropriate mathematical model, is solving it by using one of the solution techniques available. Concerning the computational mechanics, the mostly used one is without a doubt the finite element method (FEM), due to its advantages on the handling of complex geometries, restraints and loading conditions. However, every solution technique has its advantages and disadvantages and so does the finite element method i.e., FEM obtains only approximate solutions and therefore it contains inherent errors. In addition, the evaluation of element matrices, mesh generation and the assembly of element matrices into the system matrix requires substantial programming knowledge and effort.

There are alternative solution methods to FEM, some of which are; boundary element method (BEM), finite difference method (FDM), generalized differential quadrature method (GDQM), differential transform method (DTM), the Navier's method and the Galerkin's method. Among these methods, two of them i.e., DTM and GDQM can be distinguished from the others due to their superior robustness and accuracy.

The differential transform method is based on the Taylor series expansion, first proposed by Zhou [6] in 1986 for the solution of linear and nonlinear initial value problems that appear in electrical circuits. The method gives the convenience to obtain analytical solutions of the differential equations and constructs an analytical solution in the form of a polynomial. It is a semi analytical-numerical technique, which depends on the Taylor series expansion. With this technique, it is possible to obtain highly accurate results or exact solutions for differential equations, integro-differential equations [7, 8], difference equations [9, 10] and fractional differential equations [11, 12]. By using this method, the governing differential equations can be reduced to a recurrence relation and the boundary conditions can be transformed into a set of algebraic equations.

On the other hand, differential quadrature method (DQM) is a collocation scheme first introduced by Bellman et al. for the solution of nonlinear partial differential equations [13]. This method, in its first proposed form, produced ill-conditioned matrices for large systems, from which the weighting coefficients are obtained. This drawback was overcome with the introduction of the generalized differential quadrature method (GDQM) by Shu et al. [14], which presents an explicit algebraic formula for the evaluation of weighting coefficients. This robust and reliable numerical technique can produce very accurate results with considerably small number of grid points.

1.1 Literature Review

A vast number of studies exist in literature, which have been devoted to the vibration analysis of viscoelastic sandwich structures. Earlier works can be traced back to 1950's to the study of Ross et al. [15], where the effects of layered shear treatments for simply-supported plates were investigated. The same year, Kerwin discussed a three-layer beam with a damping layer sandwiched between two face layers [16]. Di Taranto derived a sixth order differential equation for a sandwich beam with a viscoelastic core having complex shear modulus and evaluated the natural frequencies [17]. Mead and Markus refined the theory developed by Di Taranto and extended it to fixed-fixed beams [18, 19]. Sadasiva and Nakra [20] studied the unsymmetrically sectioned sandwich beams and plates with viscoelastic cores. Lu et al. [21] evaluated mechanical impedances for a sandwich plate with free boundary conditions by using finite element method and compared them with experimental results. Johnson and Kienholz [22] studied the vibration and damping of sandwich ring and plate structures by using modal strain energy method implemented in NASTRAN. Lall et al. studied the effects of partial coverage on the damping characteristics of sandwich beams by using the Galerkin's method [23].

More recently, Cupial and Niziol pursued Mead's plate model and studied the simply supported sandwich plates taking into account the shear deformation of the face layers and rotary inertia [24]. Kung and Singh evaluated eigensolutions for a rectangular sandwich plate with multiple damping patches by using the Rayleigh-Ritz minimization scheme [25]. Wang et al. carried out a Galerkin assumed modes analysis for the three-layer sandwich plates with a viscoelastic core and isotropic face layers [26]. They used GHM method to take into account the frequency dependency of the viscoelastic material and validated their results with experimental data. Fasana et al. studied the vibration characteristics of a sandwich beam with a viscoelastic layer by using Rayleigh Ritz method [27]. Ganesan et al. thoroughly studied the buckling behavior of sandwich beams with viscoelastic core in thermal environments for various arrangements [28, 29]. Tang et al. performed an analysis on the partially covered beam configurations with a constrained damping layer including the normal strain effects [30]. They derived a sixth order differential equation to describe the constrained portion of the beam and investigated the effect of system parameters on loss factor and loss parameter.

Yeh and Chen obtained the natural frequencies, buckling loads, loss factors and the stability behaviors of rectangular sandwich plates with electro-rheological core by using the finite element method [31].

There also exist studies on the damping optimization of sandwich structures with a viscoelastic core in literature. Mantena et al. determined the optimal tape lengths that maximize the loss factor for sandwich beams [32]. They used modal strain energy method to calculate the loss factor and compared their finite element solutions with the experimental results. Lee and Hwang investigated the optimal coverage for sandwich beams on different operation temperatures that give the maximum value for the loss factor [33]. They took into account the frequency dependency of the core layer by using a four-parameter fractional derivative viscoelastic model. Jung et al. proposed a statistical approach to model the variability of the dynamical properties of the damping material, which is sensitive to the variable operational temperature [34]. By using this approach, they determined the values of system parameters, i.e., the layer thicknesses and the length, which minimizes the frequency response of the sandwich beam. Araujo et al. used a gradient-based optimization technique to obtain the parameters that maximize the modal loss factor for symmetrical sectioned sandwich beams and plates [35]. They also considered a multi-objective optimization case, where the first objective function to be maximized is the loss factor and the second one to be minimized is a function of maximum displacement and mass.

1.2 Purpose of the Thesis

The objectives of the thesis are listed as follows:

1- Accurately model the frequency dependent behavior of the viscoelastic core layer: For this purpose, use the modified version of the five parameter fractional Zener model.

2- Obtain the unknown parameters of the viscoelastic model from the experimental data that exist in literature for different polymeric damping materials.

3- Obtain the governing equations and boundary conditions of sandwich beams and plates.

4- Utilize the solution techniques DTM and GDQM for the vibration analysis of sandwich beams and plates respectively.

5- Compare results of these techniques to already existing ones in literature for validation.

6- Develop FEM models for sandwich beams and plates for comparison and further verification of the results of DTM and GDQM.

7- Investigate the effects of system parameters on the modal characteristics of sandwich beams and plates.

8- Solve the multi-parameter optimization problem of determining the best configuration for the layer materials, layer thicknesses and lamination angles that present the best damping characteristics, by using genetic algorithms.

1.3 Structure of the Thesis

The thesis is structured into six chapters. The first chapter includes the state of the art of vibration and damping analysis of sandwich structures followed by the objectives of the present work.

In chapter two, the concepts of viscoelasticity, details of the fractional order viscoelastic models and the evaluation of the unknown parameters, which appear in the theoretical model, from the experimental data, are presented. A new methodology that depends on fitting the theoretical model and the experimental data simultaneously is introduced. In addition, master curves for the shear modulus and loss factor of four polymeric damping materials are obtained.

In chapter three, the vibration analysis of sandwich beams is carried out. First, the equations of motion that govern the free vibrations of the sandwich beams are derived by using the principle of virtual work. Then, these equations are solved by using DTM in the frequency domain. It is shown that this semi analytical–numerical technique is accurate by comparing the results with the ones in open literature. The variation of loss factor and the frequency with system parameters are evaluated and presented graphically, in comparison to the developed FE model.

In chapter four, vibration and damping analyses of sandwich plates are considered. The governing equations and related boundary conditions are derived in terms of sectional force and moment resultants by using the principle of virtual work for the free vibrations of the plate. The eigenvalue problem defined by these equations is solved by using GDQM to obtain the frequencies and loss factors. Results are compared with the ones that exist in literature for three plate problems. Then, the effects of system parameters on the loss factor and frequency are investigated for the sandwich plates with carbon fiber reinforced plastic face layers and frequency dependent viscoelastic core. The results are verified against the developed FE model.

In chapter five, the principles of genetic algorithms are explained in detail. Then, the multi-parameter optimization problem is defined, formulated and solved for the sandwich beams and plates. Initial and optimal designs are presented graphically in terms of frequency response functions.

Lastly, the sixth chapter concludes this study by an assessment of the results and the future studies that can be carried out.

2. VISCOELASTICITY

Viscoelasticity is a property of materials such as polymers, industrial plastics and metals at high temperatures. These materials present both elastic and viscous characteristics when deformed by an external force.

The conventional models of viscoelasticity and the notions of viscoelastic behavior in time domain are presented in Section 2.1. Then, the four and five parameter fractional order viscoelastic models that arise from the conventional Zener model are investigated in detail in Section 2.2. Lastly, estimation of the unknown parameters that appear in the theoretical model and evaluation of the master curves from the experimental data are carried out in Section 2.3.

2.1 Time Domain Analysis of Conventional Models

There are three important stages that the viscoelastic materials undergo when deformed by an external force, which are creep, relaxation and recovery. Creep is the time-dependent increase in strain when a constant stress is applied to the material. Relaxation is the decrease of stress with time, when the strain is held constant. Recovery is the tendency of the deformed material to return to its original shape with time, when the applied force is removed. It can be separated in two parts; elastic-instantaneous recovery that is the immediate reduction in the strain and viscous-delayed recovery that is the time-dependent reduction in the strain.

There are mainly three viscoelastic material models that consist of the different combinations of springs and dashpots, which are Maxwell, Kelvin-Voigt and Zener models. The dynamic properties of these models, their mathematical representations and their success in modeling the viscoelastic behavior are investigated in the following text.

2.1.1 Maxwell Model

This model consists of a spring and a dashpot in series as presented in Figure 2.1.

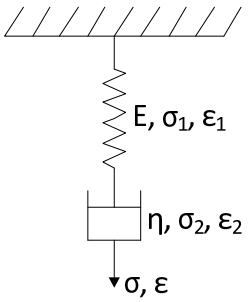

Figure 2.1: Representation of the Maxwell model.

One can notice that the following relations hold:

$$\varepsilon = \varepsilon_1 + \varepsilon_2,\ \sigma = \sigma_1 = \sigma_2, \sigma_1 = E\varepsilon_1 \text{ and } \sigma_2 = \eta \frac{d\varepsilon_2}{dt} \tag{2.1}$$

By using Eq. (2.1), the stress-strain relation for this type of modeling can be evaluated as follows:

$$\frac{d\varepsilon}{dt} = \frac{1}{E}\frac{d\sigma}{dt} + \frac{1}{\eta}\sigma \tag{2.2}$$

This equation can be written in the integral form to understand the physics underlying:

$$\varepsilon = \frac{1}{E}\sigma + \frac{1}{\eta}\int_{t_0}^{t} \sigma dt \tag{2.3}$$

Equation (2.3) shows that, at the time the stress is applied to this type of material, an instant strain occurs, which increases linearly with time. Solution of Eqs. (2.2) and (2.3) is presented in Figure 2.2 for constant stress and constant strain scenarios.

As one can see from Figure 2.2, Maxwell model accounts for creep, relaxation and recovery, however in a very poor manner. The creep motion is linear and increases boundlessly for constant stress. When the stress is removed, there is an instantaneous recovery of the elastic part of the strain however, the model does not account for the viscous part of the recovery. For the constant strain, the relaxation motion is observed however, the value of stress decreases to zero, which is not expected.

When all these properties are summed up, one can notice that the model is more appropriate for the elasto-viscous fluids rather than the viscoelastic solids.

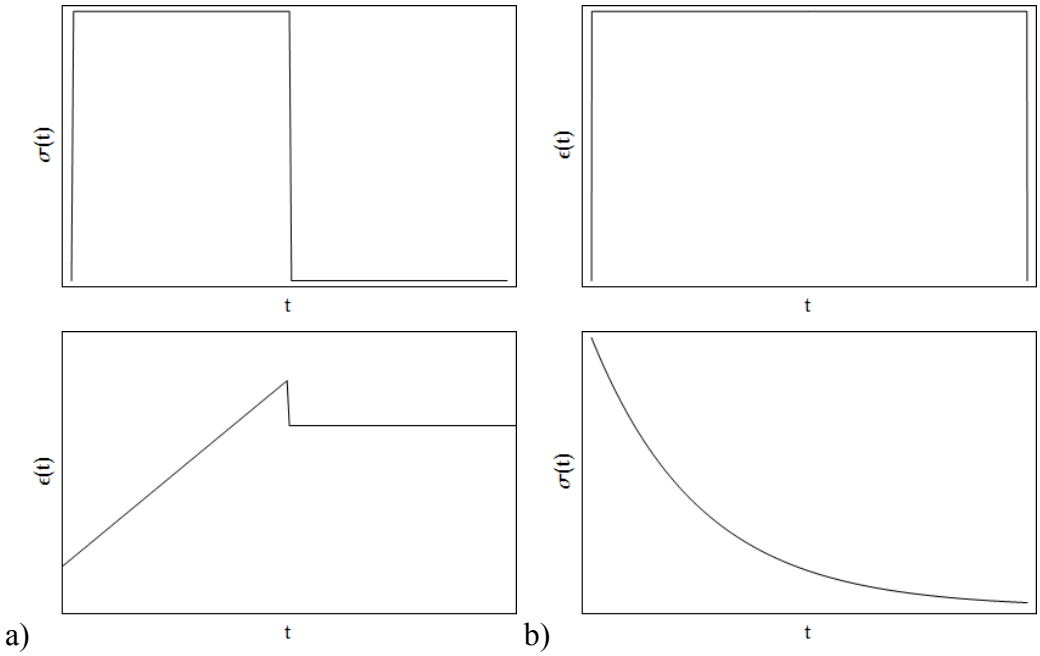

Figure 2.2: Viscoelastic behavior of Maxwell model: a) under constant stress; b) under constant strain.

2.1.2 Kelvin-Voigt Model

The second model that is investigated consists of a dashpot and a spring, as it was in the Maxwell model; however this time connected in parallel as presented in Figure 2.3.

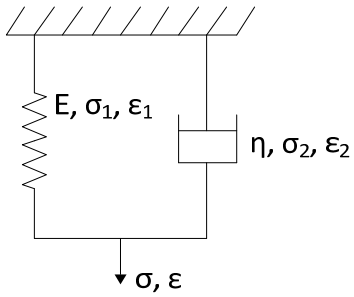

Figure 2.3: Representation of the Kelvin-Voigt model.

One can obtain the following relations for this viscoelastic model:

$$\varepsilon = \varepsilon_1 = \varepsilon_2\,,\ \sigma = \sigma_1 + \sigma_2\,,\ \sigma_1 = E\varepsilon_1 \text{ and } \sigma_2 = \eta\frac{d\varepsilon_2}{dt} \tag{2.4}$$

The stress-strain relation emerges from the relations in Eq.(2.4) as follows:

$$\sigma = E\varepsilon + \eta \frac{d\varepsilon}{dt} \tag{2.5}$$

Solution of Eq. (2.5) is presented in Figure 2.4 for the one dimensional tension case.

As observed from the figure, the model is capable to capture the creep, elastic recovery and viscous recovery behaviors quite successfully. However, it does not account for relaxation as one can see from the constant strain scenario.

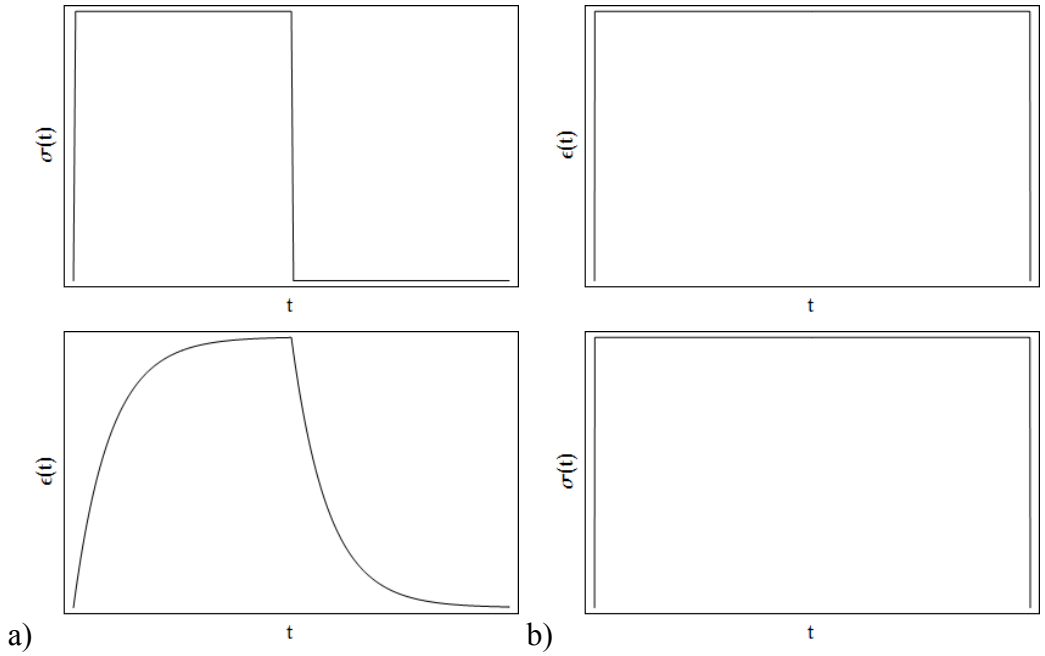

Figure 2.4: Viscoelastic behavior of Kelvin-Voigt Model: a) under constant stress; b) under constant strain.

2.1.3 Zener Model

This model is also known as the standard linear solid model and consists of a spring and a dashpot in series, connected to a spring in parallel as in Figure 2.5.

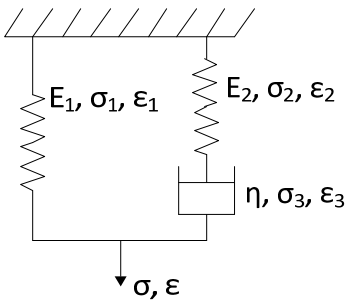

Figure 2.5: Representation of the Zener model.

The relations between stress and strain can be obtained from Figure 2.5 as follows:

$\varepsilon = \varepsilon_1 = \varepsilon_2 + \varepsilon_3$, $\sigma = \sigma_1 + \sigma_2$, $\sigma_3 = \sigma_2$, $\sigma_1 = E_1\varepsilon_1$, $\sigma_2 = E_2\varepsilon_2$ and

$$\sigma_3 = \eta \frac{d\varepsilon_3}{dt} \tag{2.6}$$

By using the relations in Eq. (2.6), one dimensional stress-strain relation for this model can be derived as follows:

$$\sigma + \frac{\eta}{E_2}\frac{d\sigma}{dt} = E_1\varepsilon + \eta\left(1 + \frac{E_1}{E_2}\right)\frac{d\varepsilon}{dt} \tag{2.7}$$

The solution of Eq. (2.7) is presented in Figure 2.6.

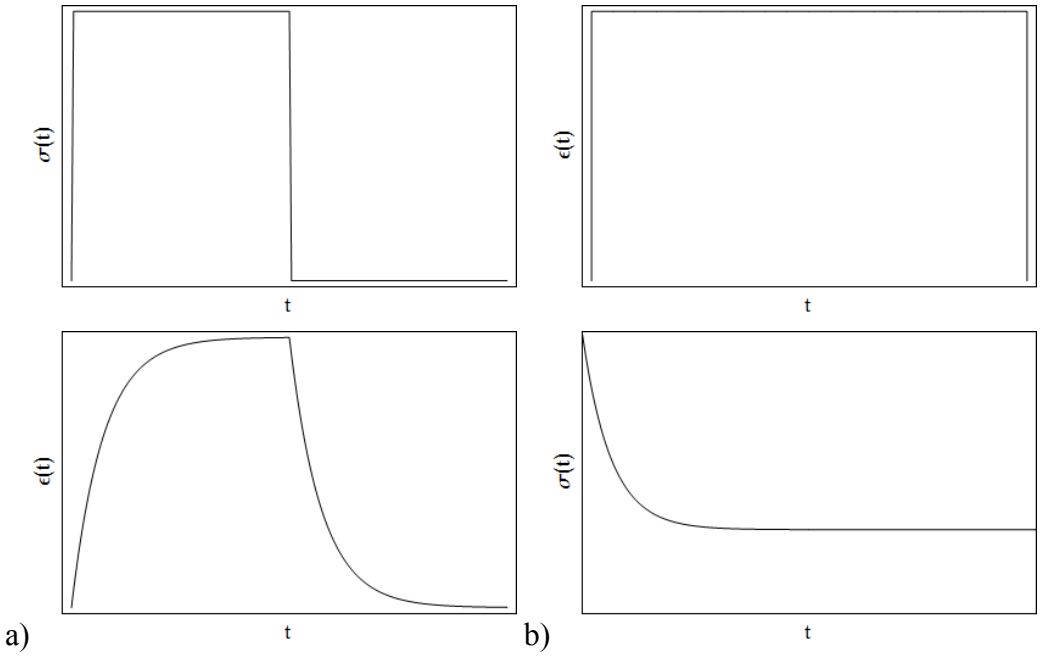

Figure 2.6: Viscoelastic behavior of Zener model: a) under constant stress; b) under constant strain.

As one can observe from Figure 2.6, this model successfully accounts for creep, elastic recovery, viscous recovery and stress-relaxation. The Zener model combines the aspects of Kelvin model and Maxwell model, which were described earlier. This model has three material constants, which are E_1, E_2 and η that are to be determined from the experimental data. Also, note that, to improve the fitting between the theoretical model and the experimental data, the model can be generalized by adding Maxwell elements to the right side of the Zener element in Figure 2.6 as demonstrated in [36].

2.2 Fractional-Order Viscoelastic Models

The earliest studies on fractional order viscoelasticity can be traced back to 1920's to the study of Nutting [37], where the experiments on hard stearine pitch revealed out that the stress-relaxation of this viscoelastic material depended on the fractional powers of time. Gemant suggested a fractional Maxwell model, with only the order of stress being fractional, for the modeling of elasto-viscous fluids [38]. Also, compared this model with the relaxation experiment for flour dough and concluded that the best match is obtained for a fractional order of 0.5 [38]. Later, Blair et al. used fractional derivatives to model the time dependent stress and strain for viscoelastic materials and compared the stress relaxation results of theory and experiments [39, 40]. After two and a half decades, Caputo et al. showed that fractional order Zener model was quite successful in the modeling of the variation of dynamical mechanical properties of glass and several metals at high temperature with frequency [41].

Though researchers, some of which are mentioned above, have realized that viscoelasticity and fractional calculus are closely related, the concept of fractional order derivatives in viscoelasticity was mostly used as a method of curve fitting until the beginning of 80's [4]. It is only after a series of publications made by Bagley and Torvik [42-46] that the fractional order models of viscoelasticity found theoretical basis. Since then, many studies have been devoted to fractional-calculus-viscoelasticity, both on the engineering and the theory sides. The fractional derivative models have superiorities over other models, which can be summarized as follows:

- The creep and relaxation behavior observed in viscoelastic polymeric materials are quite successfully modeled with relatively small number of unknown material constants [47].
- The effect of vibration frequency on the mechanical properties such as storage modulus, loss modulus and loss factor are reflected correctly [43, 47].
- Molecular theories such as Rouse's theory for chain molecules arrive at fractional order derivative of order 0.5 non-empirically, showing that fractional calculus models of viscoelastic materials are consistent with the physical principles that govern the behavior of such materials [42].

- Fractional derivatives are non-local operators, which provide a powerful instrument for the modeling of memory and heredity properties of viscoelastic materials [48].
- Master curves obtained with fractional derivative models require less number of parameters and are valid in wider frequency ranges when compared to other techniques such as Golla-Hughes-McTavish (GHM) and anelastic displacements field (ADF) methods.

It is obvious that fractional order constitutive material models are efficient and successful tools in modeling the viscoelastic behavior and as it has been shown in Section 2.1, Zener model is the best choice to describe the creep, stress-relaxation and recovery among the others. Therefore, the fractional order Zener model will be used to model the dynamical-mechanical properties of polymeric damping materials in this thesis.

Firstly, the four-parameter Zener model will be discussed and then the five-parameter model will be analyzed in detail.

2.2.1 Four-Parameter Zener Model

The four parameter fractional Zener model has solid theoretical basis, it is casual and it satisfies the thermodynamic constraints, such as predicting nonnegative internal work and energy dissipation [45]. The one-dimensional constitutive equation for this model can be written as follows [4, 43]:

$$\sigma(t) + \tau^{\alpha} \frac{d^{\alpha}\sigma(t)}{dt^{\alpha}} = E_0 \varepsilon(t) + \tau^{\alpha} E_{\infty} \frac{d^{\alpha}\varepsilon(t)}{dt^{\alpha}} \tag{2.8}$$

where, E_0 is the relaxed elastic moduli, E_∞ is the non-relaxed elastic moduli, τ is the relaxation time and α is the order of fractional derivative. Also, notice that Eq. (2.8) is a fractional order variation of the integer order Zener model presented in Eq. (2.7).

Since this model will be investigated in the frequency domain, the Fourier transform of Eq. (2.8) is required. Fourier transform of the fractional order derivative of a function g(t) can be evaluated as follows [49]:

$$F_e\left\{D^{\alpha} g(t), \omega\right\} = (i\,\omega)^{\alpha} g^{*}(\omega) \tag{2.9}$$

where, g* is the Fourier transform of g. By using the identity in Eq. (2.9), Fourier transform of Eq. (2.8) can be evaluated as follows:

$$\sigma^*(\omega)+\tau^\alpha(i\omega)^\alpha\sigma^*(\omega)=E_0\varepsilon^*(\omega)+\tau^\alpha E_\infty(i\omega)^\alpha\varepsilon^*(\omega) \tag{2.10}$$

The complex elastic moduli can be extracted from Eq. (2.10) by arranging the terms for stress and strain as follows [4]:

$$E^*(\omega)=\frac{\sigma^*(\omega)}{\varepsilon^*(\omega)}=\frac{E_0+E_\infty(i\omega\tau)^\alpha}{1+(i\omega\tau)^\alpha} \tag{2.11}$$

One can derive the following relations from Eq. (2.11) for the limit cases of the frequency:

$$\lim_{\omega\to 0}E^*(\omega)=E_0 \text{ and } \lim_{\omega\to\infty}E^*(\omega)=E_\infty \tag{2.12}$$

which is consistent with the definitions of E_0 and E_∞ for the four parameter model. The real part of the complex modulus in Eq. (2.11) corresponds to the stored strain energy and named as the storage modulus. The imaginary part of the complex modulus is related with the mechanical energy dissipated as heat and named as the loss modulus. By carrying out necessary derivations and simplifications on Eq. (2.11), one can arrive at the following relations for the storage modulus (E_d) and loss modulus (E_l) [4, 5]:

$$E_d(\omega)=\frac{E_0+E_\infty(\omega\tau)^{2\alpha}+\left(E_0+E_\infty\right)(\omega\tau)^\alpha\cos\left(\pi\alpha/2\right)}{1+(\omega\tau)^{2\alpha}+2(\omega\tau)^\alpha\cos\left(\pi\alpha/2\right)} \tag{2.13}$$

$$E_l(\omega)=\frac{\left(E_\infty-E_0\right)(\omega\tau)^\alpha\sin\left(\pi\alpha/2\right)}{1+(\omega\tau)^{2\alpha}+2(\omega\tau)^\alpha\cos\left(\pi\alpha/2\right)} \tag{2.14}$$

The ratio of the loss modulus to the storage modulus is the mechanical loss factor and can be evaluated from Eqs. (2.13) and (2.14) for the four parameter Zener model as follows:

$$\eta(\omega)=\frac{\left(E_\infty-E_0\right)(\omega\tau)^\alpha\sin\left(\pi\alpha/2\right)}{E_0+E_\infty(\omega\tau)^{2\alpha}+\left(E_0+E_\infty\right)(\omega\tau)^\alpha\cos\left(\pi\alpha/2\right)} \tag{2.15}$$

For this model, there are four parameters which are to be determined from the experimental data. The relaxed and non-relaxed elastic moduli are evaluated from the low and high frequency regime as stated in Eq. (2.12). The order of the fractional derivative α can be obtained in terms of loss factor peak (η_{max}) from the derivative of Eq. (2.15) with respect to the frequency, as follows [4]:

$$\alpha = \frac{2}{\pi}\arcsin\left[\eta_{\max}\left(E_\infty - E_0\right)\frac{2\sqrt{E_0 E_\infty} + \left(E_\infty + E_0\right)\sqrt{1+\eta_{\max}^2}}{\eta_{\max}^2\left(E_\infty + E_0\right)^2 + \left(E_\infty - E_0\right)^2}\right] \tag{2.16}$$

The last unknown parameter, the relaxation time (τ), can be obtained from the derivative of loss modulus in Eq. (2.14) with respect to the frequency, as follows [5]:

$$\tau = 1/\omega_l \tag{2.17}$$

where, ω_l is the value of frequency that corresponds to the loss modulus peak. Alternatively, as Galucio et al. [4] suggests, the relaxation time can also be obtained by minimizing the variation between theoretical model and experimental data via the least squares method. The effects of α and τ on the dynamical-mechanical properties are presented in Figure 2.7 and Figure 2.8.

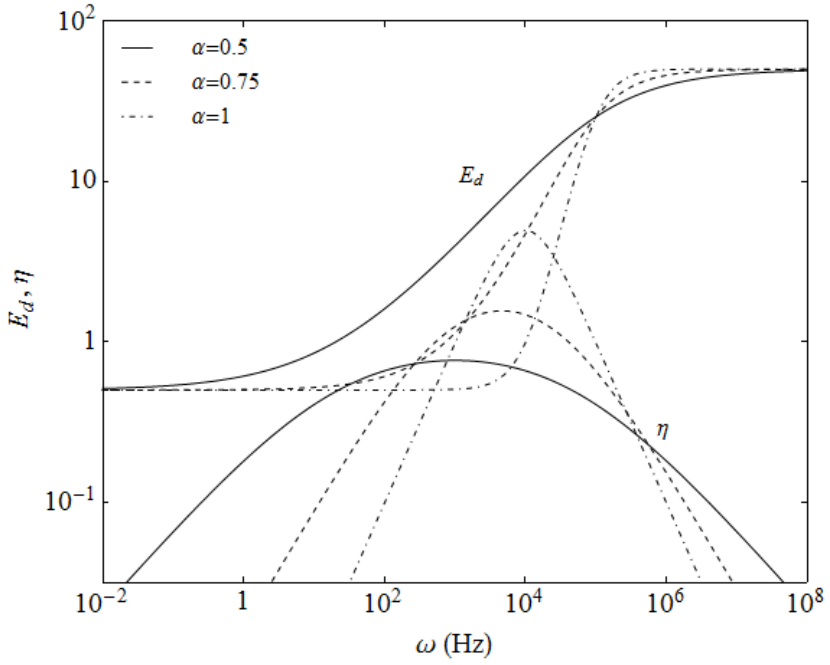

Figure 2.7: Effect of α on the storage modulus and the loss factor.

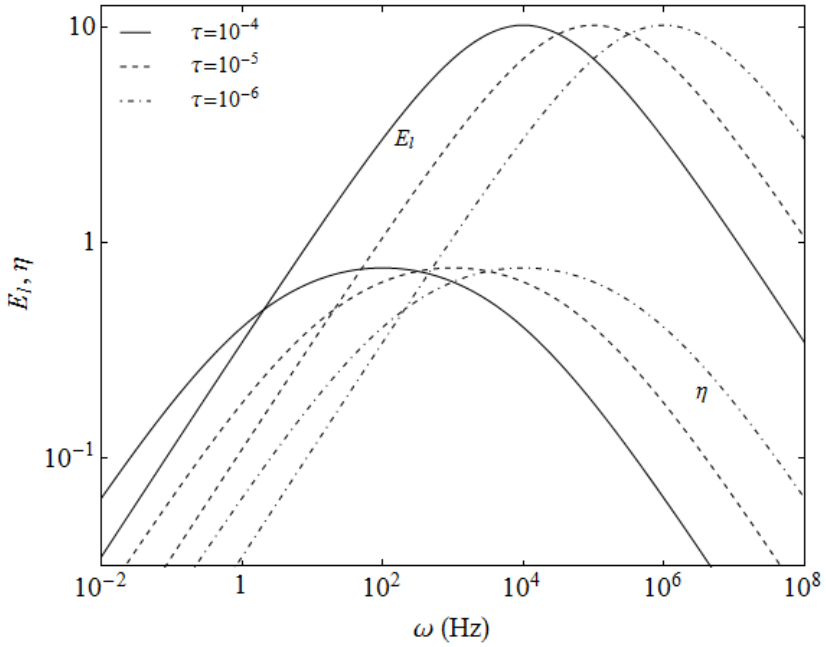

Figure 2.8: Effect of τ on the loss modulus and the loss factor.

As the order of fractional derivative α increases, the change from low frequency behavior to the high frequency behavior takes place in a narrower frequency band for the storage modulus. On the other hand, the loss factor peak increases and shifts to right with increasing α. Effect of the relaxation time is observed from Figure 2.8 as a shifting of the dynamical properties to left with increasing τ.

Also, notice that, the loss functions decrease monotonically with frequency and they are symmetrical for all values of the parameters.

2.2.2 Five Parameter Zener Model

The four-parameter fractional model analyzed previously has been used to define the viscoelastic behavior by many researchers. This model has solid theoretical basis; besides, all the unknown parameters in the model can be obtained from the experimental data without the use of a curve fitting technique. However, the four-parameter model lacks the ability to predict asymmetrical loss factor peak, which is the case usually encountered in experimental data that exist in literature.

The first attempt for a five parameter model was made by Bagley et al. [43]. The model proposed in their study is a modification of the four-parameter model in Eq. (2.8) with the assumption that the fractional order time derivatives of the stress and the strain are different. By using this model, they evaluated the master curves for the loss modulus and the storage modulus for corning glass. The matching between the experimental data and the theory was excellent; moreover, the asymmetry in the loss modulus was captured quite successfully. However, in a later study by the same authors [45], it is proven that this model was not physically meaningful in terms of thermodynamics.

Later, Friedrich et al. proposed a model with the usage of different fractional orders for stress and strain in the complex modulus [50]. Pritz pursued this model and arrived at the following five parameter fractional order stress-strain relation [5].

$$\sigma(t)+\tau^{\beta}\frac{d^{\beta}\sigma(t)}{dt^{\beta}}=E_0\varepsilon(t)+E_0\tau^{\beta}\frac{d^{\beta}\varepsilon(t)}{dt^{\beta}}+\left(E_{\infty}-E_0\right)\tau^{\alpha}\frac{d^{\alpha}\varepsilon(t)}{dt^{\alpha}} \qquad \textbf{(2.18)}$$

The parameters that appear in Eq. (2.18) are formally the same with the ones in Eq. (2.8) however, E_∞ is not the high frequency moduli (non-relaxed moduli) but a parameter related to the high frequency behavior. Also, note that τ is the relaxation time as it was in the four-parameter model, however the value of it is different from that in the four parameter model [5].

Fourier transform of Eq. (2.18) gives the following relation for the complex modulus after carrying out necessary simplifications:

$$E^{*}(\omega)=E_0+\frac{\left(E_{\infty}-E_0\right)(i\omega\tau)^{\alpha}}{1+(i\omega\tau)^{\beta}} \qquad \textbf{(2.19)}$$

The storage modulus and the loss modulus can be evaluated from the real and the imaginary parts of Eq. (2.19) respectively, as follows:

$$E_d(\omega)=E_0+(E_{\infty}-E_0)\frac{\cos\left(\alpha\pi/2\right)(\omega\tau)^{\alpha}+\cos\left[\left(\alpha-\beta\right)\pi/2\right](\omega\tau)^{\alpha+\beta}}{1+2\cos\left(\beta\pi/2\right)(\omega\tau)^{\beta}+\left(\omega\tau\right)^{2\beta}} \qquad \textbf{(2.20)}$$

$$E_l(\omega) = (E_\infty - E_0)\frac{\sin(\alpha\pi/2)(\omega\tau)^\alpha + \sin\left[(\alpha-\beta)\pi/2\right](\omega\tau)^{\alpha+\beta}}{1+2\cos(\beta\pi/2)(\omega\tau)^\beta + (\omega\tau)^{2\beta}} \tag{2.21}$$

The loss factor can be evaluated from the ratio of the loss moduli to the storage moduli as follows:

$$\eta(\omega) = (d-1)\left\{\sin(\pi\alpha/2)(\omega\tau)^\alpha + \sin\left[\pi(\alpha-\beta)/2\right](\omega\tau)^{\alpha+\beta}\right\} \Bigg/ \left\{1+(\omega\tau)^{2\beta} + 2\cos\left(\frac{\pi\beta}{2}\right)(\omega\tau)^\beta + (d-1)\left[\cos\left(\frac{\pi\alpha}{2}\right)(\omega\tau)^\alpha + \cos\left(\pi\frac{\alpha-\beta}{2}\right)(\omega\tau)^{\alpha+\beta}\right]\right\} \tag{2.22}$$

where, d is the ratio E_∞/E_0, which has values usually greater than 1 for viscoelastic materials. The unknown material constants can be obtained from the approximate low and high frequency behaviors of the dynamic moduli and the loss factor [5]:

ω<<1:

$$E_d(\omega) \cong E_0,\ \eta(\omega) \cong \frac{E_\infty}{E_0}\sin(\alpha\pi/2)(\omega\tau)^\alpha \tag{2.23}$$

ω>>1:

$$E_d(\omega) \cong E_\infty \cos\left[(\alpha-\beta)\pi/2\right](\omega\tau)^{\alpha-\beta},\ \eta(\omega) \cong \tan\left[(\alpha-\beta)\pi/2\right] \tag{2.24}$$

The thermodynamic requirements are satisfied when the following inequalities hold:

$$E_d(\omega) \geq 0 \text{ and } E_l(\omega) \geq 0 \text{ for } 0 < \omega < \infty \tag{2.25}$$

As indicated by Pritz [5], loss modulus can take negative values at some frequencies if α<β. Therefore, for the five-parameter fractional model to be physically meaningful for all frequencies, the following inequalities are necessary to satisfy [5]:

$$E_0 \geq 0,\ E_\infty \geq 0,\ d \geq 1 \text{ and } \alpha > \beta \tag{2.26}$$

and the causality condition requires that the relaxation time is positive:

$$\tau > 0 \tag{2.27}$$

Note that, there is no difference between the five and the four-parameter models for α=β, since Eqs. (2.20)-(2.22) are identical with Eqs. (2.13)-(2.15) for that case. Effects of α and β on the dynamical-mechanical properties are presented in Figure 2.9.

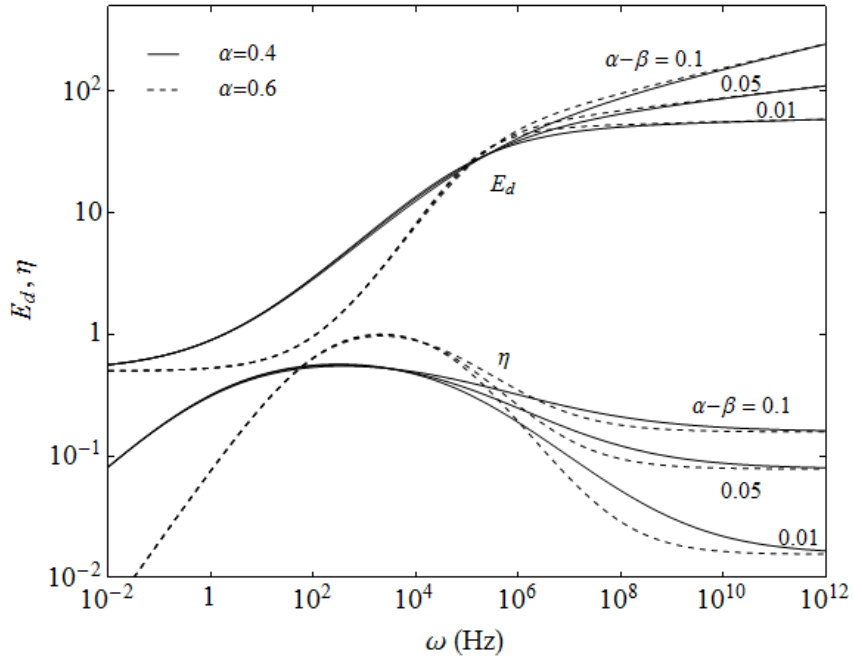

Figure 2.9: Effects of α and β on the storage modulus and the loss factor.

Figure 2.9 shows that β has no effect on the low frequency behavior. This is consistent with the comment in [5] that the four and five parameter models are identical at low frequencies.

On the other hand, the difference between α and β is the dominant parameter that determines the high frequency behavior for both the storage modulus and the loss factor. The symmetry of the loss factor peak is deformed as the difference between α and β increases. Another difference when compared with the four-parameter model is that the storage modulus does not converge to a constant value but linearly increases with frequency for the five-parameter model. The effect of relaxation time is presented in Figure 2.10.

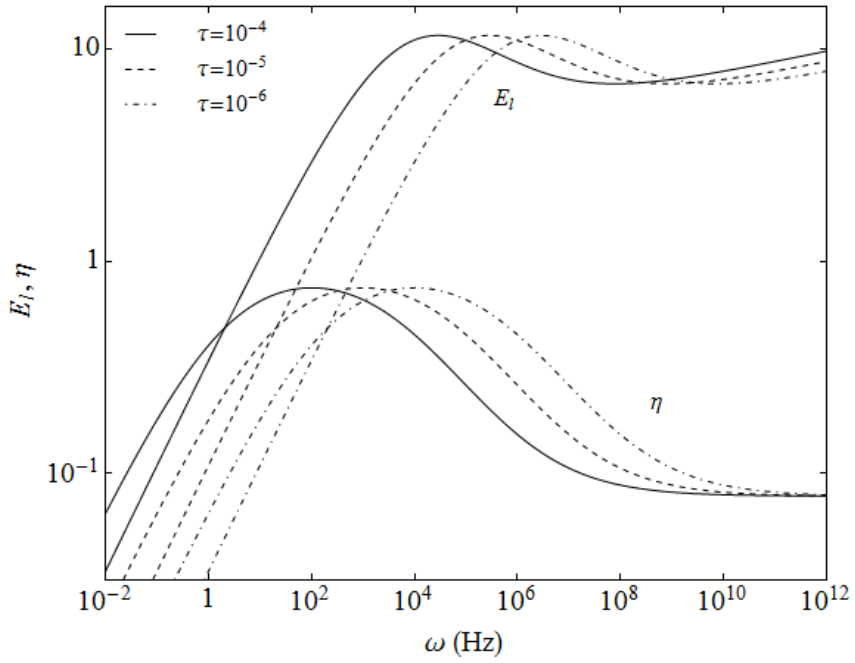

Figure 2.10: Effect of τ on the loss modulus and the loss factor.

Figure 2.10 shows that the effect of τ on the mechanical properties is a shifting of curves to left or right as it was in the four-parameter model. The striking difference between the four and five parameter models is again observed for the high frequency regime. In the four-parameter model, the loss functions were decaying with increasing frequency (Figure 2.8). However, in the five-parameter model, the loss factor converges to a constant value as also stated in Eq. (2.24) and the loss modulus constantly increases.

2.3 Analysis of the Experimental Data

It is not usually possible to obtain reliable experimental data over a broad frequency range at a desired temperature. Therefore, the experimental results for the shear modulus and loss factor are obtained for relatively narrow frequency ranges at different temperatures. The results of an experiment for 3M-ISD110 [36] is presented in Figure 2.11 and Figure 2.12, as an example.

The effects of temperature and frequency are combined as a compound variable to obtain the master curves for the viscoelastic material, as follows:

$$E^*(\omega,T) = E^*(\omega f(T)) \tag{2.28}$$

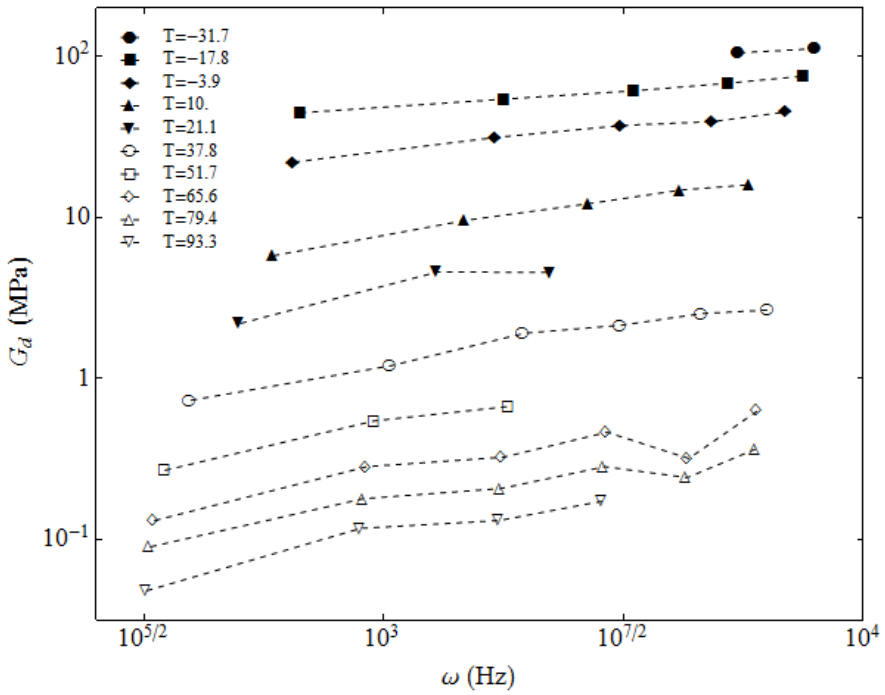

Figure 2.11: Experimental data for the storage modulus of 3M-ISD110 [36].

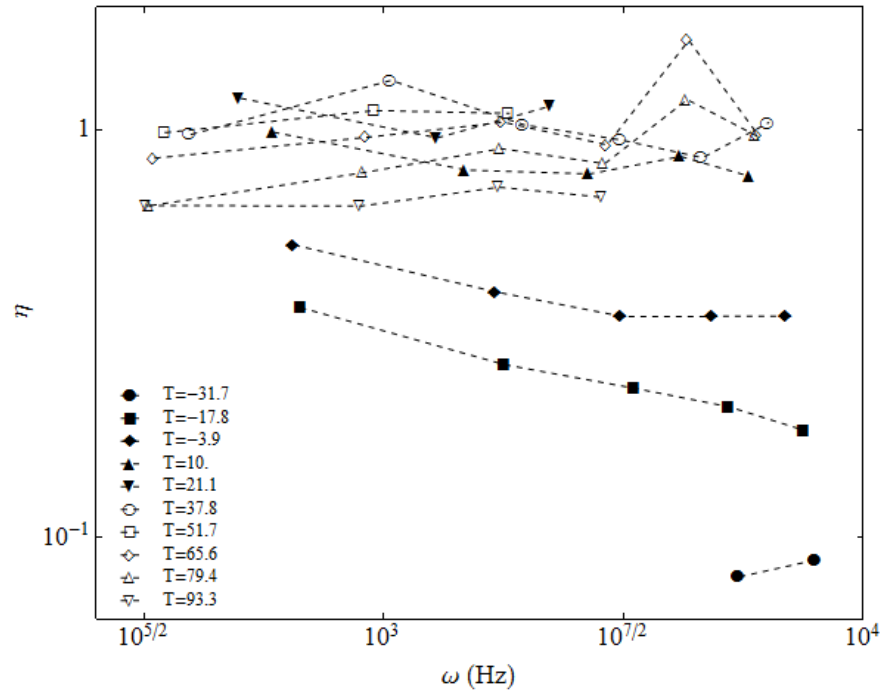

Figure 2.12: Experimental data for the loss factor of 3M-ISD110 [36].

Note that, the temperature-frequency equivalence principle in Eq. (2.28) holds for thermorheologically simple viscoelastic materials. Since the viscoelastic core is isotropic with the Poisson's ratio assumed as frequency independent, the following relation between the shear modulus and the elastic moduli holds:

$$E^* = \frac{G^*}{2(1+\nu)} \tag{2.29}$$

The complex shear modulus can be written as follows:

$$G^* = G_d\left(1+i\eta\right) \tag{2.30}$$

The simple yet successful Arrhenius shift factor equation is used to model the relationship between temperature and frequency in this work:

$$\log f(T) = T_A\left(\frac{1}{T}-\frac{1}{T_0}\right) \tag{2.31}$$

where, T_A is the activation temperature, T_0 is the reference temperature and T is the actual temperature. The value of T_A is usually determined by minimizing the scatter in the logarithmic plots of the experimental data for the shear modulus and the loss factor versus frequency. As an example, the effect of the activation temperature T_A on the master curves of 3M-ISD110 is presented in Figure 2.13.

One can conclude that minimum scatter is around a value T_A=5000. In this thesis, T_A is evaluated by a program code, which minimizes the difference between the theoretical model and the experimental results.

The curve fitting process is applied to the experimental data presented in Refs. [51] and [36] for four commercial damping polymers. The first two are self-adhesive soft acrylic polymers from 3M, i.e. 3M ISD-110 and 3M 467. The other two are relatively stiff polyurethane polymers from Soundcoat, which are DYAD 606 and DYAD 609. The unknown material constants α, β, E_0 and E_∞ are obtained from the transcendental equation system presented in Eqs. (2.23) and (2.24) by using the built-in function FindRoot in MATHEMATICA, which utilizes the Newton-Raphson method to obtain the solution. On the other hand, the relaxation time τ is estimated by minimizing the difference between the experimental and theoretical data by using the least squares method, as suggested by Galucio et al [4].

The master curves are presented in Figure 2.14 and the values of the unknown parameters for these four viscoelastic materials are presented in Table 2.1 together with the data for two other damping polymers that already exist in literature [5].

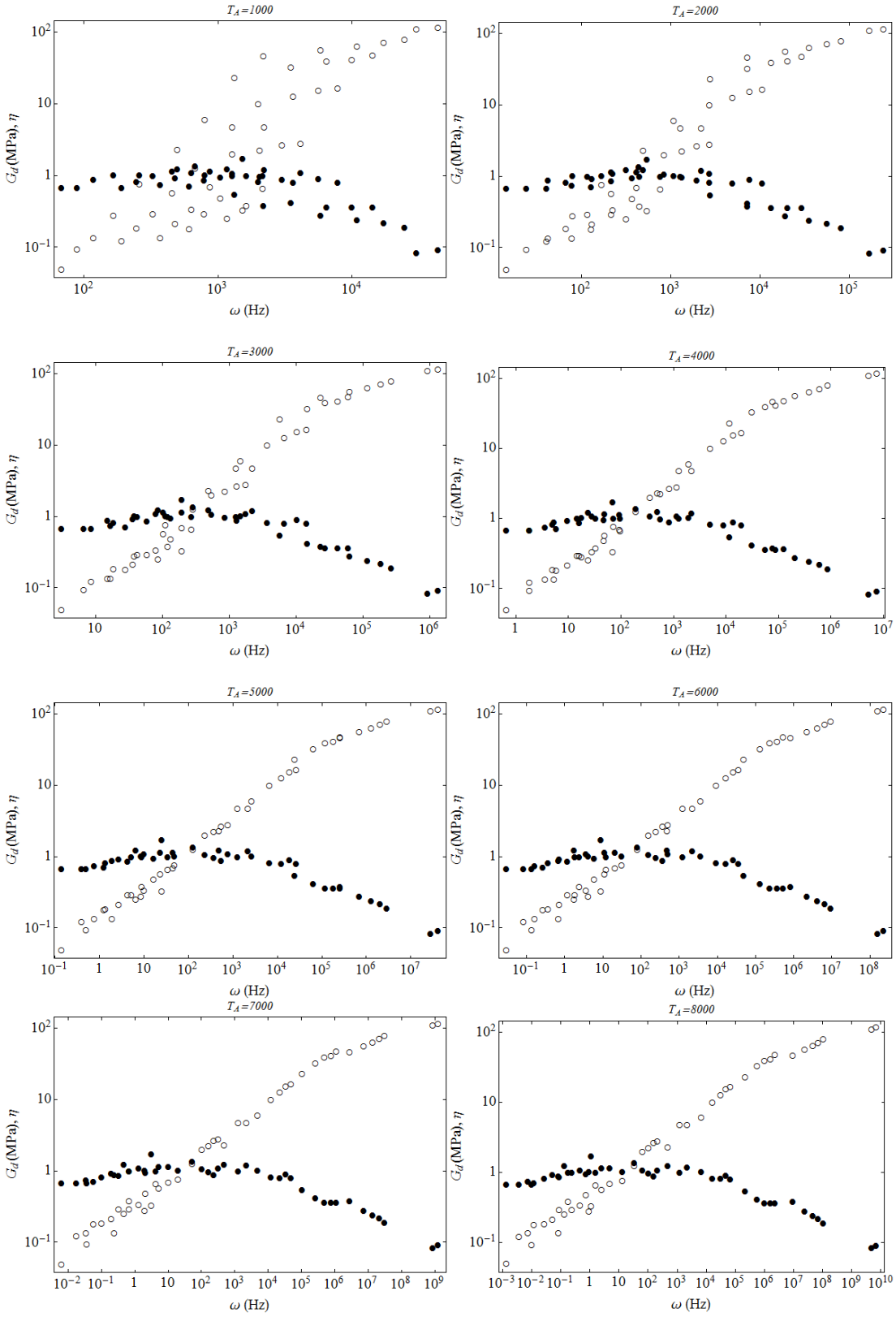

Figure 2.13: Variation of master curves with T_A for 3M-ISD110 at T_0=21.1 ^{0}C (○ Storage modulus, ● Loss factor).

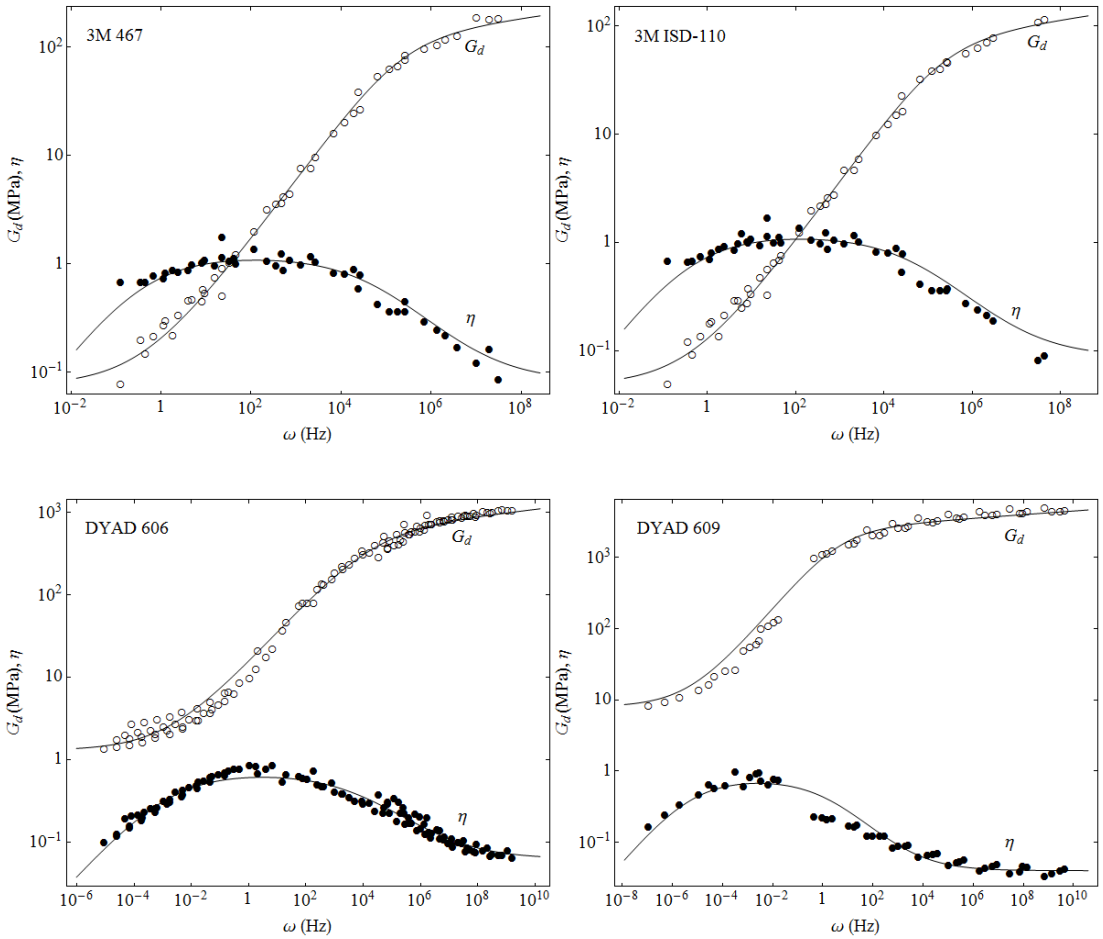

Figure 2.14: Master curves of viscoelastic materials compared with the experimental data (T_0=21.1 ^{0}C).

There is a good matching between the experimental and theoretical results, which shows that the five parameter fractional model is quite successful in capturing the viscoelastic behavior. Also, note that the experimental data for DYAD 606 and DYAD 609 are given in English system in [51] so they are converted to SI system.

Table 2.1: Viscoelastic material properties.

ID	Material	G_0, Pa	d	α	β	τ, s	ρ_2, kg/m^3	T_A, ^{0}K
1	3M ISD-110	48×10^3	1685	0.550	0.494	7.73×10^{-6}	965	5050
2	3M 467	76×10^3	1753	0.553	0.501	7.98×10^{-6}	1080	5050
3	DYAD 606	1.29×10^6	499	0.383	0.343	8.66×10^{-5}	969	10450
4	DYAD 609	7.98×10^6	324	0.421	0.396	3.75×10^{-1}	1107	10950
5	GE.SMRD[5]	5×10^6	36	0.605	0.554	2.09×10^{-4}	709	-
6	EAR C-1002[5]	8×10^6	1570	0.566	0.558	7.23×10^{-10}	1300	-

3. VIBRATION ANALYSIS OF SANDWICH BEAMS

3.1 Equation of Motion

The assumptions used to derive the kinematic relations and the governing equations are as follows:

- The shear angles of the top and bottom face layers are neglected.
- The core layer is relatively soft and viscoelastic with a complex modulus.
- The contribution from the core layer is only by transverse shear stresses.
- Layers are assumed as incompressible through the thickness.
- Transverse displacement does not change between the layers.
- The beam deflection is small.
- There is no slip between the layers.

The configuration of the sandwich beam and the displacement of its layers are presented in Figure 3.1 and Figure 3.2 respectively.

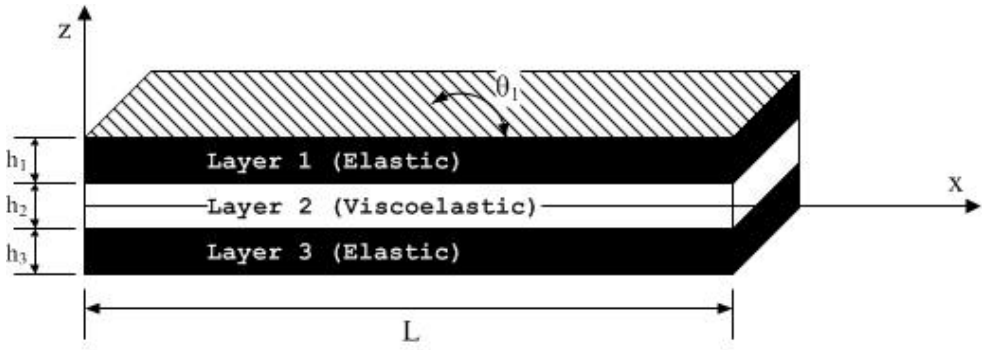

Figure 3.1: The geometry and configuration of the sandwich beam.

Using the geometry in Figure 3.2, the kinematic relations are derived as follows:

$$u^{(1)} = u_0(x,t) - \frac{h_2}{2}\varphi(x,t) - \left(z^{(1)} + \frac{h_1}{2}\right)\frac{\partial}{\partial x}w(x,t) \qquad \textbf{(3.1)}$$

$$u^{(2)} = u_0(x,t) - z^{(2)}\varphi(x,t) \tag{3.2}$$

$$u^{(3)} = u_0(x,t) + \frac{h_2}{2}\varphi(x,t) - \left(z^{(3)} - \frac{h_3}{2}\right)\frac{\partial}{\partial x}w(x,t) \tag{3.3}$$

$$w^{(i)} = w(x,t)\ ,\ i = 1,2,3 \tag{3.4}$$

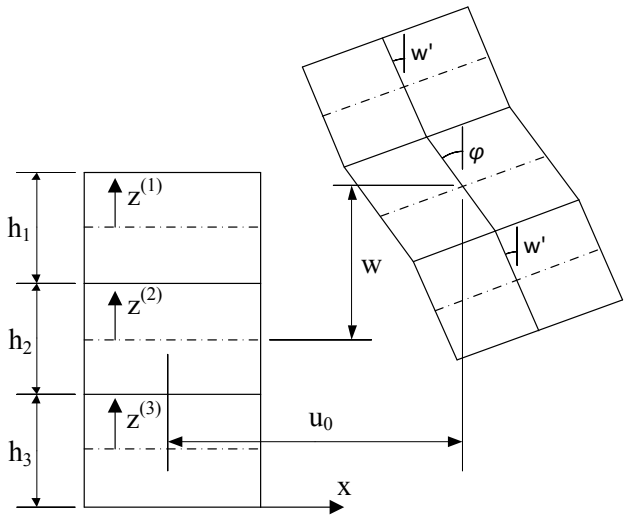

Figure 3.2: Coordinate system and displacement of layers of the sandwich beam.

where, φ(x,t) is the rotation, u_0(x,t) is the longitudinal displacement and w(x,t) is the transverse displacement of the centroid of viscoelastic core. In addition, $u^{(i)}$ and $w^{(i)}$ correspond to the longitudinal and transverse displacement fields of the i'th layer. One can find similar beam models and kinematic relations that exist in literature for three-layered sandwich beams [27, 52, 53].

The strain-displacement relations for the sandwich beam can be evaluated from Eqs. (3.1) - (3.4) as follows:

$$\varepsilon_{xx}^{(1)} = \frac{\partial u_0}{\partial x} - \frac{h_2}{2}\frac{\partial \varphi}{\partial x} - \left(z^{(1)} + \frac{h_1}{2}\right)\frac{\partial^2 w}{\partial x^2} \tag{3.5}$$

$$\gamma_{xz}^{(2)} = \frac{\partial w}{\partial x} - \varphi \tag{3.6}$$

$$\varepsilon_{xx}^{(3)} = \frac{\partial u_0}{\partial x} + \frac{h_2}{2}\frac{\partial \varphi}{\partial x} - \left(z^{(3)} - \frac{h_3}{2}\right)\frac{\partial^2 w}{\partial x^2} \tag{3.7}$$

The stress-strain relations can be given as follows:

$$\sigma_{xx}^{(1)} = E_1 \varepsilon_{xx}^{(1)} \tag{3.8}$$

$$\sigma_{xz}^{(2)} = G_2^* \gamma_{xz}^{(2)} \tag{3.9}$$

$$\sigma_{xx}^{(3)} = E_3 \varepsilon_{xx}^{(3)} \tag{3.10}$$

where $G_2^* = G_2(1+i\eta)$ is the complex shear modulus of the viscoelastic core and E_1, E_3 correspond to the Young's moduli of the constraining layer and base layer respectively. Let us consider the face layers as orthotropic. Then, the Young's moduli of these layers can be calculated as follows:

$$E_i = Q_{11} cos^4(\theta_i) + Q_{22} sin^4(\theta_i) + 2\left(Q_{12} + 2Q_{66}\right) sin^2(\theta_i) cos^2(\theta_i)\,,\ i = 1,3 \tag{3.11}$$

where, θ_i is the angle of lamination of the i'th layer and

$$Q_{11} = \frac{E_{11}}{1-\nu_{12}\nu_{21}},\ Q_{12} = \frac{\nu_{12}E_{22}}{1-\nu_{12}\nu_{21}},\ Q_{22} = \frac{E_{22}}{1-\nu_{12}\nu_{21}},\ Q_{66} = G_{12},$$
$$\nu_{21} = \nu_{12}\frac{E_{22}}{E_{11}} \tag{3.12}$$

are the material properties of the composite face layers. For the free vibrations of the beam, Hamilton's principle can be expressed as follows:

$$\int_0^T (\delta U - \delta K) dt = 0 \tag{3.13}$$

where U and K correspond to the elastic strain energy and the kinetic energy respectively. For the problem considered, Eq. (3.13) becomes:

$$\int_0^T\int_0^L\int_{-h_1/2}^{h_1/2}\left[\sigma_{xx}^{(1)}\delta\varepsilon_{xx}^{(1)}-\rho_1\left(\frac{\partial w}{\partial t}\delta\frac{\partial w}{\partial t}+\frac{\partial u^{(1)}}{\partial t}\delta\frac{\partial u^{(1)}}{\partial t}\right)\right]dz^{(1)}dxdt$$
$$+\int_0^T\int_0^L\int_{-h_2/2}^{h_2/2}\left[\sigma_{xz}^{(2)}\delta\gamma_{xz}^{(2)}-\rho_2\left(\frac{\partial w}{\partial t}\delta\frac{\partial w}{\partial t}+\frac{\partial u^{(2)}}{\partial t}\delta\frac{\partial u^{(2)}}{\partial t}\right)\right]dz^{(2)}dxdt \qquad \textbf{(3.14)}$$
$$+\int_0^T\int_0^L\int_{-h_3/2}^{h_3/2}\left[\sigma_{xx}^{(3)}\delta\varepsilon_{xx}^{(3)}-\rho_3\left(\frac{\partial w}{\partial t}\delta\frac{\partial w}{\partial t}+\frac{\partial u^{(3)}}{\partial t}\delta\frac{\partial u^{(3)}}{\partial t}\right)\right]dz^{(3)}dxdt=0$$

From Eq. (3.14), the governing equations are obtained as follows:

$$(E_1h_1+E_3h_3)\frac{\partial^2u_0}{\partial x^2}+\frac{h_2}{2}(E_3h_3-E_1h_1)\frac{\partial^2\varphi}{\partial x^2}+\frac{1}{2}(E_3h_3^2-E_1h_1^2)\frac{\partial^3w}{\partial x^3}$$
$$=(h_1\rho_1+h_2\rho_2+h_3\rho_3)\frac{\partial^2u_0}{\partial t^2}+\frac{h_2}{2}(h_3\rho_3-h_1\rho_1)\frac{\partial^2\varphi}{\partial t^2}+\frac{1}{2}(h_3^2\rho_3-h_1^2\rho_1)\frac{\partial^3w}{\partial t^2\partial x} \qquad \textbf{(3.15)}$$

$$(E_3h_3-E_1h_1)\frac{\partial^2u_0}{\partial x^2}+\frac{h_2}{2}(E_1h_1+E_3h_3)\frac{\partial^2\varphi}{\partial x^2}+\frac{1}{2}(E_1h_1^2+E_3h_3^2)\frac{\partial^3w}{\partial x^3}+2G_2(\frac{\partial w}{\partial x}-\varphi)$$
$$=(h_3\rho_3-h_1\rho_1)\frac{\partial^2u_0}{\partial t^2}+\frac{h_2}{6}(3h_1\rho_1+h_2\rho_2+3h_3\rho_3)\frac{\partial^2\varphi}{\partial t^2}+\frac{1}{2}(h_1^2\rho_1+h_3^2\rho_3)\frac{\partial^3w}{\partial t^2\partial x} \qquad \textbf{(3.16)}$$

$$G_2h_2(\frac{\partial\varphi}{\partial x}-\frac{\partial^2w}{\partial x^2})+\frac{1}{2}(E_3h_3^2-E_1h_1^2)\frac{\partial^3u_0}{\partial x^3}+\frac{h_2}{4}(E_1h_1^2+E_3h_3^2)\frac{\partial^3\varphi}{\partial x^3}$$
$$+\frac{1}{3}(E_1h_1^3+E_3h_3^3)\frac{\partial^4w}{\partial x^4}=\frac{1}{2}(h_3^2\rho_3-h_1^2\rho_1)\frac{\partial^3u_0}{\partial^2t\partial x}-(h_1\rho_1+h_2\rho_2+h_3\rho_3)\frac{\partial^2w}{\partial t^2} \qquad \textbf{(3.17)}$$
$$+\frac{h_2}{4}(h_1^2\rho_1+h_3^2\rho_3)\frac{\partial^3\varphi}{\partial^2t\partial x}+\frac{1}{3}(h_1^3\rho_1+h_3^3\rho_3)\frac{\partial^4w}{\partial x^2\partial t^2}$$

Notice that, Eq. (3.15) that governs the axial motion of the sandwich beam is uncoupled with the rotation and the transverse displacement for a symmetrically sectioned beam, where the material and geometric properties of Layers 1 and 3 are identical.

The boundary conditions are evaluated as follows:

$$\left(N_x^{(1)}+N_x^{(3)}\right)\delta u_0\Big|_0^L=0 \qquad \textbf{(3.18)}$$

$$\frac{h_2}{2}\left(N_x^{(3)}-N_x^{(1)}\right)\delta\varphi\Big|_0^L=0 \qquad \textbf{(3.19)}$$

$$\left(Q_x^{(2)} + \frac{\partial}{\partial x} M_x^{(1)} + \frac{\partial}{\partial x} M_x^{(3)} + \frac{h_1}{2} \frac{\partial}{\partial x} N_x^{(1)} - \frac{h_3}{2} \frac{\partial}{\partial x} N_x^{(3)} \right) \delta w \Big|_0^L = 0 \tag{3.20}$$

$$\left(\frac{h_3}{2} N_x^{(3)} - \frac{h_1}{2} N_x^{(1)} - M_x^{(1)} - M_x^{(3)} \right) \delta \left(\frac{\partial w}{\partial x} \right) \Big|_0^L = 0 \tag{3.21}$$

where;

$$N_x^{(i)} = \int_{-h_i/2}^{h_i/2} \sigma_{xx}^{(i)} dz^{(i)} \,,\; Q_x^{(i)} = \int_{-h_i/2}^{h_i/2} \sigma_{xz}^{(i)} dz^{(i)} \,,\; M_x^{(i)} = \int_{-h_i/2}^{h_i/2} z^{(i)} \sigma_{xx}^{(i)} dz^{(i)} \,, \quad i = 1,2,3 \tag{3.22}$$

For the problem considered, the sectional moment and forces are obtained from Eqs. (3.5) - (3.10) together with Eq. (3.22) as follows:

$$N_x^{(1)} = E_1 \left(h_1 \frac{\partial u_0}{\partial x} - \frac{1}{2} h_1 h_2 \frac{\partial \varphi}{\partial x} - \frac{1}{2} h_1^2 \frac{\partial^2 w}{\partial x^2} \right) \tag{3.23}$$

$$N_x^{(3)} = E_3 \left(h_3 \frac{\partial u_0}{\partial x} + \frac{1}{2} h_2 h_3 \frac{\partial \varphi}{\partial x} + \frac{1}{2} h_3^2 \frac{\partial^2 w}{\partial x^2} \right) \tag{3.24}$$

$$Q_x^{(2)} = G_2 h_2 \left(\frac{\partial w}{\partial x} - \varphi \right) \tag{3.25}$$

$$M_x^{(1)} = -\frac{1}{12} E_1 h_1^3 \frac{\partial^2 w}{\partial x^2} \tag{3.26}$$

$$M_x^{(3)} = -\frac{1}{12} E_3 h_3^3 \frac{\partial^2 w}{\partial x^2} \tag{3.27}$$

For the harmonic vibrations of the sandwich beam, the displacement field can be assumed as follows:

$$u_0(x,t) = \overline{u}_0(x,\omega) e^{i\omega t} \,,\; w(x,t) = \overline{w}(x,\omega) e^{i\omega t} \,,\; \varphi(x,t) = \overline{\varphi}(x,\omega) e^{i\omega t} \tag{3.28}$$

Then, Eqs. (3.15) - (3.17) become:

$$(E_1h_1+E_3h_3)\bar{u}_0''+\frac{h_2}{2}(E_3h_3-E_1h_1)\bar{\varphi}''+\frac{1}{2}(E_3h_3^2-E_1h_1^2)\bar{w}'''$$
$$=-\omega^2\left[(h_1\rho_1+h_2\rho_2+h_3\rho_3)\bar{u}_0+\frac{h_2}{2}(h_3\rho_3-h_1\rho_1)\bar{\varphi}+\frac{1}{2}(h_3^2\rho_3-h_1^2\rho_1)\bar{w}'\right] \quad \textbf{(3.29)}$$

$$(E_3h_3-E_1h_1)\bar{u}_0''+\frac{h_2}{2}(E_1h_1+E_3h_3)\bar{\varphi}''+\frac{1}{2}(E_1h_1^2+E_3h_3^2)\bar{w}'''+2G_2(\bar{w}'-\bar{\varphi})$$
$$=-\omega^2\left[(h_3\rho_3-h_1\rho_1)\bar{u}_0+\frac{h_2}{6}(3h_1\rho_1+h_2\rho_2+3h_3\rho_3)\bar{\varphi}+\frac{1}{2}(h_1^2\rho_1+h_3^2\rho_3)\bar{w}'\right] \quad \textbf{(3.30)}$$

$$G_2h_2(\bar{\varphi}'-\bar{w}'')+\frac{1}{2}(E_3h_3^2-E_1h_1^2)\bar{u}_0'''+\frac{h_2}{4}(E_1h_1^2+E_3h_3^2)\bar{\varphi}'''$$
$$+\frac{1}{3}(E_1h_1^3+E_3h_3^3)\bar{w}^{iv}=-\omega^2\left[\frac{1}{2}(h_3^2\rho_3-h_1^2\rho_1)\bar{u}_0'-(h_1\rho_1+h_2\rho_2+h_3\rho_3)\bar{w}\right. \quad \textbf{(3.31)}$$
$$\left.+\frac{h_2}{4}(h_1^2\rho_1+h_3^2\rho_3)\bar{\varphi}'+\frac{1}{3}(h_1^3\rho_1+h_3^3\rho_3)\bar{w}''\right]$$

The boundary conditions are presented for various end conditions in Table 3.1.

Table 3.1: Boundary conditions for the sandwich beam.

End Configuration	Boundary Conditions
Clamped	$\bar{u}_0=0,\ \bar{\varphi}=0,\ \bar{w}=0,\ \bar{w}'=0$
Free	$2(E_1h_1+E_3h_3)\bar{u}_0'+h_2(E_3h_3-E_1h_1)\bar{\varphi}'+(E_3h_3^2-E_1h_1^2)\bar{w}''=0$
	$2(E_3h_3-E_1h_1)\bar{u}_0'+h_2(E_1h_1+E_3h_3)\bar{\varphi}'+(E_1h_1^2+E_3h_3^2)\bar{w}''=0$
	$12G_2h_2(\bar{w}'-\bar{\varphi})+6(E_1h_1^2-E_3h_3^2)\bar{u}_0''-3h_2(E_1h_1^2+E_3h_3^2)\bar{\varphi}''$ $-4(E_1h_1^3+E_3h_3^3)\bar{w}'''=0$
	$6(E_3h_3^2-E_1h_1^2)\bar{u}_0'+3h_2(E_1h_1^2+E_3h_3^2)\bar{\varphi}'+4(E_1h_1^3+E_3h_3^3)\bar{w}''=0$
Simply Supported (Sliding)	$\bar{w}=0,\ 2(E_1h_1+E_3h_3)\bar{u}_0'+h_2(E_3h_3-E_1h_1)\bar{\varphi}'+(E_3h_3^2-E_1h_1^2)\bar{w}''=0$
	$2(E_3h_3-E_1h_1)\bar{u}_0'+h_2(E_1h_1+E_3h_3)\bar{\varphi}'+(E_1h_1^2+E_3h_3^2)\bar{w}''=0$
	$6(E_3h_3^2-E_1h_1^2)\bar{u}_0'+3h_2(E_1h_1^2+E_3h_3^2)\bar{\varphi}'+4(E_1h_1^3+E_3h_3^3)\bar{w}''=0$
Simply Supported (Non-Sliding)	$\bar{u}_0=0,\bar{w}=0$
	$2(E_3h_3-E_1h_1)\bar{u}_0'+h_2(E_1h_1+E_3h_3)\bar{\varphi}'+(E_1h_1^2+E_3h_3^2)\bar{w}''=0$
	$6(E_3h_3^2-E_1h_1^2)\bar{u}_0'+3h_2(E_1h_1^2+E_3h_3^2)\bar{\varphi}'+4(E_1h_1^3+E_3h_3^3)\bar{w}''=0$

3.2 Differential Transform Method

Differential transform method (DTM) is a semi analytical-numerical technique based on Taylor series and it is promising for the solution of various types of equations. It is possible to obtain highly accurate results or exact solutions for differential equations, fractional differential equations [11, 12], integro-differential equations [7, 8] and difference equations [9, 10] with this technique.

The differential transform of the k^{th} derivative of a function f(x) with one variable, at $x=x_0$ is as follows:

$$F_k = \frac{1}{k!}\left[\frac{d^k f(x)}{dx^k}\right]_{x=x_0} \tag{3.32}$$

and the inverse transformation is defined as:

$$f(x) = \sum_{k=0}^{\infty} F_k (x - x_0)^k \tag{3.33}$$

The resulting differential equation system, which is presented in Eqs. (3.29) - (3.31) are transformed by using the basic rules of DTM that are given in Table 3.2 and arranged to give the following recurrence relations:

$$\begin{aligned} U_{k+2} &= \frac{1}{4}(k+3)(h_1 - h_3)W_{k+3} - \frac{2G_2(E_1h_1 - E_3h_3) + \omega^2 h_1 h_3 (E_1h_3\rho_3 - E_3h_1\rho_1)}{4(k+2)E_1E_3h_1h_3}W_{k+1} \\ &+ \frac{12G_2(E_1h_1 - E_3h_3) + \omega^2 h_2\left[E_3h_3(6h_1\rho_1 + h_2\rho_2) - E_1h_1(h_2\rho_2 + 6h_3\rho_3)\right]}{24(k+1)(k+2)E_1E_3h_1h_3}\Psi_k \\ &- \frac{\omega^2\left[E_3h_3(2h_1\rho_1 + h_2\rho_2) + E_1h_1(h_2\rho_2 + 2h_3\rho_3)\right]}{4(k+1)(k+2)E_1E_3h_1h_3}U_k \end{aligned} \tag{3.34}$$

$$\begin{aligned} \Psi_{k+2} &= \frac{12G_2(E_1h_1 + E_3h_3) - \omega^2 h_2(6E_3h_1h_3\rho_1 + E_1h_1h_2\rho_2 + E_3h_2h_3\rho_2 + 6E_1h_1h_3\rho_3)}{12(k+1)(k+2)E_1E_3h_1h_2h_3}\Psi_k \\ &- \frac{(k+3)(h_1 + h_3)}{2h_2}W_{k+3} - \frac{2G_2(E_1h_1 + E_3h_3) + \omega^2 h_1h_3(E_3h_1\rho_1 + E_1h_3\rho_3)}{2(k+2)E_1E_3h_1h_2h_3}W_{k+1} \\ &+ \frac{\omega^2\left[E_3h_3(2h_1\rho_1 + h_2\rho_2) - E_1h_1(h_2\rho_2 + 2h_3\rho_3)\right]}{2(k+1)(k+2)E_1E_3h_1h_2h_3}U_k \end{aligned} \tag{3.35}$$

$$W_{k+4}=\frac{1}{2(k+1)(k+2)(k+3)(k+4)(E_1h_1^3+E_3h_3^3)}\Big\{6\omega^2h_2(h_3-h_1)\rho_2(k+1)U_{k+1}$$
$$+2\Big[6G_2(h_1+2h_2+h_3)-\omega^2(h_1^3\rho_1+h_3^3\rho_3)\Big](k+1)(k+2)W_{k+2} \qquad \textbf{(3.36)}$$
$$+24\omega^2(h_1\rho_1+h_2\rho_2+h_3\rho_3)W_k+\Big[\omega^2h_2^2(h_1+h_3)\rho_2-12G_2(h_1+2h_2+h_3)\Big](k+1)\Psi_{k+1}\Big\}$$

where U_k, W_k and Ψ_k correspond to the differential transform of $\bar{u}_0$, $\bar{w}$ and $\bar{\varphi}$ respectively. The boundary conditions in Table 3.1 are transformed at x=0 and arranged to give the relations in Table 3.3.

The end conditions are transformed at x=L and presented in Table 3.4.

Table 3.2: Basic rules of DTM.

Original Function	Differential Transform
$f(x)=g(x)\pm h(x)$	$F_k=G_k\pm H_k$
$f(x)=\lambda g(x)$	$F_k=\lambda G_k$
$f(x)=g(x)h(x)$	$F_k=\sum_{l=0}^{k}G_lH_{k-l}$
$f(x)=\dfrac{d^ng(x)}{dx^n}$	$F_k=\dfrac{(k+n)!}{k!}G_{k+n}$
$f(x)=x^n$	$F_k=\delta(k-n)=\begin{cases}1 & k=n\\ 0 & k\neq n\end{cases}$

Table 3.3: Differential transform of the boundary conditions at x=0.

End Configuration	Boundary Conditions
Clamped	$U_0=0,\ \Psi_0=0,\ W_0=0,\ W_1=0$
Free	$U_1=0,\ \Psi_1=0,\ W_2=0$ $W_3=\dfrac{2h_2G_2(W_1-\Psi_0)+E_1h_1^2(2U_2-h_2\Psi_2)-E_3h_3^2(2U_2+h_2\Psi_2)}{4(E_1h_1^3+E_3h_3^3)}$
Simply S. (Sliding)	$U_1=0,\ \Psi_1=0,\ W_0=0,\ W_2=0$
Simply Supported (Non-Sliding)	$U_0=0, W_0=0, W_2=\dfrac{6E_1E_3h_1(h_1-h_3)h_3U_1}{E_1^2h_1^4+E_3^2h_3^4+2E_1E_3h_1h_3(2h_1^2-3h_1h_3+2h_3^2)}$ $\Psi_1=\dfrac{2\Big[E_1^2h_1^4-E_3^2h_3^4+4E_1E_3h_1h_3(h_3^2-h_1^2)\Big]U_1}{h2\Big[E1^2h1^4+E3^2h3^4+2E_1E_3h_1h_3(2h_1^2-3h_1h_3+2h_3^2)\Big]}$

Table 3.4: Differential transform of the boundary conditions at x=L.

End Conf.	Boundary Conditions
Clamped	$\sum_{k=0}^{N} U_k L^k = 0\,,\ \sum_{k=0}^{N} \Psi_k L^k = 0\,,\ \sum_{k=0}^{N} W_k L^k = 0\,,\ \sum_{k=0}^{N} k W_k L^{k-1} = 0$
Free	$\sum_{k=0}^{N} \begin{bmatrix} 2(E_1h_1 + E_3h_3)kU_kL + h_2(E_3h_3 - E_1h_1)k\Psi_kL \\ +(E_3h_3^2 - E_1h_1^2)k(k-1)W_k \end{bmatrix} L^{k-2} = 0$
	$\sum_{k=0}^{N} \begin{bmatrix} 2(E_3h_3 - E_1h_1)kU_kL + h_2(E_1h_1 + E_3h_3)k\Psi_kL \\ +(E_1h_1^2 + E_3h_3^2)k(k-1)W_k \end{bmatrix} L^{k-2} = 0$
	$\sum_{k=0}^{N} \begin{bmatrix} 12G_2h_2\left(L^2kW_k - L^3\Psi_k\right) + 6(E_1h_1^2 - E_3h_3^2)Lk(k-1)U_k \\ -3h_2(E_1h_1^2 + E_3h_3^2)Lk(k-1)\Psi_k - 4(E_1h_1^3 + E_3h_3^3)k(k-1)(k-2)W_k \end{bmatrix} L^{k-3} = 0$
	$\sum_{k=0}^{N} \begin{bmatrix} 6(E_3h_3^2 - E_1h_1^2)LkU_k + 3h_2(E_1h_1^2 + E_3h_3^2)Lk\Psi_k \\ +4(E_1h_1^3 + E_3h_3^3)k(k-1)W_k \end{bmatrix} L^{k-2} = 0$
Simply Supported (Sliding)	$\sum_{k=0}^{N} W_k L^k = 0\,,\ \sum_{k=0}^{N} \begin{bmatrix} 2(E_1h_1 + E_3h_3)kU_kL + h_2(E_3h_3 - E_1h_1)k\Psi_kL \\ +(E_3h_3^2 - E_1h_1^2)k(k-1)W_k \end{bmatrix} L^{k-2} = 0$
	$\sum_{k=0}^{N} \begin{bmatrix} 2(E_3h_3 - E_1h_1)kU_kL + h_2(E_1h_1 + E_3h_3)k\Psi_kL \\ +(E_1h_1^2 + E_3h_3^2)k(k-1)W_k \end{bmatrix} L^{k-2} = 0$
	$\sum_{k=0}^{N} \begin{bmatrix} 6(E_3h_3^2 - E_1h_1^2)LkU_k + 3h_2(E_1h_1^2 + E_3h_3^2)Lk\Psi_k \\ +4(E_1h_1^3 + E_3h_3^3)k(k-1)W_k \end{bmatrix} L^{k-2} = 0$
Simply Supported (Non-Sliding)	$\sum_{k=0}^{N} U_k L^k = 0\,,\ \sum_{k=0}^{N} W_k L^k = 0$
	$\sum_{k=0}^{N} \begin{bmatrix} 2(E_3h_3 - E_1h_1)kU_kL + h_2(E_1h_1 + E_3h_3)k\Psi_kL \\ +(E_1h_1^2 + E_3h_3^2)k(k-1)W_k \end{bmatrix} L^{k-2} = 0$
	$\sum_{k=0}^{N} \begin{bmatrix} 6(E_3h_3^2 - E_1h_1^2)LkU_k + 3h_2(E_1h_1^2 + E_3h_3^2)Lk\Psi_k \\ +4(E_1h_1^3 + E_3h_3^3)k(k-1)W_k \end{bmatrix} L^{k-2} = 0$

where, N is number of terms calculated. By using Eqs. (3.34) - (3.36) together with the transformed boundary conditions in Table 3.3 and Table 3.4, one arrives at the following eigenvalue problem:

$$\begin{bmatrix} M_{11}(\omega) & M_{12}(\omega) & M_{13}(\omega) & M_{14}(\omega) \\ M_{21}(\omega) & M_{22}(\omega) & M_{23}(\omega) & M_{24}(\omega) \\ M_{31}(\omega) & M_{32}(\omega) & M_{33}(\omega) & M_{34}(\omega) \\ M_{41}(\omega) & M_{42}(\omega) & M_{43}(\omega) & M_{44}(\omega) \end{bmatrix} . \lfloor D \rfloor = 0 \qquad \textbf{(3.37)}$$

where, $\lfloor D \rfloor$ correspond to the missing boundary conditions at x=0. For the non-trivial solutions of Eq. (3.37), it is necessary that the determinant of the coefficient matrix is equal to zero:

$$\begin{vmatrix} M_{11}(\omega) & M_{12}(\omega) & M_{13}(\omega) & M_{14}(\omega) \\ M_{21}(\omega) & M_{22}(\omega) & M_{23}(\omega) & M_{24}(\omega) \\ M_{31}(\omega) & M_{32}(\omega) & M_{33}(\omega) & M_{34}(\omega) \\ M_{41}(\omega) & M_{42}(\omega) & M_{43}(\omega) & M_{44}(\omega) \end{vmatrix} = 0 \qquad \textbf{(3.38)}$$

Solution of Eq. (3.38) is simply a polynomial root-finding problem. Many techniques such as Newton's method, Laguerre's method etc. can be used to find the roots of this frequency equation.

In this study, the built in function "NSolve" in MATHEMATICA that works with Jenkins-Traub algorithm is utilized. This is a fast and reliable algorithm for finding the real and imaginary roots of a polynomial, which is also globally convergent.

3.3 Finite Element Method

In order to validate the results of DTM for the composite beams, a two-node sandwich beam finite element with four degrees of freedom per node is utilized. Element matrices are evaluated with the face layers modeled with Euler beam theory and the core layer modeled with Timoshenko beam theory. The kinematic relations used for the analytical model, given in Eqs. (3.1) - (3.4), are used for the FE model.

For the transverse displacement, C^1 continuous polynomial shape functions are used:

$$w = N_1 w^1 + N_2 \vartheta^1 + N_3 w^2 + N_4 \vartheta^2 \qquad \textbf{(3.39)}$$

with

$$N_1 = 1 - \frac{3x^2}{l_e^2} + \frac{2x^3}{l_e^3}, N_2 = x - \frac{2x^2}{l_e} + \frac{x^3}{l_e^2}, N_3 = \frac{3x^2}{l_e^2} - \frac{2x^3}{l_e^3}, N_4 = -\frac{x^2}{l_e} + \frac{x^3}{l_e^2} \qquad \textbf{(3.40)}$$

where, w^i is the displacement and $\vartheta^i=(\partial w/\partial x)^i$ is the rotation at i'th node and l_e is the length of the beam element. For the axial displacement and the rotation, C^0 continuous shape functions are used to interpolate the displacement field:

$$u_0 = N_5 u_0^1 + N_6 u_0^2 \,,\ \varphi = N_5 \varphi^1 + N_6 \varphi^2 \tag{3.41}$$

with

$$N_5 = \frac{l_e - x}{l_e},\ N_6 = \frac{x}{l_e} \tag{3.42}$$

The sandwich beam finite element is presented in Figure 3.3.

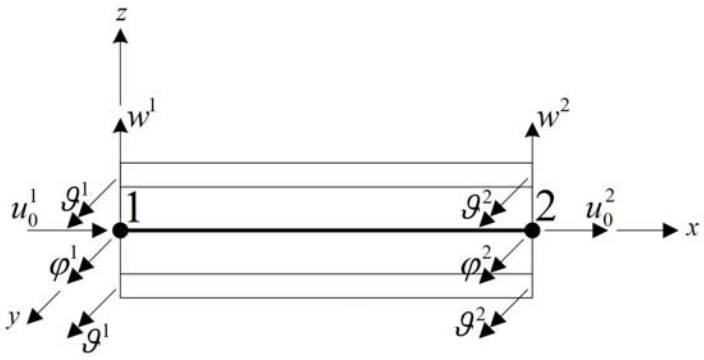

Figure 3.3: The nodal degrees of freedom of the 2-node sandwich beam finite element.

The displacement field in each layer depends on the degrees of freedom of the sandwich beam:

$$\begin{Bmatrix} u^{(i)} \\ w^{(i)} \end{Bmatrix} = \mathbf{T}_i \begin{Bmatrix} u_0 \\ \varphi \\ w \end{Bmatrix} \tag{3.43}$$

where $\mathbf{T}_i$ is the transverse thickness interpolation matrix that can be obtained for each layer by using the kinematic relations given in Eqs. (3.1) - (3.4), as follows:

$$\mathbf{T}_1 = \begin{bmatrix} 1 & -\frac{h_2}{2} & -\left(z^{(1)} + \frac{h_1}{2} \right) \frac{\partial}{\partial x} \\ 0 & 0 & 1 \end{bmatrix} \tag{3.44}$$

$$\mathbf{T}_2 = \begin{bmatrix} 1 & -z^{(2)} & 0 \\ 0 & 0 & 1 \end{bmatrix} \tag{3.45}$$

$$\mathbf{T}_3 = \begin{bmatrix} 1 & \frac{h_2}{2} & -\left(z^{(3)} - \frac{h_3}{2}\right)\frac{\partial}{\partial x} \\ 0 & 0 & 1 \end{bmatrix} \tag{3.46}$$

The vector of displacements $\{u_0, \varphi, w\}^T$, can be expressed in terms of nodal degrees of freedom $\mathbf{U} = \{u_0^1, \varphi^1, w^1, \vartheta^1, u_0^2, \varphi^2, w^2, \vartheta^2\}^T$ by using Eqs. (3.39) and (3.41) as follows:

$$\begin{Bmatrix} u_0 \\ \varphi \\ w \end{Bmatrix} = \mathbf{NU} \tag{3.47}$$

where **N** is the matrix of interpolation functions:

$$\mathbf{N} = \begin{bmatrix} N_5 & 0 & 0 & 0 & N_6 & 0 & 0 & 0 \\ 0 & N_5 & 0 & 0 & 0 & N_6 & 0 & 0 \\ 0 & 0 & N_1 & N_2 & 0 & 0 & N_3 & N_4 \end{bmatrix} \tag{3.48}$$

Combining Eqs. (3.43) and (3.47), the displacement field can be expressed in terms of the nodal degrees of freedom as follows:

$$\begin{Bmatrix} u^{(i)} \\ w^{(i)} \end{Bmatrix} = \mathbf{T}_i\mathbf{NU} \tag{3.49}$$

Mass and stiffness matrices for each layer are obtained from the following relations:

$$\mathbf{M}^{(i)} = \rho_i \int_0^{l_e} \int_{-h_i/2}^{h_i/2} (\mathbf{T}_i\mathbf{N})^T (\mathbf{T}_i\mathbf{N})\, dz^{(i)} dx \tag{3.50}$$

$$\mathbf{K}^{(i)} = \int_0^{l_e} \int_{-h_i/2}^{h_i/2} \mathbf{B}^{(i)T}\mathbf{E}^{(i)}\mathbf{B}^{(i)}\, dz^{(i)} dx \tag{3.51}$$

where, **E** is the elastic coefficient matrix given as follows:

$$\mathbf{E}^{(i)} = \begin{bmatrix} E_i & 0 \\ 0 & G_i \end{bmatrix} \tag{3.52}$$

Also, $\mathbf{B}^{(i)}$ is the deformation matrix of i'th layer obtained from the following relation:

$$\mathbf{B}^{(i)} = \mathbf{D}\mathbf{T}_i\mathbf{N} \tag{3.53}$$

with:

$$\mathbf{D} = \begin{bmatrix} \partial/\partial x & 0 \\ \partial/\partial z & \partial/\partial x \end{bmatrix} \tag{3.54}$$

The mass and stiffness matrices of layers 1-3 are derived and assembled to obtain the sandwich beam finite element matrices of 8x8 dimension:

$$\mathbf{M} = \sum_{i=1}^{3} \mathbf{M}^{(i)}, \ \mathbf{K} = \sum_{i=1}^{3} \mathbf{K}^{(i)} \tag{3.55}$$

These matrices are quite large so they are not presented here.

3.4 Results and Discussion

3.4.1 Validation

In order to validate both the beam model and the solution technique, firstly a symmetrical sectioned sandwich beam with clamped-free boundary conditions is considered. The material and geometric properties are given in Table 3.5.

Table 3.5: Material properties and dimensions (Example 1)

Elastic layers (Layers 1 and 3)	
Young's modulus	$E_1 = E_3 = 69$ GPa
Density	$\rho_1 = \rho_3 = 2800$ kg/m^3
Thickness	$h_1 = h_3 = 1.52$ mm
Viscoelastic layer (Layer 2)	
Shear modulus	$G_2 = 0.69$ MPa
Density	$\rho_2 = 968.3$ kg/m^3
Thickness	$h_2 = 0.127$ mm
Loss Factor	$\eta = 0.1, 0.2, 0.3, 0.6, 1.0, 1.5$
Whole beam	
Length	L=177.8 mm

This problem has attracted the attention of several researchers [18, 30, 53-55] and it has been used as a benchmark problem to test new beam theories and solution techniques. The vibration frequencies and loss factors defined in Eqs. (3.56) and (3.57) are obtained with DTM and presented in Table 3.6 and Table 3.7.

$$LossFactor = \frac{\mathrm{Im}(\omega_n^2)}{\mathrm{Re}(\omega_n^2)} \tag{3.56}$$

$$Frequency = \sqrt{\mathrm{Re}(\omega_n^2)} \tag{3.57}$$

where, ω_n is the n'th complex natural frequency.

Table 3.6: Natural frequencies (Hz).

η		Mode 1	Mode 2	Mode 3	Mode 4	Mode 5	Mode 6
0.1	DTM	63.608	294.215	738.006	1382.899	2242.596	3315.220
	Ref. [18]	64.075	296.41	743.7	1393.9	2261.09	-
	Ref. [30]	63.607	294.22	738.08	1383.27	2243.68	3317.77
	Ref. [53]	63.61	294.20	738.02	1383.06	2243.21	-
	Ref. [54]	60.9	288.8	732.9	1381.4	2246.6	3327.3
	Ref. [55]	64.2	297.0	747.2	1408.3	2304.0	3446.1
0.2	DTM	63.741	294.440	738.160	1382.983	2242.653	3315.257
	Ref. [18]	64.21	296.64	743.85	1394.0	2261.15	
	Ref. [30]	63.740	294.447	738.236	1383.36	2243.74	3317.81
	Ref. [53]	63.74	294.43	738.18	1383.14	2243.27	-
	Ref. [54]	61.2	289.0	733.4	1381.7	2246.9	3327.5
	Ref. [55]	64.4	297.6	748.0	1409.0	2304.0	3446.4
0.3	DTM	63.958	294.809	738.415	1383.122	2242.746	3315.318
	Ref. [18]	64.43	297.01	744.1	1394.0	2261.24	-
	Ref. [30]	63.957	294.816	738.492	1383.496	2243.832	3317.87
	Ref. [53]	63.957	294.796	738.432	1383.283	2243.357	-
	Ref. [54]	61.5	289.8	734.0	1382.3	2247.2	3327.8
	Ref. [55]	64.7	298.0	748.2	1409.5	2305.0	3447.0
0.6	DTM	65.006	296.689	739.779	1383.860	2243.242	3315.644
	Ref. [18]	65.48	298.9	745.48	1394.9	2261.7	-
	Ref. [30]	65.005	296.696	739.854	1384.234	2244.326	3318.19
	Ref. [53]	65.005	296.675	739.793	1384.016	2243.847	-
	Ref. [54]	62.7	292.4	737.4	1385.2	2249.7	3329.6
	Ref. [55]	65.5	301.0	753.0	1414.0	2310.0	3450.0
1.0	DTM	66.914	300.550	742.911	1385.539	2244.389	3316.386
	Ref. [18]	67.41	302.8	748.6	1396.6	2262.88	-
	Ref. [30]	66.913	300.556	742.983	1385.912	2245.468	3318.94
	Ref. [53]	66.913	300.533	742.92	1385.684	2244.98	-
	Ref. [54]	64.3	296.7	744.3	1391.0	2254.8	3334.8
	Ref. [55]	67.4	307.0	762.0	1422.0	2316.0	3455.0
1.5	DTM	69.367	306.575	748.724	1388.643	2246.550	3317.766
	Ref. [18]	69.88	308.85	754.0	1397.7	2265.0	-
	Ref. [30]	69.366	306.582	748.792	1389.017	2247.623	3320.32
	Ref. [53]	69.366	306.555	748.725	1388.773	2247.120	-
	Ref. [54]	64.4	303.5	755.3	1400.6	2263.8	3341.2
	Ref. [55]	70.0	315.0	774.0	1433.0	2328.0	3448.5

Table 3.7: Loss factors (%).

		Mode 1	Mode 2	Mode 3	Mode 4	Mode 5	Mode 6
0.1	DTM	2.8132	2.426	1.544	0.891	0.574	0.392
	Ref. [18]	2.815	2.424	1.54	0.889	0.573	-
	Ref. [30]	2.8132	2.427	1.544	0.891	0.574	0.391
	Ref. [53]	2.81	2.43	1.54	0.89	0.574	-
	Ref. [54]	2.646	2.713	1.328	0.742	0.463	0.305
	Ref. [55]	2.817	2.425	1.534	0.878	0.559	0.377
0.2	DTM	5.556	4.834	3.086	1.782	1.149	0.783
	Ref. [18]	5.56	4.83	3.08	1.776	1.144	-
	Ref. [30]	5.556	4.834	3.086	1.782	1.148	0.783
	Ref. [53]	5.56	4.83	3.09	1.78	1.14	-
	Ref. [54]	5.292	4.346	2.656	1.484	0.926	0.610
	Ref. [55]	5.564	4.832	3.066	1.756	1.118	0.744
0.3	DTM	8.165	7.205	4.623	2.672	1.722	1.174
	Ref. [18]	8.169	7.197	4.614	2.664	1.716	-
	Ref. [30]	8.165	7.205	4.6228	2.672	1.722	1.174
	Ref. [53]	8.165	7.204	4.622	2.670	1.720	-
	Ref. [54]	7.938	6.519	3.984	2.226	1.389	0.915
	Ref. [55]	8.175	7.203	4.593	2.634	1.68	1.116
0.6	DTM	14.750	13.950	9.181	5.330	3.441	2.347
	Ref. [18]	14.76	13.938	9.168	5.316	3.432	-
	Ref. [30]	14.750	13.952	9.180	5.329	3.439	2.346
	Ref. [53]	14.750	13.949	9.178	5.326	3.437	-
	Ref. [54]	15.876	13.038	7.968	4.452	2.778	1.830
	Ref. [55]	14.772	13.956	9.126	5.256	3.36	2.262
1.0	DTM	20.202	21.786	15.056	8.833	5.719	3.909
	Ref. [18]	20.22	21.77	15.02	8.81	5.7	-
	Ref. [30]	20.202	21.790	15.055	8.833	5.717	3.905
	Ref. [53]	20.202	21.72	15.023	8.828	5.714	-
	Ref. [54]	26.46	21.72	13.28	7.42	4.63	3.05
	Ref. [55]	20.19	21.8	15	8.73	5.6	3.77
1.5	DTM	22.938	29.650	21.935	13.128	8.541	5.845
	Ref. [18]	22.956	29.625	21.9	13.095	8.52	-
	Ref. [30]	22.938	29.655	21.934	13.128	8.538	5.844
	Ref. [53]	22.938	29.651	21.931	13.122	8.534	-
	Ref. [54]	26.46	32.58	19.92	11.13	6.945	4.575
	Ref. [55]	22.83	29.28	21.855	13.02	8.385	5.67

As one can see, the results are in good agreement with the already existing ones. An important point is that, the beam model used in this study predicts higher frequencies for the lower modes and lower frequencies for the higher modes when compared with the results of Ref. [30] . This is due to the longitudinal and rotary inertial effects, which are neglected in Ref. [30].

The real and imaginary parts of normalized mode shapes for the transverse displacement are presented in Figure 3.4 for the first three modes.

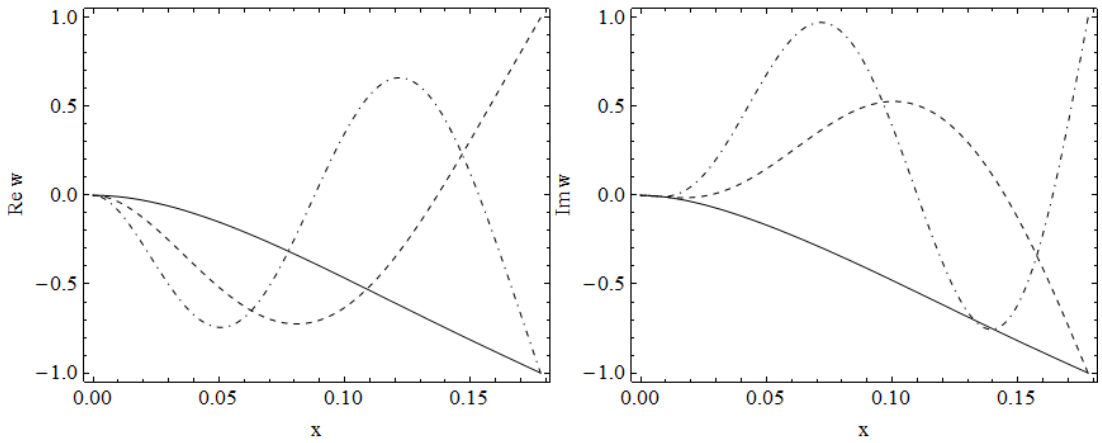

Figure 3.4: Real and imaginary parts of the first three mod shapes (- 1st mode, -- 2nd mode, -.- 3rd mode).

The convergence of the loss factor for the first four modes with increasing number of terms considered is presented in Figure 3.5. The figure presents a rapid convergence for the loss factors. Another important point is that, it is necessary to consider more number of terms in the DTM calculations in order to evaluate higher modes.

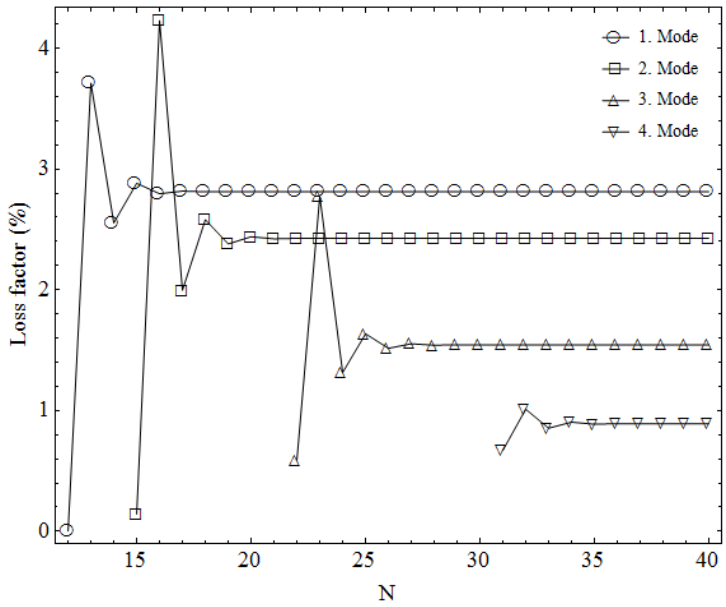

Figure 3.5: Convergence of the modal loss factor with N.

The next example is a sandwich beam with a non-symmetrical section, simply supported at both ends with the properties given in Table 3.8. Calculations are carried out for three different cases and the results are presented in Table 3.9 and Table 3.10 for the first four natural frequencies and modal loss factors.

The real and the imaginary parts of the first three mode shapes are presented in Figure 3.6.

Table 3.8: Material properties and dimensions (Example 2).

	Problem 1	Problem 2	Problem 3
	Elastic layers (Layers 1 and 3)		
Young's modulus	E_1= E_3=207 GPa	E_1= E_3=207 GPa	E_1= E_3=207 GPa
Density	ρ_1= ρ_3=7800 kg/m^3	ρ_1= ρ_3=7800 kg/m^3	ρ_1= ρ_3=7800 kg/m^3
Thicknesses	h_1=0.5 mm	h_1=0.5 mm	h_1=0.5 mm
	h_3=5 mm	h_3=5 mm	h_3=5 mm
	Viscoelastic layer (Layer 2)		
Shear modulus	G_2=0.2615 MPa	G_2=4 MPa	G_2=20 MPa
Density	ρ_2=2000 kg/m^3	ρ_2=2000 kg/m^3	ρ_2=2000 kg/m^3
Thickness	h_2=2.5 mm	h_2=2.5 mm	h_2=2.5 mm
Loss factor	η=0.38	η=0.38	η=0.38
	Whole Beam		
Length	L=300 mm	L=242.5 mm	L=1084.498 mm

Table 3.9: Natural frequencies (rad/s).

Problem		Mode 1	Mode 2	Mode 3	Mode 4
1	DTM	740.487	2947.775	6623.476	11763.052
	Ref. [19]	740.564	2949.00	6629.68	11782.60
	Ref. [23]	740.56	2948.29	6629.66	11782.60
	Ref. [30]	740.564	2949.00	6629.68	11782.61
	Ref. [52]	741	2952	6647	-
	Ref. [56]	741	2949	6630	11783
	Ref. [57]	740.6	2949.0	6629.7	11783.0
2	DTM	1187.768	4570.159	10192.612	18047.974
	Ref. [19]	1187.96	4573.08	10207.22	18093.90
	Ref. [23]	1187.93	4573.05	10207.19	18093.87
	Ref. [30]	1187.98	4573.14	10207.35	18094.13
3	DTM	81.728	309.331	652.785	1096.834
	Ref. [19]	81.730	309.35	652.85	1097.01
	Ref. [23]	81.73	309.35	652.85	1097.01
	Ref. [30]	81.742	309.39	652.92	1097.10

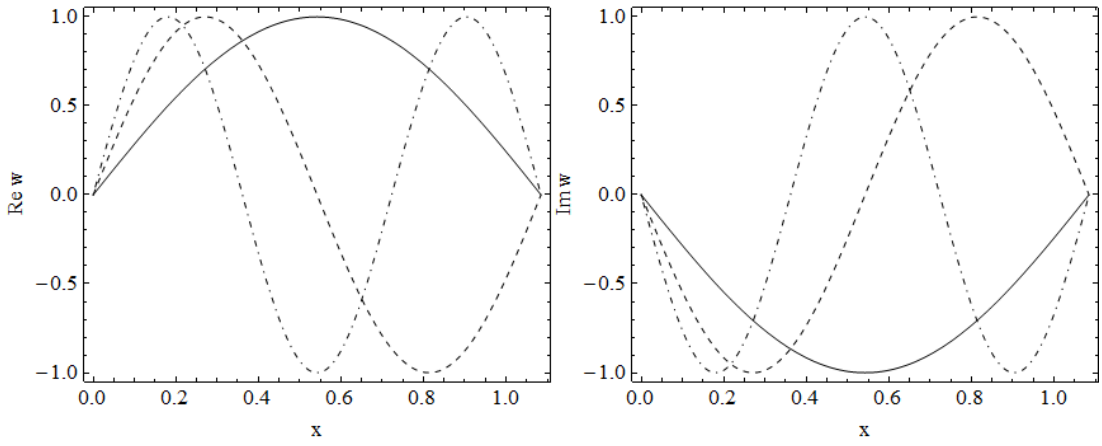

Figure 3.6: Real and imaginary parts of the first three mod shapes (- 1st mode, -- 2nd mode, -.- 3rd mode).

Table 3.10: Loss factors (%).

Problem		Mode 1	Mode 2	Mode 3	Mode 4
1	DTM	0.44818	0.11477	0.051232	0.028859
	Ref. [19]	0.44819	0.11478	0.051243	0.028870
	Ref. [23]	0.44790	0.11470	0.051209	0.028850
	Ref. [30]	0.44825	0.11484	0.051306	0.028932
	Ref. [52]	0.45	0.11	0.051	-
	Ref. [56]	0.45	0.11	0.051	0.029
	Ref. [57]	0.450	0.110	0.0513	0.0289
2	DTM	3.4257	1.0679	0.49577	0.28317
	Ref. [19]	3.4261	1.0682	0.49597	0.28336
	Ref. [23]	3.4250	1.0677	0.49577	0.28324
	Ref. [30]	3.4271	1.0691	0.49693	0.28431
3	DTM	1.5837	4.5748	6.5899	7.1579
	Ref. [19]	1.5838	4.5758	6.5921	7.1608
	Ref. [23]	1.5839	4.5758	6.5921	7.6079
	Ref. [30]	1.5966	4.5877	6.6024	7.1694

Again, the results show good agreement, validating both the solution technique and the beam model.

The first two examples previously considered are hypothetical test problems, where the viscoelastic material properties are assumed as frequency independent. The third example is a free-free sandwich beam with randomly oriented glass-fiber reinforced plastic (GFRP) face layers and a viscoelastic core that consist of vibrachoc VIB12 damping material. The results of an experimental test exist for the first three frequencies and loss factors of the problem considered [54]. In addition, the damping contribution of GFRP face layers have not been omitted, instead, have been attributed a constant value in this study. The material properties and dimensions for the problem are presented in Table 3.11.

Table 3.11: Material properties and dimensions (Example 3).

GFRP composite layers (Layers 1 and 3)	
Young's modulus	$E_1= E_3=24$ GPa
Density	$\rho_1= \rho_3=1890$ kg/m^3
Thickness	$h_1= h_3=10.2$ mm
Loss Factor	$\eta_1= \eta_3=0.005$ (0-2000Hz band)
VIB12 viscoelastic layer (Layer 2)	
Shear modulus	$G_2= G_2(\omega)$ (Figure 3.7)
Density	$\rho_2=1100$ kg/m^3
Thickness	$h_2=1$ mm
Loss Factor	$\eta_2= \eta_2(\omega)$ (Figure 3.7)
Whole beam	
Length	L=0.6 m

The experimental data for the frequency dependent shear modulus and loss factor of VIB12 damping material have been extracted from a figure in Ref. [54]. Interpolation functions that go through the experimental data are evaluated for the dynamic shear modulus and loss factor as presented in Figure 3.7. In the solutions carried out, an initial guess for the desired mode is made and then the problem is solved for the corresponding material properties of the viscoelastic core. Then, the numerical result obtained for the natural frequency of the sandwich beam is used as the next guess. The iteration is repeated until the vibration frequency converges to a value:

$$\frac{\left\| f_n^{i+1} - f_n^i \right\|}{f_n^i} \leq \xi \tag{3.58}$$

where, ξ is the error tolerance and f_n^i is the n'th natural frequency at i'th iteration. The results of this iterative process, for the first natural frequency with the initial guess f_1^1=15 Hz, are presented in Figure 3.7. Figure shows that the iteration converges rapidly and the frequencies f_1^3 and f_1^4 overlap.

The numerical results for the third example are presented in **Table 3.12**.

Table 3.12: Natural frequencies and the loss factors.

	Mode 1		Mode 2		Mode 3	
	f (Hz)	η (%)	f (Hz)	η (%)	f (Hz)	η (%)
DTM	206.16	7.33	518.99	15.71	936.96	20.95
Ref. [27]	205	7.4	516	15.7	938	20.8
Ref. [53]	209.51	6.19	516.73	15.76	897.05	21.49
Ref. [54]	193	8.8	493	17.5	900	22.3
Ref. [54] (Exp.)	202	8.9	512	18	941	24.7

The calculated frequencies show good agreement with the already existing ones. However, the loss factors show some discrepancy with the experimental results, most probably due to the incorrect evaluation of the material properties of the viscoelastic core as indicated by Shi et al. [53].

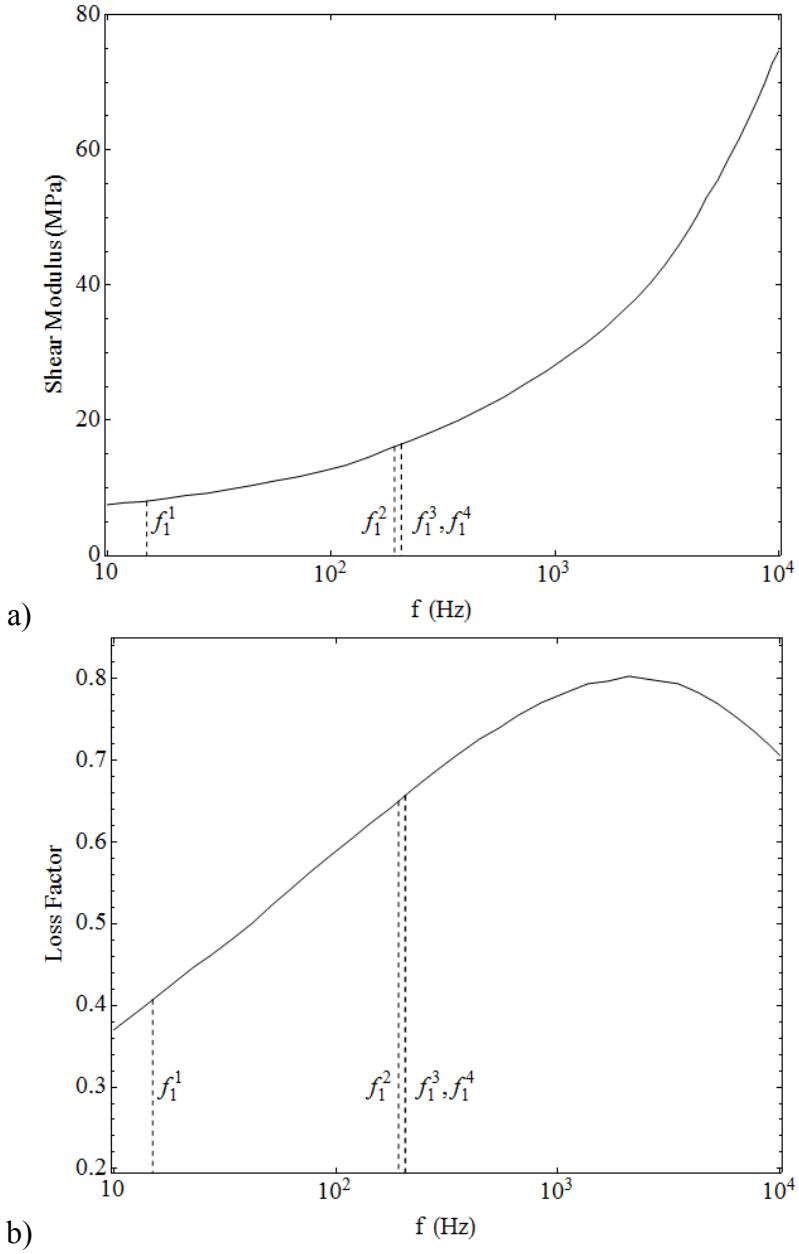

Figure 3.7: Graphical presentation of the iterative process: a) shear modulus; b) loss factor.

3.4.2 Parametric Analysis for the Composite Beams

In this section, the effects of system parameters on the vibration and damping characteristics of clamped-free composite beams, with the properties given in Table 3.13, are investigated. The material for the composite face layers is selected as carbon fiber reinforced plastic (CFRP) and the core material is chosen as 3M ISD-110 damping polymer. The five-parameter fractional derivative viscoelastic model, which is presented in Section 2.2.2 in detail, is used to describe the dynamical properties of the viscoelastic material.

Table 3.13: Properties and dimensions of the composite beam.

CFRP composite layers (Layers 1 and 3)	
Young's modulus	E_{11}=138.6 GPa, E_{22}=8.27 GPa
Shear modulus	G_{12}=4.12 GPa
Density	ρ_1= ρ_3=1824 kg/m^3
Poisson's ratio	ν_{12}=0.26
Thickness	h_1+ h_3=6 mm
Loss factor	η_1= η_3=0.003
3M ISD-110 viscoelastic layer (Layer 2)	
Shear modulus	G_2= $G_2(\omega)$ (Table 2.1)
Density	ρ_2=1600 kg/m^3
Thickness	h_2=0.127 mm
Loss factor	η_2= $\eta_2(\omega)$ (Table 2.1)
Poisson's ratio	ν_2=0.5
Whole beam	
Length	Variable

The loss factors of CFRP's vary in the range $0.001<\eta<0.005$ [58]. Though they are quite small when compared with the loss factor of the viscoelastic material, it may not be safe to omit them since the contribution to the total loss factor is also proportional with the stored strain energy [32]. Therefore, an approximate average value η=0.003 is attributed to the CFRP material, in order to include the damping contribution of the face layers.

The FE model used to make comparison with the results of DTM consists of 20 elements with the same length.

Figure 3.8 shows the effect of angle of lamination over the modal loss factor and natural frequency for the first four modes. The viscoelastic damping is maximized for the fundamental mode for θ=0°. The maximum values for the other modal loss factors are reached at higher values of θ for higher modes. The frequency is maximum for θ=0° for all modes since the stiffness of the face layers are maximum at this value. The figure is presented in the range $0°<\theta<90°$ since the results are symmetrical beyond the point θ=90°.

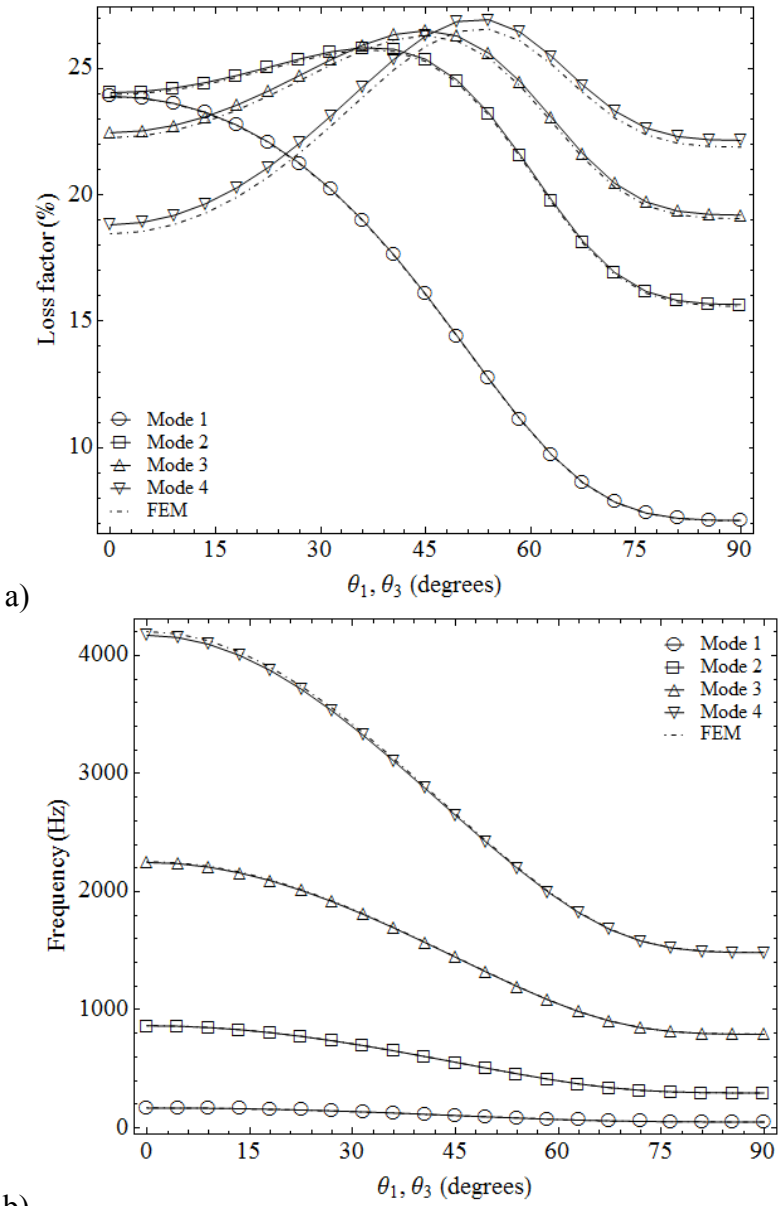

Figure 3.8: Variation with angle of lamination (L=0.2 m, h_1= h_3=3 mm): a) loss factor; b) frequency.

The effect of beam length for a symmetrically sectioned beam is presented in Figure 3.9. The general trend for the loss factors is that, there is an increase up to a maximum value with increasing L and then, there is a continuous decrease. In other words, there is a maximum for the magnitude of damping for a specific beam length. On the other hand, the vibration frequency continuously decreases with increasing beam length, as expected.

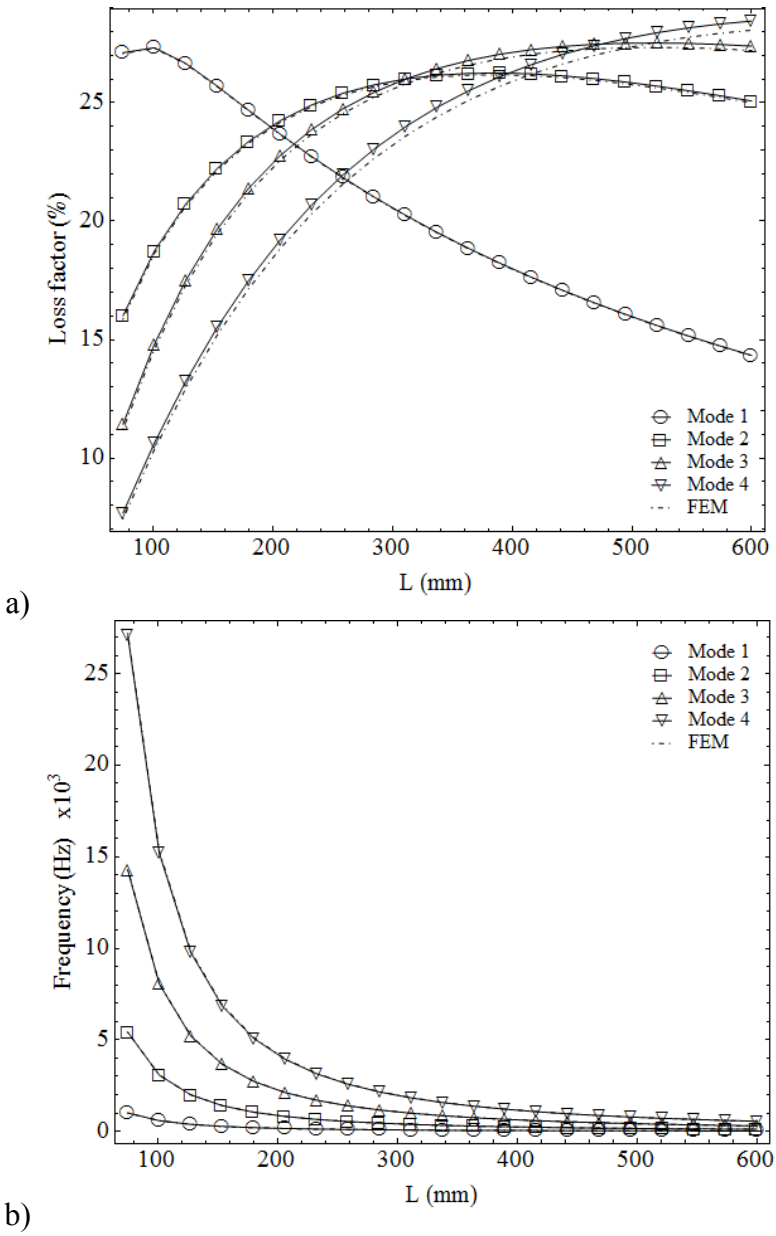

Figure 3.9: Variation with beam length ($\theta_1=\theta_3=0°$, $h_1=h_3=3$ mm): a) loss factor; b) frequency.

The effect of the location of the viscoelastic core inside the beam is shown in Figure 3.10. For all modal loss factors, the maximum values correspond to symmetrical configurations, where $h_1=h_3$. This is quite natural since the core experiences the greatest magnitudes of shear stress for symmetrical configurations. On the frequency side, this effect is vice versa; the minimum value of the natural frequency corresponds to the symmetrical case. Since the core material is quite soft when compared to the stiff face layers, it undergoes a large amount of shear deformation. This in turn reduces the compression and extension that the base and constraining layers experience during the bending of the beam.

Therefore, the natural frequencies are higher for the case the core layer is closer to beam surface than the case it is in the middle of the sandwich beam.

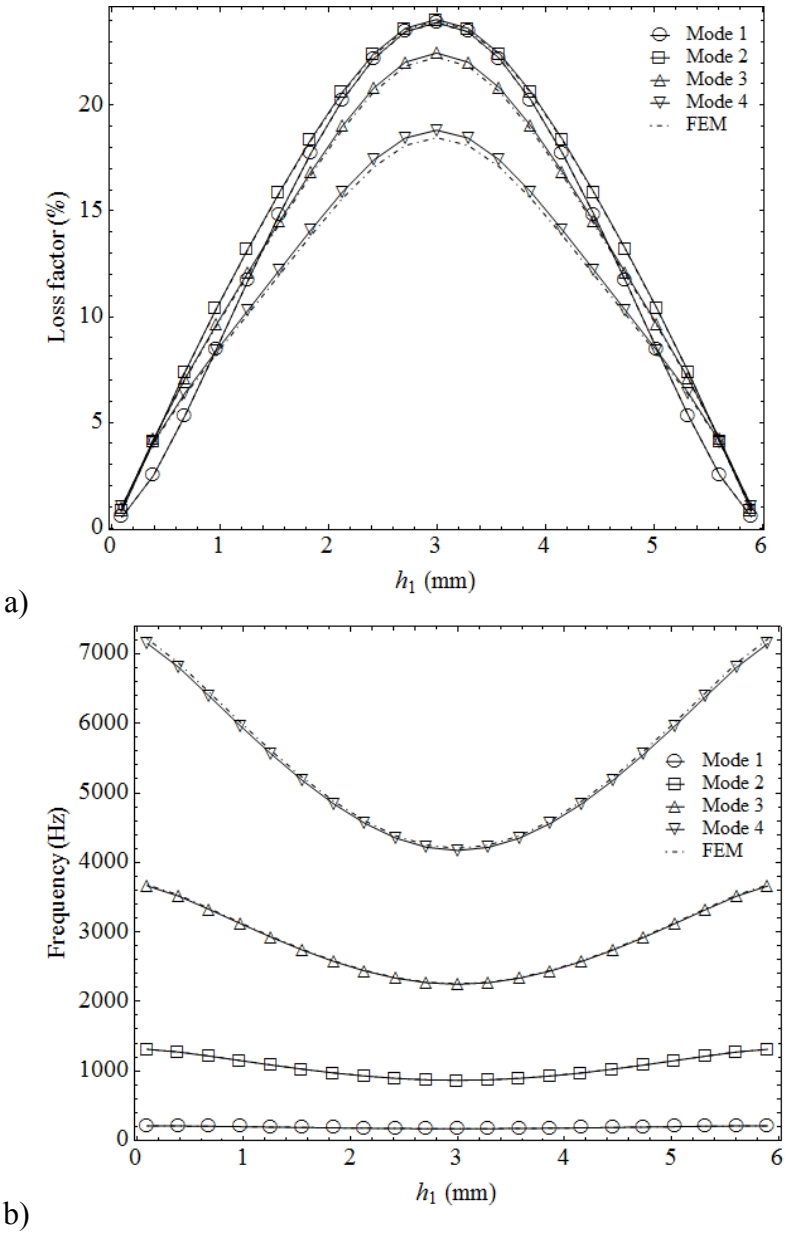

Figure 3.10: Variation with the location of viscoelastic core (L=0.2 m and $\theta_1=\theta_3=0°$): a) loss factor; b) frequency.

Lastly, Figure 3.11 shows the effect of core thickness on the loss factor and resonant frequencies of the system. As mentioned before, the system loss factor depends on both the material loss factor and stored strain energy. As the thickness of the viscoelastic core increases, the average material loss factor of the beam increases, however, the strain energy stored by the core due to the shear stress decreases. Therefore, the loss factors of the beam do not linearly increase with the core thickness. Instead, an increase to a maximum and then a decrease is observed.

On the other hand, the frequencies decrease with increasing core thickness. This is mainly because the shear deformation of the core layer increases with its thickness. The stiff face layers start acting independently during the bending motion and they cannot extend and compress effectively, for thicker cores. Therefore, the stiffness of the sandwich beam decreases, resulting in a decrease of the natural frequencies, as observed from the figure.

The deformed sections for the first mode are presented in Figure 3.12 for different values of the core thickness, to visualize the phenomena mentioned above.

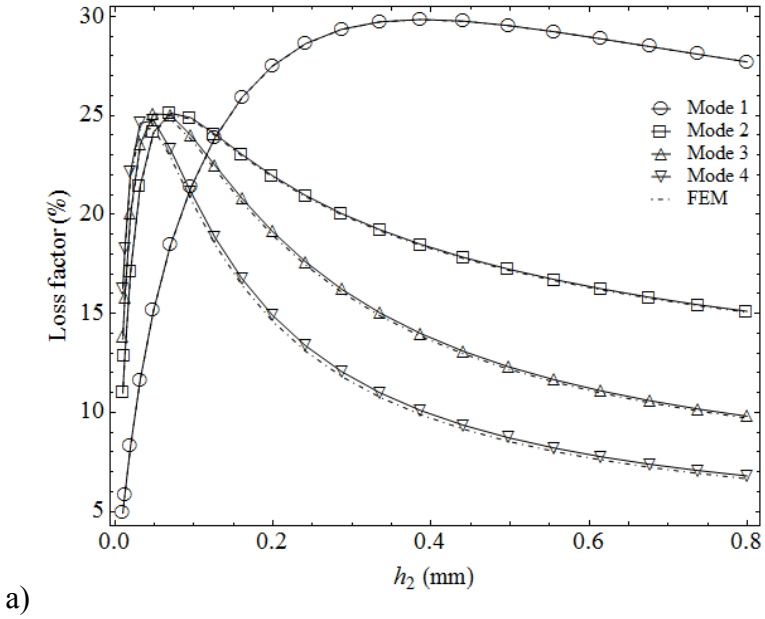

a)

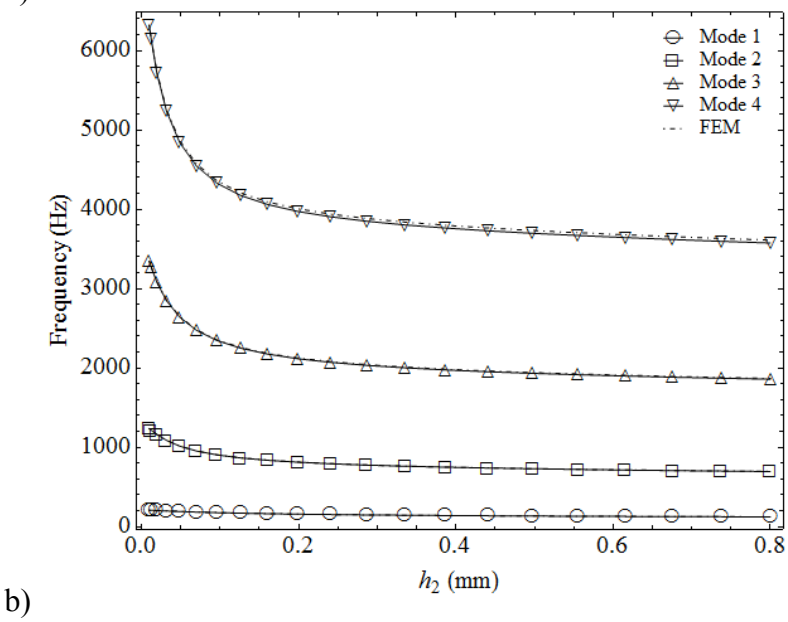

b)

Figure 3.11: Variation with the core thickness (L=0.2 m, h_1= h_3=3 mm): a) loss factor; b) frequency.

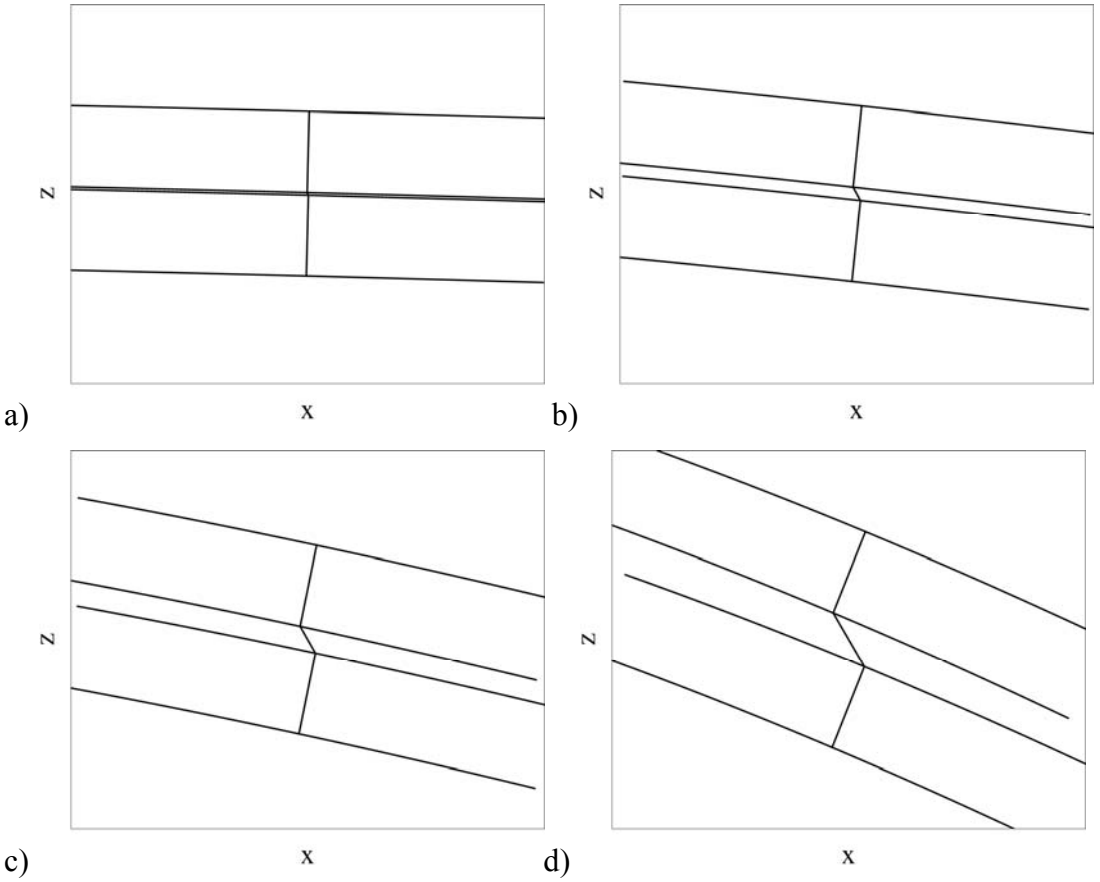

Figure 3.12: Deformed sections for the sandwich beams with a soft-core layer: a) h_2=0.1 mm; b) h_2=0.5 mm; c) h_2=1 mm; d) h_2=2 mm.

All figures show excellent agreement between the results of FEM and DTM especially for the first modes. The results for the frequency and loss factor of a clamped-free sandwich beam with CFRP face layers and 3M ISD-112 core modeled with a four parameter fractional derivative viscoelastic model exist in Ref. [59]. The results obtained in this section are consistent with the findings of [59].

4. VIBRATION ANALYSIS OF SANDWICH PLATES

4.1 Equation of Motion

The assumptions used to derive the kinematic relations and the governing equations are as follows [60]:

- The viscoelastic core is represented by the complex modulus approach.
- Deformation through thickness is negligible.
- Transverse displacement does not change between the layers.
- The plate deflection is small.
- There is no slip between the layers.

The geometry of the sandwich plate and the displacement of its layers are presented in Figure 4.1 and Figure 4.2 respectively.

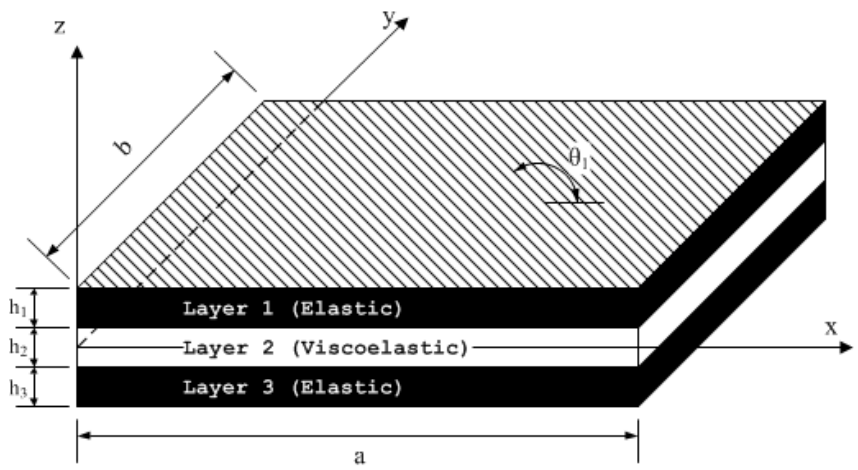

Figure 4.1: Geometry and configuration of the sandwich plate.

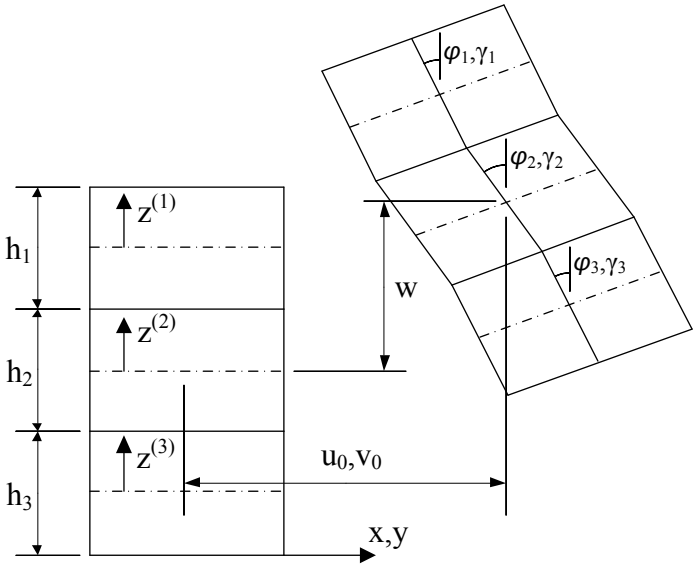

Figure 4.2: Coordinate system and displacement of layers.

The kinematic relations are derived from the geometry in Figure 4.2 based on the first-order shear deformation theory (FSDT) as follows:

$$u^{(1)} = u_0 - \frac{h_2}{2}\varphi_2 - \left(z^{(1)} + \frac{h_1}{2}\right)\varphi_1 \tag{4.1}$$

$$v^{(1)} = v_0 - \frac{h_2}{2}\gamma_2 - \left(z^{(1)} + \frac{h_1}{2}\right)\gamma_1 \tag{4.2}$$

$$u^{(2)} = u_0 - z^{(2)}\varphi_2 \tag{4.3}$$

$$v^{(2)} = v_0 - z^{(2)}\gamma_2 \tag{4.4}$$

$$u^{(3)} = u_0 + \frac{h_2}{2}\varphi_2 + \left(\frac{h_3}{2} - z^{(3)}\right)\varphi_3 \tag{4.5}$$

$$v^{(3)} = v_0 + \frac{h_2}{2}\gamma_2 + \left(\frac{h_3}{2} - z^{(3)}\right)\gamma_3 \tag{4.6}$$

$$w^{(i)} = w,\ i = 1,2,3 \tag{4.7}$$

where, φ_i and γ_i are the rotations of normals to mid-plane, $u^{(i)}$ and $v^{(i)}$ are the axial displacements and $w^{(i)}$ is the transverse displacement of the i'th layer. Also, u_0 and v_0 are the longitudinal displacements of the centroid of viscoelastic core. One can find similar plate models and kinematic relations that exist in literature [24, 26, 31, 61].

The strain-displacement relation for the linear vibrations of the sandwich plate is given by:

$$\begin{Bmatrix} \varepsilon_{xx}^{(i)} \\ \varepsilon_{yy}^{(i)} \\ 2\varepsilon_{xy}^{(i)} \\ 2\varepsilon_{yz}^{(i)} \\ 2\varepsilon_{xz}^{(i)} \end{Bmatrix} = \begin{bmatrix} \partial/\partial x & 0 & 0 \\ 0 & \partial/\partial y & 0 \\ \partial/\partial y & \partial/\partial x & 0 \\ 0 & \partial/\partial z & \partial/\partial y \\ \partial/\partial z & 0 & \partial/\partial x \end{bmatrix} \begin{Bmatrix} u^{(i)} \\ v^{(i)} \\ w^{(i)} \end{Bmatrix}, \; i = 1,2,3 \tag{4.8}$$

The stress-strain relation for the composite-orthotropic base and constraining layers can be expressed as follows:

$$\begin{Bmatrix} \sigma_{xx}^{(i)} \\ \sigma_{yy}^{(i)} \\ \sigma_{xy}^{(i)} \\ \sigma_{yz}^{(i)} \\ \sigma_{xz}^{(i)} \end{Bmatrix} = \begin{bmatrix} \bar{Q}_{11}^{(i)} & \bar{Q}_{12}^{(i)} & \bar{Q}_{16}^{(i)} & 0 & 0 \\ \bar{Q}_{12}^{(i)} & \bar{Q}_{22}^{(i)} & \bar{Q}_{26}^{(i)} & 0 & 0 \\ \bar{Q}_{16}^{(i)} & \bar{Q}_{26}^{(i)} & \bar{Q}_{66}^{(i)} & 0 & 0 \\ 0 & 0 & 0 & \bar{Q}_{44}^{(i)} & \bar{Q}_{45}^{(i)} \\ 0 & 0 & 0 & \bar{Q}_{45}^{(i)} & \bar{Q}_{55}^{(i)} \end{bmatrix} \begin{Bmatrix} \varepsilon_{xx}^{(i)} \\ \varepsilon_{yy}^{(i)} \\ 2\varepsilon_{xy}^{(i)} \\ 2\varepsilon_{yz}^{(i)} \\ 2\varepsilon_{xz}^{(i)} \end{Bmatrix}, \; i = 1,3 \tag{4.9}$$

where, $\bar{Q}_{mn}^{(i)}$ are the transformed stiffness coefficients for the i'th layer that can be expressed in terms of the lamina stiffness coefficients in principal material coordinates as follows:

$$\begin{aligned}
\bar{Q}_{11}^{(i)} &= Q_{11}cos^4\theta_i + 2(Q_{12}+2Q_{66})sin^2\theta_i cos^2\theta_i + Q_{22}Sin^4\theta_i \\
\bar{Q}_{12}^{(i)} &= (Q_{11}+Q_{22}-4Q_{66})sin^2\theta_i cos^2\theta_i + Q_{12}(sin^4\theta_i + cos^4\theta_i) \\
\bar{Q}_{22}^{(i)} &= Q_{11}sin^4\theta_i + 2(Q_{12}+2Q_{66})sin^2\theta_i cos^2\theta_i + Q_{22}cos^4\theta_i \\
\bar{Q}_{16}^{(i)} &= (Q_{11}-Q_{12}-2Q_{66})sin\theta_i cos^3\theta_i + (Q_{12}-Q_{22}+2Q_{66})sin^3\theta_i cos\theta_i \\
\bar{Q}_{26}^{(i)} &= (Q_{11}-Q_{12}-2Q_{66})sin^3\theta_i cos\theta_i + (Q_{12}-Q_{22}+2Q_{66})sin\theta_i cos^3\theta_i \\
\bar{Q}_{66}^{(i)} &= (Q_{11}+Q_{22}-2Q_{12}-2Q_{66})sin^2\theta_i cos^2\theta_i + Q_{66}(sin^4\theta_i + cos^4\theta_i) \\
\bar{Q}_{44}^{(i)} &= Q_{44}cos^2\theta_i + Q_{55}sin^2\theta_i \\
\bar{Q}_{45}^{(i)} &= (Q_{55}-Q_{44})cos\theta_i sin\theta_i \\
\bar{Q}_{55}^{(i)} &= Q_{55}cos^2\theta_i + Q_{44}sin^2\theta_i
\end{aligned} \tag{4.10}$$

where, θ_i is the angle of lamination of the i'th layer and Q_{mn} are related to the engineering constants as follows:

$$Q_{11}=\frac{E_1}{1-\nu_{12}\nu_{21}}, Q_{12}=\frac{\nu_{12}E_2}{1-\nu_{12}\nu_{21}}, Q_{22}=\frac{E_2}{1-\nu_{12}\nu_{21}}, Q_{66}=G_{12},$$
$$Q_{44}=G_{23}, Q_{55}=G_{13}, \nu_{21}=\frac{E_2\nu_{12}}{E_1} \tag{4.11}$$

Since the viscoelastic core is isotropic with the Poisson's ratio assumed as frequency independent, the following stress-strain relation holds:

$$\begin{Bmatrix}\sigma_{xx}^{(2)}\\ \sigma_{yy}^{(2)}\\ \sigma_{xy}^{(2)}\\ \sigma_{yz}^{(2)}\\ \sigma_{xz}^{(2)}\end{Bmatrix}=\frac{E_2^*}{1-\nu_2^2}\begin{bmatrix}1 & \nu_2 & 0 & 0 & 0\\ \nu_2 & 1 & 0 & 0 & 0\\ 0 & 0 & 1-\nu_2 & 0 & 0\\ 0 & 0 & 0 & 1-\nu_2 & 0\\ 0 & 0 & 0 & 0 & 1-\nu_2\end{bmatrix}\begin{Bmatrix}\varepsilon_{xx}^{(2)}\\ \varepsilon_{yy}^{(2)}\\ \varepsilon_{xy}^{(2)}\\ \varepsilon_{yz}^{(2)}\\ \varepsilon_{xz}^{(2)}\end{Bmatrix} \tag{4.12}$$

where, $E_2^*=E_2(1+i\eta_2)$ is the complex modulus of the viscoelastic core. For the free vibrations of the sandwich plate, Hamilton's principle can be expressed as follows:

$$\int_0^T(\delta U-\delta K)dt=0 \tag{4.13}$$

where, U and K correspond to the elastic strain energy and the kinetic energy respectively. For the problem considered, Eq. (4.13) becomes:

$$\sum_{i=1}^{3}\int_0^T\int_0^b\int_0^a\int_{-h_i/2}^{h_i/2}\left(\sigma_{xx}^{(i)}\delta\varepsilon_{xx}^{(i)}+\sigma_{yy}^{(i)}\delta\varepsilon_{yy}^{(i)}+2\sigma_{xy}^{(i)}\delta\varepsilon_{xy}^{(i)}+2\sigma_{yz}^{(i)}\delta\varepsilon_{yz}^{(i)}+2\sigma_{xz}^{(i)}\delta\varepsilon_{xz}^{(i)}\right)dz^{(i)}dxdydt$$
$$-\sum_{i=1}^{3}\rho_i\int_0^T\int_0^b\int_0^a\int_{-h_i/2}^{h_i/2}\left(\frac{\partial u^{(i)}}{\partial t}\delta\frac{\partial u^{(i)}}{\partial t}+\frac{\partial v^{(i)}}{\partial t}\delta\frac{\partial v^{(i)}}{\partial t}+\frac{\partial w^{(i)}}{\partial t}\delta\frac{\partial w^{(i)}}{\partial t}\right)dz^{(i)}dxdydt=0 \tag{4.14}$$

The governing equations in terms of sectional moments and forces are obtained from Eq. (4.14) by using the calculus of variations. These equations for the harmonic vibrations of the plate are presented as follows:

$$\frac{\partial N_{xx}^{(1)}}{\partial x}+\frac{\partial N_{xx}^{(2)}}{\partial x}+\frac{\partial N_{xx}^{(3)}}{\partial x}+\frac{\partial N_{xy}^{(1)}}{\partial y}+\frac{\partial N_{xy}^{(2)}}{\partial y}+\frac{\partial N_{xy}^{(3)}}{\partial y}=\omega^2\left[\frac{1}{2}h_1^2\rho_1\varphi_1-\frac{1}{2}h_3^2\rho_3\varphi_3 +\frac{1}{2}h_2\left(h_1\rho_1-h_3\rho_3\right)\varphi_2-\left(h_1\rho_1+h_2\rho_2+h_3\rho_3\right)u_0\right] \tag{4.15}$$

$$\frac{\partial N_{yy}^{(1)}}{\partial y}+\frac{\partial N_{yy}^{(2)}}{\partial y}+\frac{\partial N_{yy}^{(3)}}{\partial y}+\frac{\partial N_{xy}^{(1)}}{\partial x}+\frac{\partial N_{xy}^{(2)}}{\partial x}+\frac{\partial N_{xy}^{(3)}}{\partial x}=\omega^2\left[\frac{1}{2}h_1^2\rho_1\gamma_1-\frac{1}{2}h_3^2\rho_3\gamma_3 +\frac{1}{2}h_2\left(h_1\rho_1-h_3\rho_3\right)\gamma_2-\left(h_1\rho_1+h_2\rho_2+h_3\rho_3\right)v_0\right] \tag{4.16}$$

$$\frac{\partial N_{xz}^{(1)}}{\partial x}+\frac{\partial N_{xz}^{(2)}}{\partial x}+\frac{\partial N_{xz}^{(3)}}{\partial x}+\frac{\partial N_{yz}^{(1)}}{\partial y}+\frac{\partial N_{yz}^{(2)}}{\partial y}+\frac{\partial N_{yz}^{(3)}}{\partial y}=-\omega^2\left(h_1\rho_1+h_2\rho_2+h_3\rho_3\right)w \tag{4.17}$$

$$\frac{1}{2}h_1\left(\frac{\partial N_{xx}^{(1)}}{\partial x}+\frac{\partial N_{xy}^{(1)}}{\partial y}\right)+\frac{\partial M_{xx}^{(1)}}{\partial x}+\frac{\partial M_{xy}^{(1)}}{\partial y}-N_{xz}^{(1)}=\frac{1}{12}h_1^2\rho_1\omega^2\left(4h_1\varphi_1+3h_2\varphi_2-6u_0\right) \tag{4.18}$$

$$\frac{1}{2}h_2\left(\frac{\partial N_{xx}^{(1)}}{\partial x}+\frac{\partial N_{xy}^{(1)}}{\partial y}-\frac{\partial N_{xx}^{(3)}}{\partial x}-\frac{\partial N_{xy}^{(3)}}{\partial y}\right)+\frac{\partial M_{xx}^{(2)}}{\partial x}+\frac{\partial M_{xy}^{(2)}}{\partial y}-N_{xz}^{(2)}=\frac{1}{12}h_2\omega^2 \times\left[\left(6h_3\rho_3-6h_1\rho_1\right)u_0+h_2\left(3h_1\rho_1+h_2\rho_2+3h_3\rho_3\right)\varphi_2+3h_1^2\rho_1\varphi_1+3h_3^2\rho_3\varphi_3\right] \tag{4.19}$$

$$\frac{\partial M_{xx}^{(3)}}{\partial x}+\frac{\partial M_{xy}^{(3)}}{\partial y}-\frac{1}{2}h_3\left(\frac{\partial N_{xx}^{(3)}}{\partial x}+\frac{\partial N_{xy}^{(3)}}{\partial y}\right)-N_{xz}^{(3)}=\frac{h_3^2\rho_3\omega^2}{12}\left(6u_0+4h_3\varphi_3+3h_2\varphi_2\right) \tag{4.20}$$

$$\frac{1}{2}h_1\left(\frac{\partial N_{yy}^{(1)}}{\partial y}+\frac{\partial N_{xy}^{(1)}}{\partial x}\right)+\frac{\partial M_{yy}^{(1)}}{\partial y}+\frac{\partial M_{xy}^{(1)}}{\partial x}-N_{yz}^{(1)}=\frac{h_1^2\rho_1\omega^2}{12}\left(4h_1\gamma_1+3h_2\gamma_2-6v_0\right) \tag{4.21}$$

$$\frac{1}{2}h_2\left(\frac{\partial N_{yy}^{(1)}}{\partial y}+\frac{\partial N_{xy}^{(1)}}{\partial x}-\frac{\partial N_{yy}^{(3)}}{\partial y}-\frac{\partial N_{xy}^{(3)}}{\partial x}\right)+\frac{\partial M_{yy}^{(2)}}{\partial y}+\frac{\partial M_{xy}^{(2)}}{\partial x}-N_{yz}^{(2)}=\frac{1}{12}h_2\omega^2 \times\left[\left(6h_3\rho_3-6h_1\rho_1\right)v_0+h_2\left(3h_1\rho_1+h_2\rho_2+3h_3\rho_3\right)\gamma_2+3h_1^2\rho_1\gamma_1+3h_3^2\rho_3\gamma_3\right] \tag{4.22}$$

$$\frac{\partial M_{yy}^{(3)}}{\partial y}+\frac{\partial M_{xy}^{(3)}}{\partial x}-\frac{1}{2}h_3\left(\frac{\partial N_{yy}^{(3)}}{\partial y}+\frac{\partial N_{xy}^{(3)}}{\partial x}\right)-N_{yz}^{(3)}=\frac{h_3^2\rho_3\omega^2}{12}\left(6v_0+4h_3\gamma_3+3h_2\gamma_2\right) \tag{4.23}$$

and related boundary conditions are:

$$\left(N_{xx}^{(1)}+N_{xx}^{(2)}+N_{xx}^{(3)}\right)\delta u_0\Big|_{x=0}^{a}=0,\ \left(N_{xy}^{(1)}+N_{xy}^{(2)}+N_{xy}^{(3)}\right)\delta v_0\Big|_{x=0}^{a}=0,$$
$$\left(N_{xz}^{(1)}+N_{xz}^{(2)}+N_{xz}^{(3)}\right)\delta w\Big|_{x=0}^{a}=0,\ \left(M_{xx}^{(1)}+\frac{1}{2}h_1N_{xx}^{(1)}\right)\delta\varphi_1\Big|_{x=0}^{a}=0,$$
$$\left[M_{xx}^{(2)}+\frac{1}{2}h_2\left(N_{xx}^{(1)}-N_{xx}^{(3)}\right)\right]\delta\varphi_2\Big|_{x=0}^{a}=0,\ \left(M_{xx}^{(3)}-\frac{1}{2}h_3N_{xx}^{(3)}\right)\delta\varphi_3\Big|_{x=0}^{a}=0, \quad \textbf{(4.24)}$$
$$\left(M_{xy}^{(1)}+\frac{1}{2}h_1N_{xy}^{(1)}\right)\delta\gamma_1\Big|_{x=0}^{a}=0,\ \left[M_{xy}^{(2)}+\frac{1}{2}h_2\left(N_{xy}^{(1)}-N_{xy}^{(3)}\right)\right]\delta\gamma_2\Big|_{x=0}^{a}=0,$$
$$\left(M_{xy}^{(3)}-\frac{1}{2}h_3N_{xy}^{(3)}\right)\delta\gamma_3\Big|_{x=0}^{a}=0$$

$$\left(N_{xy}^{(1)}+N_{xy}^{(2)}+N_{xy}^{(3)}\right)\delta u_0\Big|_{y=0}^{b}=0,\ \left(N_{yy}^{(1)}+N_{yy}^{(2)}+N_{yy}^{(3)}\right)\delta v_0\Big|_{y=0}^{b}=0,$$
$$\left(N_{yz}^{(1)}+N_{yz}^{(2)}+N_{yz}^{(3)}\right)\delta w\Big|_{y=0}^{b}=0,\ \left(M_{xy}^{(1)}+\frac{1}{2}h_1N_{xy}^{(1)}\right)\delta\varphi_1\Big|_{y=0}^{b}=0,$$
$$\left[M_{xy}^{(2)}+\frac{1}{2}h_2\left(N_{xy}^{(1)}-N_{xy}^{(3)}\right)\right]\delta\varphi_2\Big|_{y=0}^{b}=0,\ \left(M_{xy}^{(3)}-\frac{1}{2}h_3N_{xy}^{(3)}\right)\delta\varphi_3\Big|_{y=0}^{b}=0, \quad \textbf{(4.25)}$$
$$\left(M_{yy}^{(1)}+\frac{1}{2}h_1N_{yy}^{(1)}\right)\delta\gamma_1\Big|_{y=0}^{b}=0,\ \left[M_{yy}^{(2)}+\frac{1}{2}h_2\left(N_{yy}^{(1)}-N_{yy}^{(3)}\right)\right]\delta\gamma_2\Big|_{y=0}^{b}=0,$$
$$\left(M_{yy}^{(3)}-\frac{1}{2}h_3N_{yy}^{(3)}\right)\delta\gamma_3\Big|_{y=0}^{b}=0$$

The sectional moments and forces are obtained from the following equations:

$$N_{mn}^{(i)}=\int_{-h_i/2}^{h_i/2}\sigma_{mn}^{(i)}dz^{(i)},\ M_{mn}^{(i)}=\int_{-h_i/2}^{h_i/2}z^{(i)}\sigma_{mn}^{(i)}dz^{(i)},\ i=1,2,3 \quad \textbf{(4.26)}$$

4.2 Generalized Differential Quadrature Method

In order to approximate the derivatives of a function at a point, GDQM employs a weighted linear sum of the function values at all discrete points. The following relations hold for the uncoupled derivatives of a function w(x,y) [62]:

$$\frac{\partial^p}{\partial x^p}w\left(x_i,y_j\right)=\sum_{k=1}^{N}c_{ik}^{(p)}w\left(x_k,y_j\right) \quad \textbf{(4.27)}$$

$$\frac{\partial^r}{\partial y^r} w\left(x_i, y_j\right) = \sum_{m=1}^{M} d_{jm}^{(r)} w\left(x_i, y_m\right) \tag{4.28}$$

where, N and M are the total number of sampling points of the grid distribution in x and y directions respectively. Also, $c_{ik}^{(p)}$ and $d_{jm}^{(r)}$ correspond to the weighting coefficients, which can be evaluated for the first order derivatives as follows:

$$c_{ik}^{(1)} = \begin{cases} \dfrac{\bar{M}_x^{(1)}(x_i)}{(x_i - x_k)\bar{M}_x^{(1)}(x_k)} & for \;\; i \neq k \;\; and \;\; i,k = 1,2,...,N \\ -\sum\limits_{s=1, s\neq i}^{N} c_{is}^{(1)} & for \;\; i = k \;\; and \;\; i,k = 1,2,...,N \end{cases} \tag{4.29}$$

$$d_{jm}^{(1)} = \begin{cases} \dfrac{\bar{M}_y^{(1)}(y_j)}{(y_j - y_m)\bar{M}_y^{(1)}(y_m)} & for \;\; j \neq m \;\; and \;\; j,m = 1,2,...,M \\ -\sum\limits_{s=1, s\neq j}^{M} d_{js}^{(1)} & for \;\; j = m \;\; and \;\; j,m = 1,2,...,M \end{cases} \tag{4.30}$$

where, the function $\bar{M}$ is given by:

$$\bar{M}_x(x) = \prod_{s=1}^{N} (x - x_s), \;\; \bar{M}_y(y) = \prod_{s=1}^{M} (y - y_s) \tag{4.31}$$

The derivatives of $\bar{M}$ at discrete x_i and y_j points can be written as follows:

$$\bar{M}_x^{(1)}(x_i) = \prod_{s=1, s\neq i}^{N} (x_i - x_s), \;\; \bar{M}_y^{(1)}(y_j) = \prod_{s=1, s\neq j}^{M} (y_j - y_s) \tag{4.32}$$

The following recurrence relations hold for the weighting coefficients of higher order derivatives:

$$c_{ik}^{(p)} = \begin{cases} p\left(c_{ii}^{(p-1)} c_{ik}^{(1)} - \dfrac{c_{ik}^{(p-1)}}{x_i - x_k} \right) & for \;\; i \neq k \;\; and \;\; i,k = 1,2,...,N \\ -\sum\limits_{s=1, s\neq i}^{N} c_{is}^{(p)} & for \;\; i = k \;\; and \;\; i,k = 1,2,...,N \end{cases} \tag{4.33}$$

$$d_{jm}^{(r)} = \begin{cases} r\left(d_{jj}^{(r-1)} d_{jm}^{(1)} - \dfrac{d_{jm}^{(r-1)}}{y_j - y_m} \right) & for \;\; j \neq m \;\; and \;\; j,m = 1,2,...,M \\ -\sum\limits_{s=1, s\neq i}^{M} d_{js}^{(r)} & for \;\; j = m \;\; and \;\; j,m = 1,2,...,M \end{cases} \tag{4.34}$$

The GDQ formulation of the coupled derivative can also be given by:

$$\frac{\partial^{p+r}}{\partial x^p \partial y^r} w\left(x_i, y_j\right) = \sum_{k=1}^{N} c_{ik}^{(p)} \sum_{m=1}^{M} d_{jm}^{(r)} w\left(x_k, y_m\right) \tag{4.35}$$

It is well known that the use of a grid distribution, which is denser on the boundaries, gives much better results when compared with a uniform distribution in GDQ analysis. Therefore, Chebyshev-Gauss-Labatto grid distribution is utilized to discretize the spatial coordinates.

$$x_i = \frac{a}{2}\left[1 - \cos\left(\frac{i-1}{N-1}\pi\right)\right], \; y_j = \frac{b}{2}\left[1 - \cos\left(\frac{j-1}{M-1}\pi\right)\right], \; i = 1,2,...,N \;\; \text{and} \;\; j = 1,2,...,M \tag{4.36}$$

The grid distribution is presented in Figure 4.3.

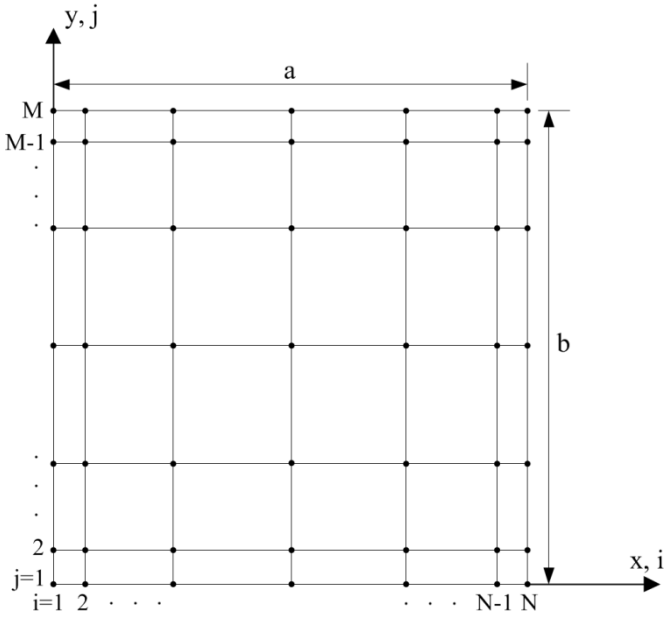

Figure 4.3: Grid distribution.

The open forms of governing equations and their GDQ representations are not presented here since these equations are quite large; however, one can easily obtain them by using Eqs. (4.8), (4.9), (4.12) and (4.26). The global assembling of the governing equations and the boundary conditions lead to the following set of linear equations [63]:

$$\begin{bmatrix} \mathbf{K}_{bb} & \mathbf{K}_{bd} \\ \mathbf{K}_{db} & \mathbf{K}_{dd} \end{bmatrix} \begin{Bmatrix} \boldsymbol{\delta}_b \\ \boldsymbol{\delta}_d \end{Bmatrix} = \omega^2 \begin{bmatrix} 0 & 0 \\ 0 & \mathbf{M}_{dd} \end{bmatrix} \begin{Bmatrix} \boldsymbol{\delta}_b \\ \boldsymbol{\delta}_d \end{Bmatrix} \tag{4.37}$$

where, the subscripts b and d stand for the degrees of freedom that belong to the boundary and the domain respectively. Kinematic condensation of non-domain degrees of freedom can be performed as follows [63]:

$$\left(\mathbf{K}_{dd} - \mathbf{K}_{db} \mathbf{K}_{bb}^{-1} \mathbf{K}_{bd} \right) = \omega^2 \mathbf{M}_{dd} \tag{4.38}$$

After solving Eq. (4.38) for the desired eigenpair, the displacements at the boundaries can also be obtained as follows:

$$\boldsymbol{\delta}_b = -\mathbf{K}_{bb}^{-1} \mathbf{K}_{bd} \boldsymbol{\delta}_d \tag{4.39}$$

In the solutions carried out, a symbolic calculation software package MATHEMATICA is utilized. The built-in function “Eigenvalues” is used, which solves the generalized eigenvalue problem in Eq. (4.38) by QZ algorithm.

4.3 Finite Element Method

In order to validate the results of GDQM for the composite plates, a simple four-node sandwich plate finite element with seven degrees of freedom per node is utilized. The mass and stiffness matrices are derived by considering classical plate theory (CPT) for the base and the constraining layers and FSDT for the core layer. The kinematic relations are obtained from Eqs. (4.1)-(4.7) by taking:

$$\varphi_1 = \varphi_3 = \frac{\partial w}{\partial x} = \vartheta_x \text{ and } \gamma_1 = \gamma_3 = \frac{\partial w}{\partial y} = \vartheta_y \tag{4.40}$$

The sandwich plate element is presented in Figure 4.4.

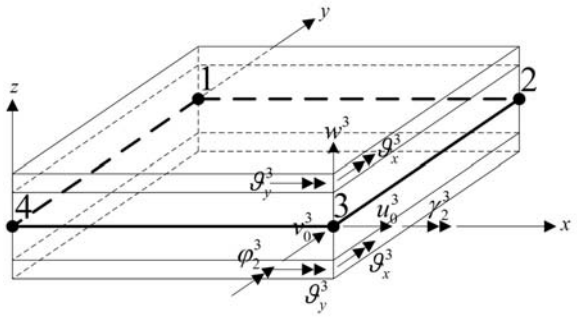

Figure 4.4: The nodal degrees of freedom of the 4-node sandwich plate finite element.

The transverse displacement is assumed to be in the following polynomial form [64]:

$$w(x,y) = a_1 + a_2 x + a_3 y + a_4 x^2 + a_5 xy + a_6 y^2 + a_7 x^3 + a_8 x^2 y + a_9 xy^2 + a_{10} y^3 + a_{11} x^3 y + a_{12} xy^3 \tag{4.41}$$

The unknown coefficients can be related to the nodal displacements by using Eq. (4.41):

$$\begin{aligned} w^i &= w(x_i, y_i) \\ \vartheta_x^i &= \frac{\partial}{\partial x} w(x_i, y_i), \ i = 1,2,3,4 \\ \vartheta_y^i &= \frac{\partial}{\partial y} w(x_i, y_i) \end{aligned} \tag{4.42}$$

where, w^i is the transverse displacement and ϑ_x^i, ϑ_y^i are the rotations of face layers at i'th node. Solution of Eq. (4.42) results in:

$$w = N_1^1 w^1 + N_2^1 \vartheta_x^1 + N_3^1 \vartheta_y^1 + N_1^2 w^2 + N_2^2 \vartheta_x^2 + N_3^2 \vartheta_y^2 + N_1^3 w^3 + N_2^3 \vartheta_x^3 + N_3^3 \vartheta_y^3 + N_1^4 w^4 + N_2^4 \vartheta_x^4 + N_3^4 \vartheta_y^4 \tag{4.43}$$

The shape functions in Eq. (4.43) can be evaluated at each node as follows:

$$\begin{Bmatrix} N_1^i \\ N_2^i \\ N_3^i \end{Bmatrix} = \frac{1}{8}(1+\xi\xi_i)(1+\eta\eta_i) \begin{Bmatrix} 2+\xi\xi_i+\eta\eta_i-\xi^2-\eta^2 \\ -\frac{a_e}{2}\xi_i(1-\xi^2) \\ -\frac{b_e}{2}\eta_i(1-\eta^2) \end{Bmatrix}, \ i = 1,2,3,4 \tag{4.44}$$

with the normalized coordinates given by:

$$\xi = \frac{2x}{a_e} \text{ and } \eta = \frac{2y}{b_e} \tag{4.45}$$

where a_e, b_e are the dimensions of the plate element and ξ_i, η_i are the values of ξ and η at the i'th node respectively. Also, note that the shape functions in Eq. (4.44) are non-conforming, since the C^1 continuity is not satisfied on the element boundaries.

For the axial displacements and the rotations of the core layer, C^0 continuous bilinear shape functions are used to interpolate the displacement field:

$$\begin{aligned} u_0 &= N_1 u_0^1 + N_2 u_0^2 + N_3 u_0^3 + N_4 u_0^4 \\ v_0 &= N_1 v_0^1 + N_2 v_0^2 + N_3 v_0^3 + N_4 v_0^4 \\ \varphi_2 &= N_1 \varphi_2^1 + N_2 \varphi_2^2 + N_3 \varphi_2^3 + N_4 \varphi_2^4 \\ \gamma_2 &= N_1 \gamma_2^1 + N_2 \gamma_2^2 + N_3 \gamma_2^3 + N_4 \gamma_2^4 \end{aligned} \tag{4.46}$$

with

$$N_i = \frac{1}{4}\left(1 + \xi\xi_i\right)\left(1 + \eta\eta_i\right) \tag{4.47}$$

The displacement field in each layer depends on the degrees of freedom of the sandwich plate:

$$\begin{Bmatrix} u^{(i)} \\ v^{(i)} \\ w^{(i)} \end{Bmatrix} = \mathbf{T}_i \begin{Bmatrix} u_0 \\ v_0 \\ \varphi_2 \\ \gamma_2 \\ w \end{Bmatrix} \tag{4.48}$$

where $\mathbf{T}_i$ is the transverse thickness interpolation matrix that can be obtained for each layer by using the kinematic relations given in Eqs. (4.1)-(4.7) together with Eq. (4.40):

$$\mathbf{T}_1 = \begin{bmatrix} 1 & 0 & -\frac{h_2}{2} & 0 & -\left(z^{(1)} + \frac{h_1}{2}\right)\frac{\partial}{\partial x} \\ 0 & 1 & 0 & -\frac{h_2}{2} & -\left(z^{(1)} + \frac{h_1}{2}\right)\frac{\partial}{\partial y} \\ 0 & 0 & 0 & 0 & 1 \end{bmatrix} \tag{4.49}$$

$$\mathbf{T}_2 = \begin{bmatrix} 1 & 0 & -z^{(2)} & 0 & 0 \\ 0 & 1 & 0 & -z^{(2)} & 0 \\ 0 & 0 & 0 & 0 & 1 \end{bmatrix} \tag{4.50}$$

$$\mathbf{T}_3 = \begin{bmatrix} 1 & 0 & \frac{h_2}{2} & 0 & \left(\frac{h_3}{2} - z^{(3)}\right)\frac{\partial}{\partial x} \\ 0 & 1 & 0 & \frac{h_2}{2} & \left(\frac{h_3}{2} - z^{(3)}\right)\frac{\partial}{\partial y} \\ 0 & 0 & 0 & 0 & 1 \end{bmatrix} \tag{4.51}$$

The vector of displacements $\{u_0, v_0, \varphi_2, \gamma_2, w\}^T$ can be expressed in terms of nodal degrees of freedom $\mathbf{U} = \{u_0^1, v_0^1, \varphi_2^1, \gamma_2^1, w^1, \vartheta_x^1, \vartheta_y^1, ..., u_0^4, v_0^4, \varphi_2^4, \gamma_2^4, w^4, \vartheta_x^4, \vartheta_y^4\}^T$ by using Eqs. (4.43) and (4.46) as follows:

$$\begin{Bmatrix} u_0 \\ v_0 \\ \varphi_2 \\ \gamma_2 \\ w \end{Bmatrix} = \mathbf{NU} \tag{4.52}$$

where **N** is the matrix of interpolation functions:

$$\mathbf{N} = \begin{bmatrix} N_1 & 0 & 0 & 0 & 0 & 0 & 0 & ... & N_4 & 0 & 0 & 0 & 0 & 0 & 0 \\ 0 & N_1 & 0 & 0 & 0 & 0 & 0 & ... & 0 & N_4 & 0 & 0 & 0 & 0 & 0 \\ 0 & 0 & N_1 & 0 & 0 & 0 & 0 & ... & 0 & 0 & N_4 & 0 & 0 & 0 & 0 \\ 0 & 0 & 0 & N_1 & 0 & 0 & 0 & ... & 0 & 0 & 0 & N_4 & 0 & 0 & 0 \\ 0 & 0 & 0 & 0 & N_1^1 & N_2^1 & N_3^1 & ... & 0 & 0 & 0 & 0 & N_1^4 & N_2^4 & N_3^4 \end{bmatrix} \tag{4.53}$$

The displacement field at each layer can be written in terms of the nodal degrees of freedom by using Eqs. (4.48) and (4.52) as follows:

$$\begin{Bmatrix} u^{(i)} \\ v^{(i)} \\ w^{(i)} \end{Bmatrix} = \mathbf{T}_i \mathbf{N} \mathbf{U} \tag{4.54}$$

Mass and stiffness matrices are obtained from the following relations for each layer:

$$\mathbf{M}^{(i)} = \rho_i \int_{-a_e/2}^{a_e/2} \int_{-b_e/2}^{b_e/2} \int_{-h_i/2}^{h_i/2} \left(\mathbf{T}_i \mathbf{N}\right)^T \left(\mathbf{T}_i \mathbf{N}\right) dz^{(i)} dy dx \tag{4.55}$$

$$\mathbf{K}^{(i)} = \int_{-a_e/2}^{a_e/2} \int_{-b_e/2}^{b_e/2} \int_{-h_i/2}^{h_i/2} \mathbf{B}^{(i)T} \mathbf{E}^{(i)} \mathbf{B}^{(i)} \, dz^{(i)} dy dx \tag{4.56}$$

where, **E** is the elastic coefficient matrix given as follows.

Face layers:

$$\mathbf{E}^{(i)} = \begin{bmatrix} \bar{Q}_{11}^{(i)} & \bar{Q}_{12}^{(i)} & \bar{Q}_{16}^{(i)} \\ \bar{Q}_{12}^{(i)} & \bar{Q}_{22}^{(i)} & \bar{Q}_{26}^{(i)} \\ \bar{Q}_{16}^{(i)} & \bar{Q}_{26}^{(i)} & \bar{Q}_{66}^{(i)} \end{bmatrix}, \; i = 1,3 \tag{4.57}$$

Core layer:

$$\mathbf{E}^{(2)} = \frac{E_2^*}{1-\nu_2^2} \begin{bmatrix} 1 & \nu_2 & 0 & 0 & 0 \\ \nu_2 & 1 & 0 & 0 & 0 \\ 0 & 0 & \dfrac{1-\nu_2}{2} & 0 & 0 \\ 0 & 0 & 0 & \dfrac{1-\nu_2}{2} & 0 \\ 0 & 0 & 0 & 0 & \dfrac{1-\nu_2}{2} \end{bmatrix} \tag{4.58}$$

Also, $\mathbf{B}^{(i)}$ is the deformation matrix of i'th layer, which can obtained from the following relation:

$$\mathbf{B}^{(i)} = \mathbf{D}^{(i)} \mathbf{T}_i \mathbf{N} \tag{4.59}$$

with:

Face layers:

$$\mathbf{D}^{(i)} = \begin{bmatrix} \partial/\partial x & 0 & 0 \\ 0 & \partial/\partial y & 0 \\ \partial/\partial y & \partial/\partial x & 0 \end{bmatrix}, \; i = 1,3 \tag{4.60}$$

Core layer:

$$\mathbf{D}^{(2)} = \begin{bmatrix} \partial/\partial x & 0 & 0 \\ 0 & \partial/\partial y & 0 \\ \partial/\partial y & \partial/\partial x & 0 \\ \partial/\partial z & 0 & \partial/\partial x \\ 0 & \partial/\partial z & \partial/\partial y \end{bmatrix} \tag{4.61}$$

The mass and stiffness matrices of layers 1- 3 are obtained and assembled to obtain the sandwich plate finite element matrices of 28x28 dimension:

$$\mathbf{M} = \sum_{i=1}^{3} \mathbf{M}^{(i)}, \; \mathbf{K} = \sum_{i=1}^{3} \mathbf{K}^{(i)} \tag{4.62}$$

These matrices are very large so they are not presented here.

4.4 Results and Discussion

In this section, three sandwich plate problems that exist in literature are considered to validate both the plate model and the solution technique. Then, a parametric analysis on the effects of system parameters on vibration and damping characteristics of a three-layered composite plate is carried out.

4.4.1 Validation

First two cases that will be considered consist of simply supported sandwich plates with elastic isotropic face layers and a viscoelastic core with constant material properties. These are hypothetical test problems, where the viscoelastic material properties are assumed as frequency independent. The last case is a clamped composite plate with a frequency dependent viscoelastic core. The material properties and the geometry for the first example are given in Table 4.1.

Table 4.1: Material properties and dimensions (Example 1).

Elastic layers (Layers 1 and 3)	
Young's modulus	$E_1=E_3=68.9$ GPa
Density	$\rho_1=\rho_3=2740$ kg/m^3
Poisson's ratio	$\nu_1=\nu_3=0.3$
Thickness	$h_1=h_3=0.762$ mm
Viscoelastic layer (Layer 2)	
Shear modulus	$G_2=0.896$ MPa
Density	$\rho_2=999$ kg/m^3
Poisson's ratio	$\nu_2=0.5$
Loss Factor	$\eta_2=0.5$
Thickness	$h_2=0.254$ mm
Whole plate	
Length	a=0.348 m, b=0.3048 m

This problem has attracted the attention of several researchers [22, 24, 26, 31, 65-67] and it has been used as a benchmark problem to test new plate theories and solution techniques. Natural frequencies and loss factors, previously defined by Eqs. (3.56) and (3.57), are presented for the first five modes in Table 4.2 and Table 4.3 respectively.

Table 4.2: Natural frequencies (Hz); N=30, M=26.

	Mode 1	Mode 2	Mode 3	Mode 4	Mode 5
GDQM	57.96	113.80	129.36	177.11	194.72
Ref. [22]	57.4	113.2	129.3	179.3	196.0
Ref. [24]	60.2	115.2	130.2	178.5	195.4
Ref. [26]	60.1	115.0	130.2	178.1	195.1
Ref. [31]	58.69	113.75	129.16	175.46	193.79
Ref. [65]	60.2	115.2	130.4	178.4	195.4
Ref. [66]	60.24	115.22	130.43	178.46	195.42
Ref. [67]	56.9	111.9	127.5	174.9	193.1

Table 4.3: Loss factors; N=30, M=26.

	Mode 1	Mode 2	Mode 3	Mode 4	Mode 5
GDQM	0.1706	0.1933	0.1927	0.1730	0.1705
Ref. [22]	0.176	0.188	0.188	0.153	0.153
Ref. [24]	0.190	0.203	0.199	0.181	0.174
Ref. [26]	0.192	0.203	0.198	0.179	0.172
Ref. [31]	0.201	0.211	0.208	0.189	0.183
Ref. [65]	0.190	0.203	0.199	0.181	0.174
Ref. [66]	0.1901	0.2034	0.1991	0.1806	0.1737
Ref. [67]	0.180	0.190	0.187	0.164	0.158

The real and the imaginary parts of the first four normalized mode shapes for the transverse displacement are presented in Figure 4.5.

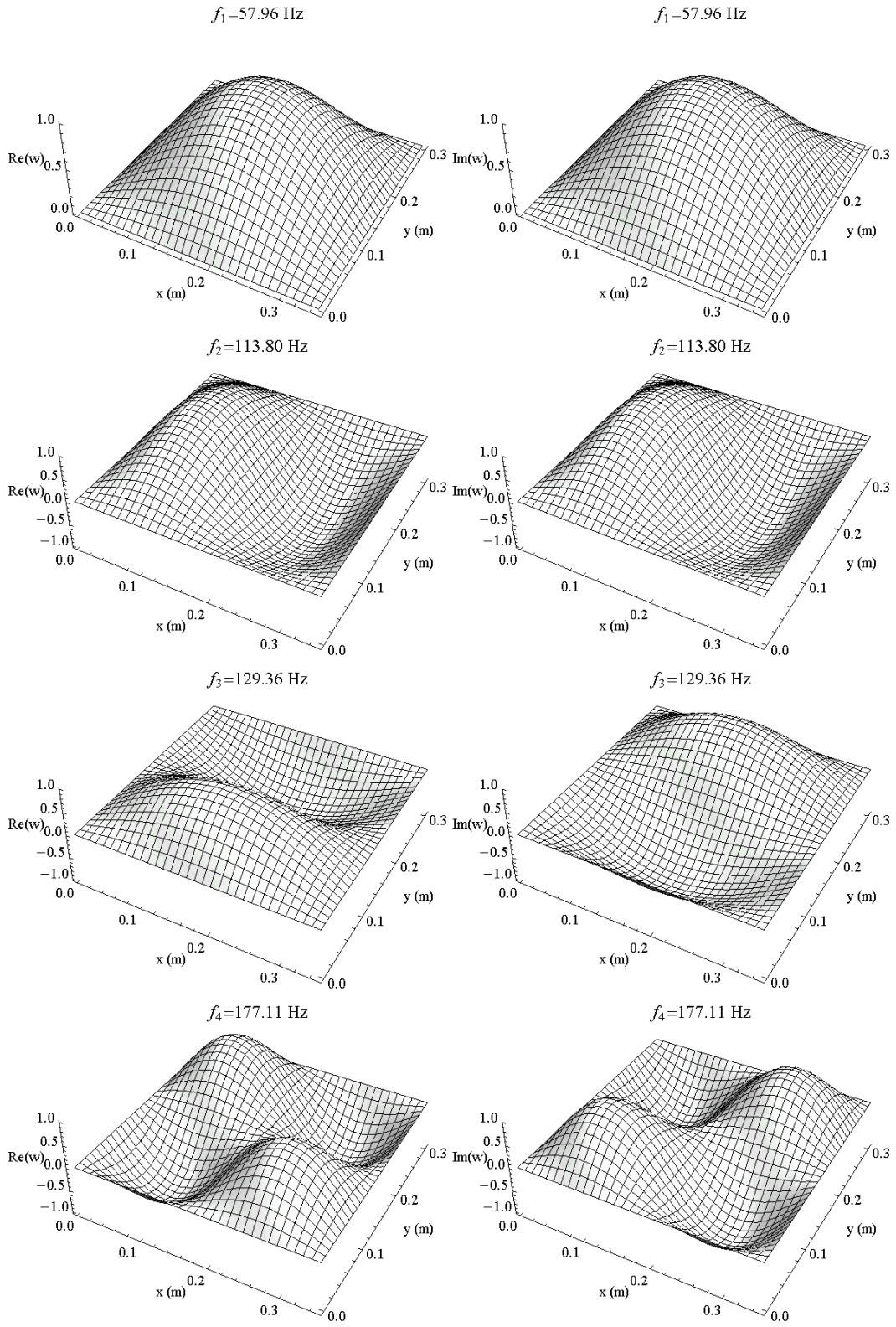

Figure 4.5: The real and the imaginary parts of the first four mode shapes.

Navier's method is utilized in Refs. [24], [26], [65] and [66] for the solution of this eigenvalue problem. Though there are some differences between the plate models used in these studies, the results show little variation probably due to the same shape functions utilized for the displacements. On the other hand, the natural frequencies and loss factors are obtained with FEM analyses in [22], [31] and [67].

The properties of the second plate are given in Table 4.4 and the results for the first four natural frequencies and loss factors are presented in Table 4.5 and Table 4.6.

Table 4.4: Material properties and dimensions (Example 2).

Elastic layers (Layers 1 and 3)	
Young's modulus	$E_1=E_3=207$ GPa
Density	$\rho_1=\rho_3=7800$ kg/m^3
Poisson's ratio	$\nu_1=\nu_3=0.334$
Thickness	$h_1=h_3=5$ mm
Viscoelastic layer (Layer 2)	
Shear modulus	$G_2=4$ MPa
Density	$\rho_2=2000$ kg/m^3
Poisson's ratio	$\nu_2=0.3$
Loss Factor	$\eta_2=0.38$
Thickness	$h_2=5$ mm
Whole plate	
Length	a=b=0.4 m

Table 4.5: Natural frequencies (rad/s); N=30, M=30.

	Mode 1	Mode 2	Mode 3	Mode 4
GDQM	970.10	2340.76	2340.76	3700.19
Ref. [25]	974.91	2350.80	2350.80	3725.60
Ref. [31]	972.89	2346.45	2346.45	3711.90
Ref. [61]	975.17	2350.79	2350.79	3725.33

Table 4.6: Loss factors (%); N=30, M=30.

	Mode 1	Mode 2	Mode 3	Mode 4
GDQM	4.391	1.919	1.919	1.232
Ref. [25]	4.386	1.911	1.911	1.221
Ref. [31]	4.4	1.9	1.9	1.2
Ref. [61]	4.431	1.918	1.918	1.224

The mode shapes for the second example are presented in Figure 4.6.

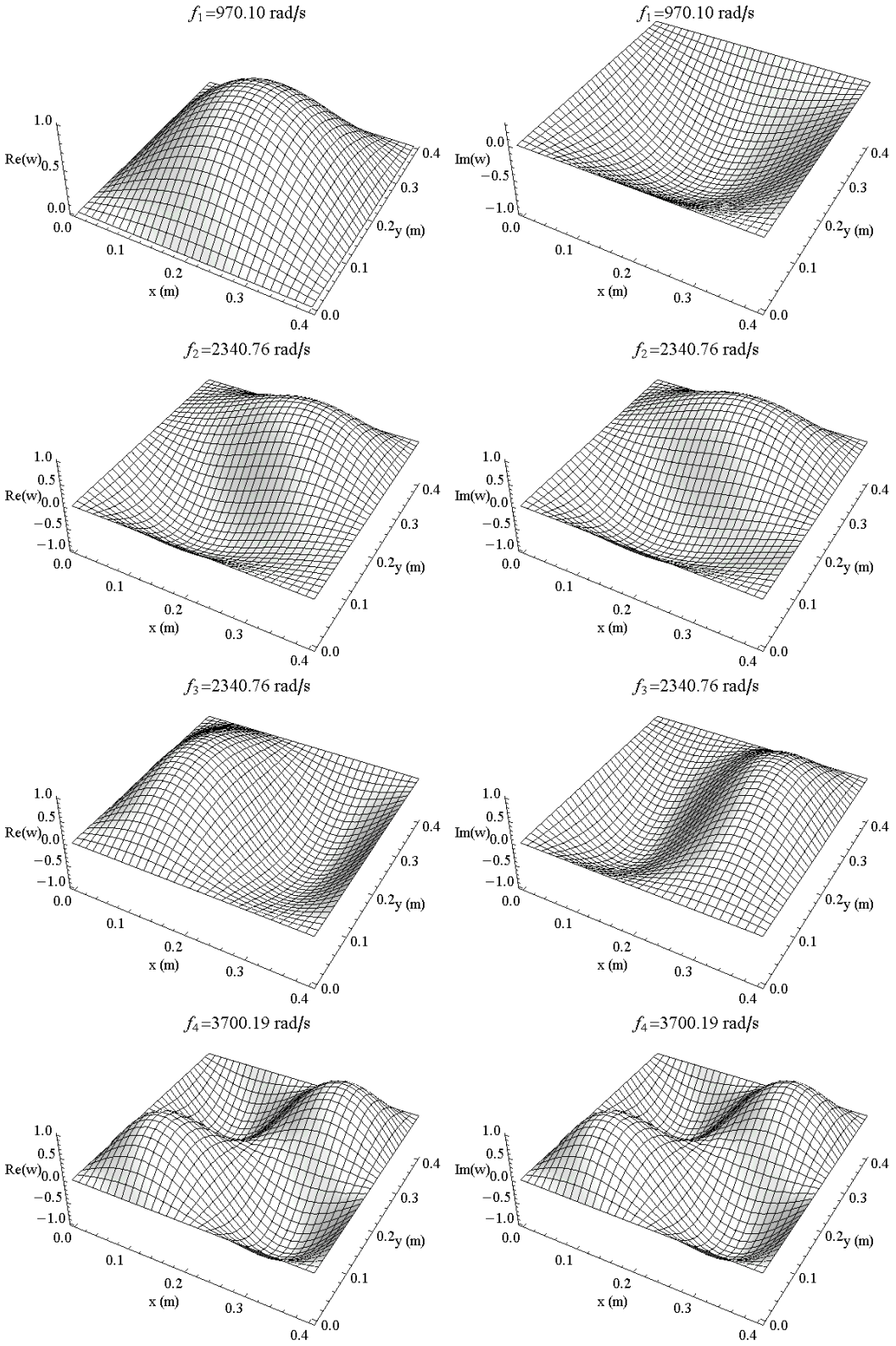

Figure 4.6: The real and the imaginary parts of the first four mode shapes.

The tables show good agreement between the results obtained with GDQM and the already existing ones. It is common to model the base and constraining layers with Kirchhoff plate theory [26, 61, 65-67], as in the FE model of this work (Section 4.3), in order to simplify the problem by decreasing the number of degrees of freedom. As a result, the neglected transverse shear strain results in an overprediction of the natural frequencies. In the GDQM analysis carried out in this thesis, all layers are modeled with Mindlin plate theory and therefore, the natural frequencies obtained are generally lower when compared with the results of other studies.

The convergence of the loss factors of the second example with increasing number of grid points considered is presented in Figure 4.7, for the first five modes.

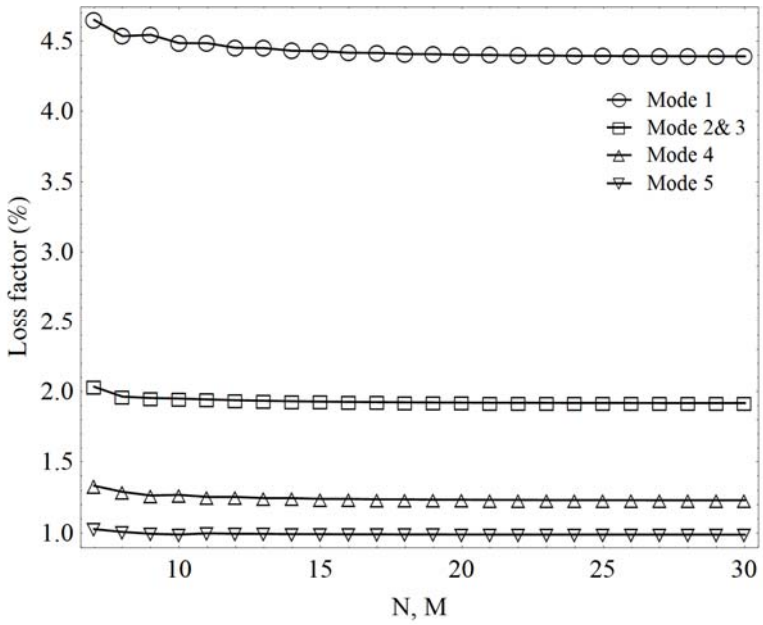

Figure 4.7: Convergence of the loss factor with N=M.

The third example is a clamped seven-layered composite plate having carbon fiber face layers and a viscoelastic core made of 3M ISD-112 damping polymer. The stacking sequence of the sandwich plate is (0/90/45/core/45/90/0) and the material properties and dimensions are as given in Table 4.7.

This problem was considered by Araujo et al. to identify the unknown parameters of fractional order viscoelastic models [68]. In their study, the core layer is modeled with a high-order shear deformation theory (HSDT) and the face layers are modeled with FSDT. In addition, an eight-node serendipity plate element with 13 mechanical degrees of freedom per node was used for the FEM analysis of this problem.

Table 4.7: Properties of the composite plate (Example 3).

Carbon fiber layers (Layers 1 and 3)	
Young's modulus	E_{11}=130.8 GPa, E_{22}=10.6 GPa
Shear modulus	G_{12}=5.6 GPa, G_{13}=4.2 GPa, G_{23}=3.0 GPa
Density	$\rho_1=\rho_3$=1543 kg/m^3
Poisson's ratio	ν_{12}=0.36
Thickness	$h_1=h_3$=1.5 mm
Viscoelastic layer (Layer 2)	
Shear modulus	$G_2= G_2(\omega)$ (Eq. (4.63))
Density	ρ_2=1000 kg/m^3
Poisson's ratio	ν_2=0.49
Loss Factor	$\eta_2= \eta_2(\omega)$ (Eq. (4.63))
Thickness	h_2=2.5 mm
Whole plate	
Length	a=0.3 m, b=0.2 m

The shear modulus and loss factor of the 3M ISD-112 viscoelastic core, for the frequency range f=5…1600 Hz, are as follows [68, 69]:

$$G_2 = 4.759 - \frac{0.9266}{0.1918 + 0.0005148\,f} + 2.405\left(0.1918 + 0.0005148\,f\right)^2 \text{ (MPa)}$$
$$\eta_2 = 1.385 - 0.03673\left(0.01 + 0.0006306\,f\right) - \frac{0.01342}{0.01 + 0.0006306\,f} \qquad \textbf{(4.63)}$$

The results for the first twelve natural frequencies and loss factors are presented in Table 4.8 and Table 4.9 with an error tolerance of ξ=0.0001 (Eq. (3.58)).

Table 4.8: Natural frequencies (Hz); N=30, M=20.

Mode	FEM [68, 69]	GDQM[a]	GDQM[b]	FEM[c]
1	211.72	216.4971	216.4971	217.1197
2	382.63	375.0547	375.0547	376.2565
3	473.22	469.5071	469.5071	472.8345
4	630.85	580.8453	580.8453	583.7805
5	674.83	635.8137	635.8137	639.0632
6	876.43	801.5226	801.5225	805.5127
7	963.66	828.7563	828.7562	840.2958
8	995.54	923.4911	923.4910	932.2388
9	1080.30	969.8134	969.8133	978.6948
10	1393.95	1054.6749	1054.6747	1061.5413
11	1440.67	1210.4852	1210.4849	1218.9995
12	1461.00	1298.7898	1298.7897	1317.9316

[a] Core modeled with FSDT, [b] Core modeled with HSDT, [c] FEM results of the present study with a 30x20 mesh

Table 4.9: Loss factors (%); N=30, M=20.

Mode	FEM [68, 69]	GDQM[a]	GDQM[b]	FEM[c]
1	46.58	50.6700	50.6700	50.7598
2	41.87	49.8528	49.8527	49.9284
3	42.52	48.2577	48.2576	48.1989
4	39.41	51.8697	51.8696	51.8075
5	31.93	40.9737	40.9737	41.0070
6	39.59	48.3322	48.3321	48.0869
7	32.92	44.6736	44.6735	44.3153
8	31.43	42.5272	42.5272	42.3802
9	33.41	38.3451	38.3451	38.2968
10	30.16	47.4708	47.4707	47.1812
11	33.90	37.9273	37.9271	37.3892
12	27.51	38.3266	38.3265	38.3406

[a] Core modeled with FSDT, [b] Core modeled with HSDT, [c] FEM results of the present study with a 30x20 mesh

This problem is also solved with the currently developed FE model presented in Section 4.3. The results of this FEM analysis are given in the last columns of Table 4.8 and Table 4.9. The GDQM estimations for the natural frequencies and loss factors, when the core layer is modeled with HSDT as in [68], are also presented.

There is some discrepancy between the results of Ref. [68] and the recent study especially for the higher modes. Since there is a good agreement between different models and solution techniques of the present work, one can conclude that the reason for this inconsistency is most probably due to the coarse mesh used in [68]. Results also show that the additional computational cost of using HSDT instead of FSDT in the modeling of the core layer is not justified since there is almost no difference between the frequencies and loss factors obtained with these two theories.

The real and imaginary parts of the mode shapes for the transverse displacement are presented in Figure 4.8 for the first four natural frequencies.

In addition, comparison of GDQ and FE methods, in terms of variation of the relative error and the CPU time with respect to the number of nodes considered, is presented in Figure 4.9 for the first natural frequency of the last example.

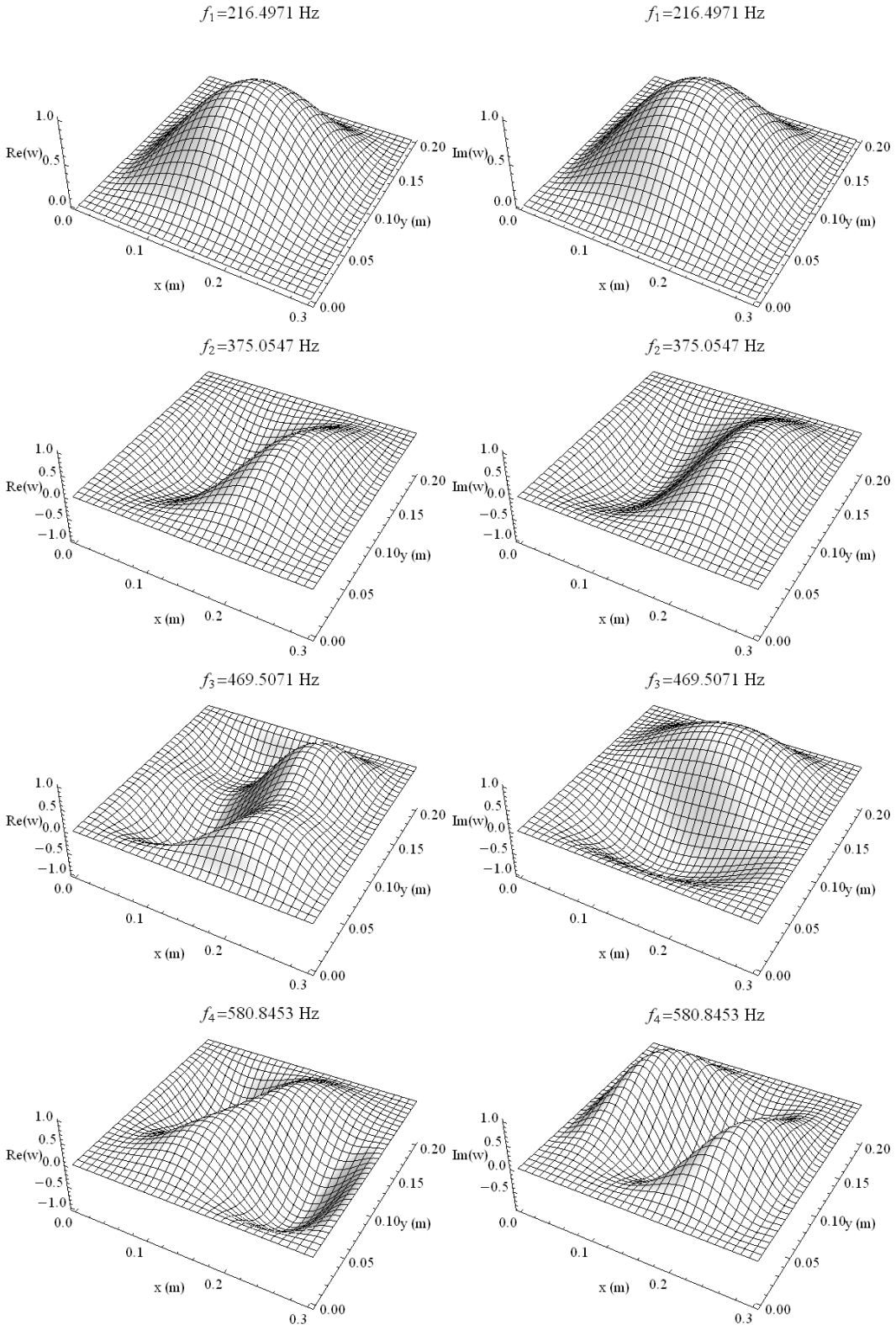

Figure 4.8: The real and the imaginary parts of the first four mode shapes.

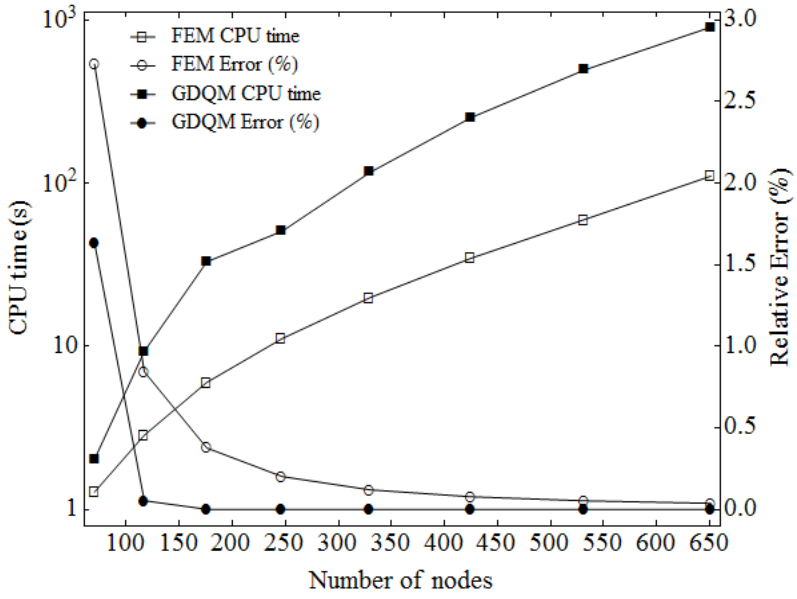

Figure 4.9: Relative error and CPU time for GDQM and FEM.

Figure 4.9 shows that, GDQM requires more CPU time to solve the problem than FEM, for the same number of nodes considered. This is mainly due to the fact that it requires more effort to solve the dense and asymmetric stiffness matrices produced by GDQ method compared to the sparse and symmetric stiffness matrices obtained with FEM. Nevertheless, the computational effort required to achieve a desired accuracy is smaller for GDQ method since it shows much better convergence characteristics when compared to FEM. Similar findings have also been reported in [70], where the CPU time and accuracy are compared between GDQM and commercial FEM software.

4.4.2 Parametric Analysis for the Sandwich Plates

The effect of geometric properties as well as the choice of core material on damping and vibration characteristics of a rectangular sandwich plate with clamped boundary conditions will be analyzed in this section. The material for the composite base and constraining layers are selected as carbon fiber reinforced plastic (CFRP) with the material properties given in Table 4.10. The shear modulus and loss factor of the viscoelastic core are calculated from Eqs. (2.20) and (2.22) together with the data in Table 2.1. The iterative approach described in Section 3.4.1 is used with the error tolerance, ξ=0.0001.

Table 4.10: Properties of the composite plate.

CFRP composite layers (Layers 1 and 3)	
Young's modulus	E_{11}=138.6 GPa, E_{22}=8.27 GPa
Shear modulus	G_{12}=G_{13}=4.96 GPa, G_{23}=4.12 GPa
Density	ρ_1=ρ_3=1824 kg/m^3
Poisson's ratio	ν_{12}=0.26
Loss Factor	η_1=η_3=0.003
Thickness	Variable
Viscoelastic layer (Layer 2)	
Shear modulus	G_2= $G_2(\omega)$ (Table 2.1)
Density	ρ_2 (Table 2.1)
Poisson's ratio	ν_2=0.5
Loss Factor	η_2= $\eta_2(\omega)$ (Table 2.1)
Thickness	Variable
Whole plate	
Length	a=0.3 m, b=0.4 m

As mentioned before, though the loss factors of elastic face layers are usually quite small when compared with the loss factor of the viscoelastic material, it may not be safe to omit them since the contribution to the total loss factor of the structure is proportional with the stored strain energy [32]. The loss factors of CFRP's usually vary in the range $0.001<\eta<0.005$ [58]; therefore, an approximate average value $\eta=0.003$ is attributed to the CFRP material in order to include the damping contribution of the face layers.

In addition, to be on the safe side, the results obtained with GDQM are compared with the results of the recent FEM model with a 15x20 mesh.

The effect of lamination angle of the constraining layer on the fundamental frequency and loss factor is presented in Figure 4.10. The plate section is geometrically symmetrical and the base layer is held at a constant lamination angle, $\theta_3=0°$. Figure shows that the frequency and the loss factor are maximized for a symmetric layup (0/core/0). The loss factor has its greatest values when the core material is a damping polymer from 3M. Moreover, the maximum values of the frequency and the minimum values of the loss factor belong to a DYAD 609 core. An interesting point observed is that the loss factor of the sandwich plate is almost constant with the lamination angle of the constraining layer, when the core material is EAR C-1002.

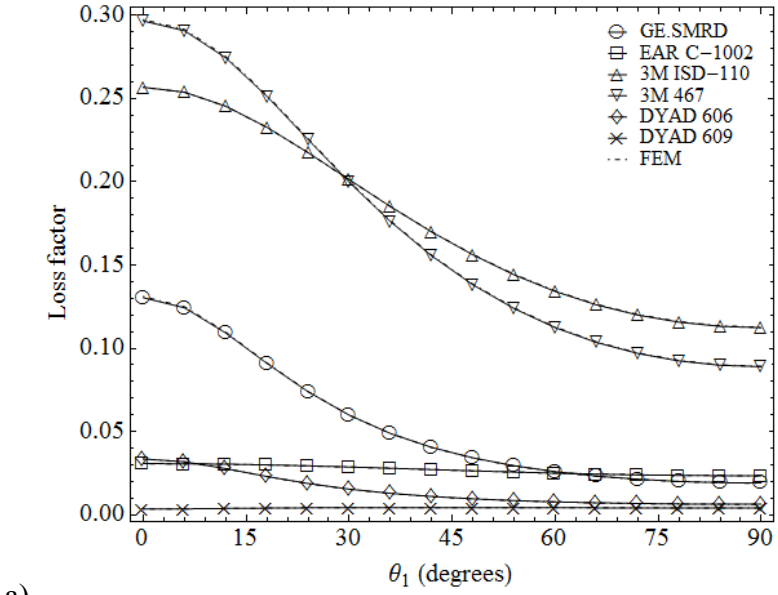

a)

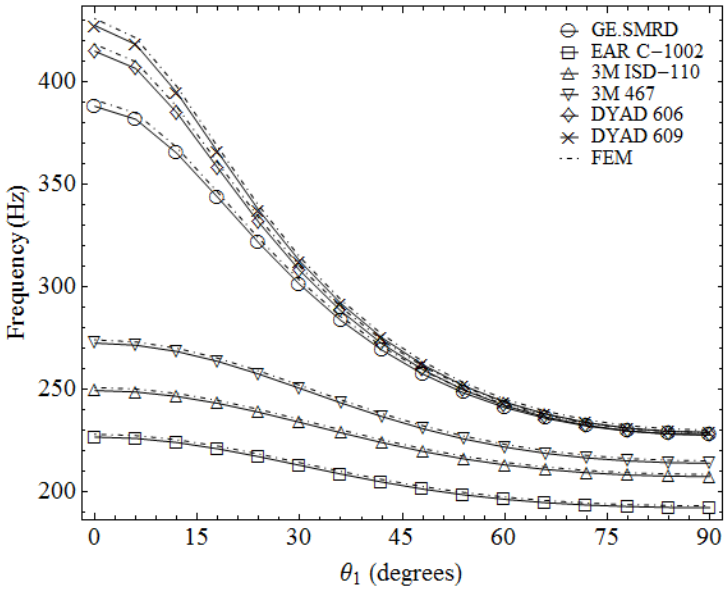

b)

Figure 4.10: Variation with the angle of lamination of the constraining layer (h_1=2mm, h_2=0.2mm, h_3=2mm): a) loss factor; b) frequency.

The effect of face layer thicknesses on the vibration and damping characteristics of the sandwich plate is shown in Figure 4.11, where the base and constraining layers are taken of equal thickness. Because of increasing sectional stiffness, the frequency increases with h_1 and h_3 for all types of the core material, as expected. On the other hand, the loss factor has a global maximum at a specific thickness of the face layers for each core material.

Again, the viscoelastic materials from 3M show the best damping characteristics for this plate configuration. Also, note that, the deviation of predicted frequencies between FEM and GDQM solutions increase with increasing thicknesses, h_1 and h_3. This is quite natural since the transverse shear stresses ignored in the FEM model dominate as the thicknesses of the face layers increase and the thin plate model starts to fail.

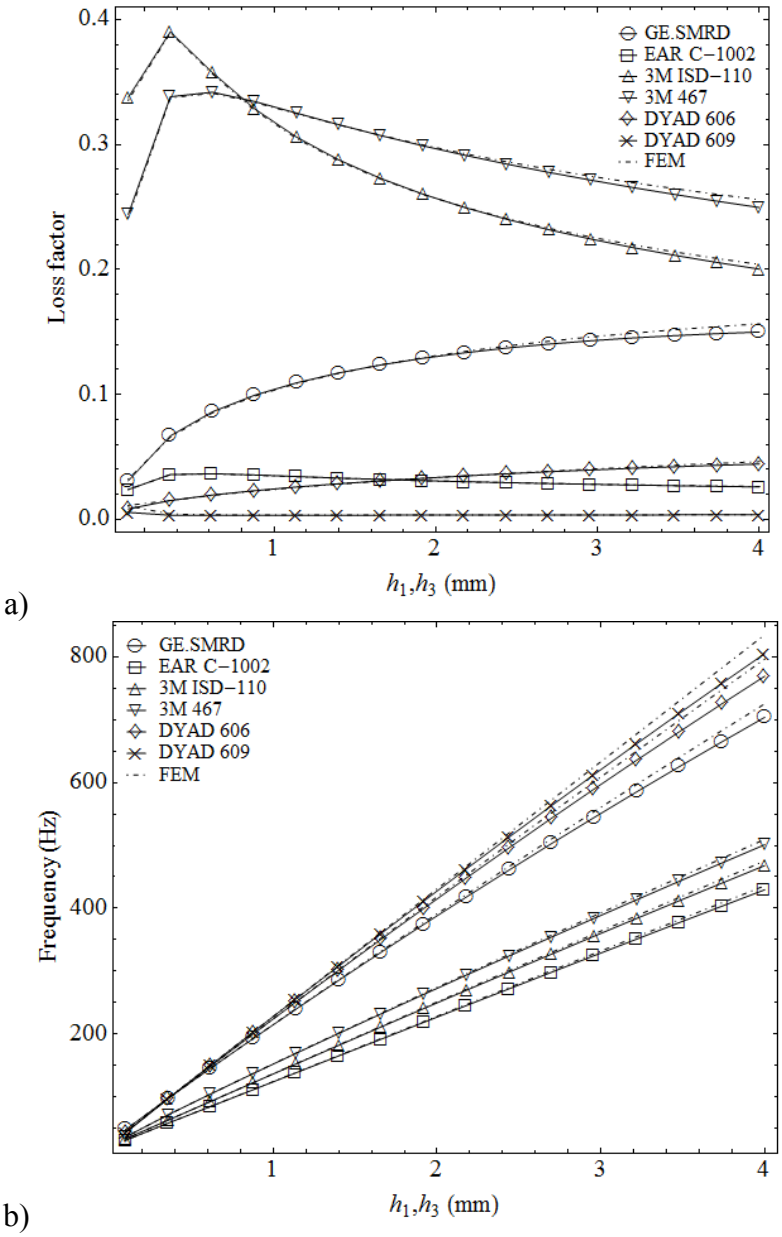

Figure 4.11: Variation with face layer thicknesses for $h_1=h_3$ ($h_2=0.2$mm, $\theta_1=\theta_3=0°$): a) loss factor; b) frequency.

The effect of core thickness on the natural frequency and modal loss factor is presented in Figure 4.12. The frequencies decrease with increasing core thickness for the relatively soft damping materials i.e. 3M ISD-110, 3M 467 and EAR C-1002. Particularly for soft cores, the shear deformation of the core layer increases with its thickness. As a result, the constraining and base layers can no longer be compressed and extended effectively and the stiffness of the plate decreases. For the stiff materials, this effect is vice versa since the core layer can resist shear deformation.

To better visualize this, the deformed plate sections are presented for soft and stiff core materials in Figure 4.13 and Figure 4.14 respectively, for the first mode.

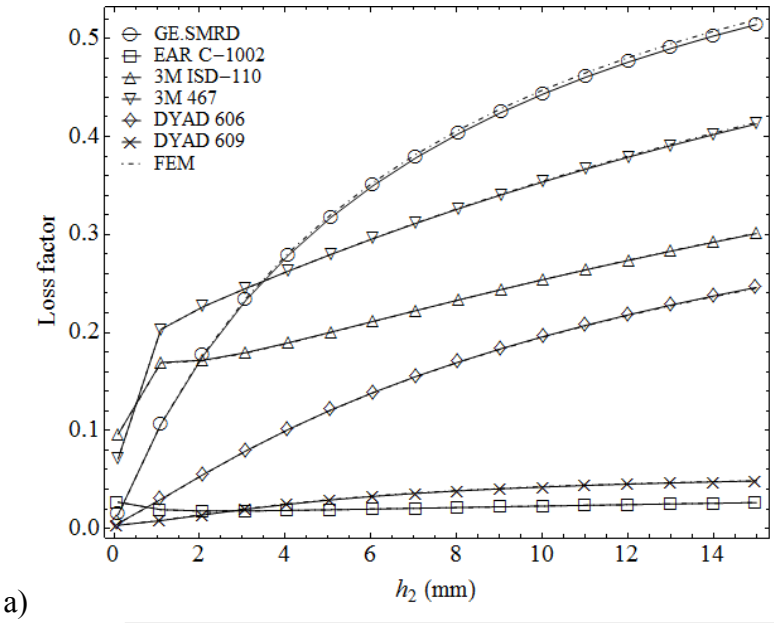

a)

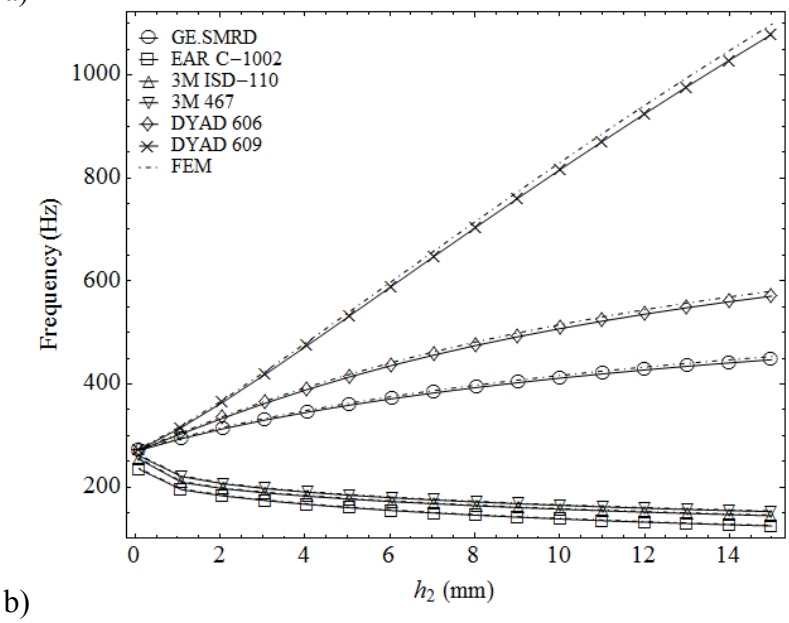

b)

Figure 4.12: Variation with core thickness (h_1=2mm, h_3=3mm, θ_1=0°, θ_3=90°): a) loss factor; b) frequency.

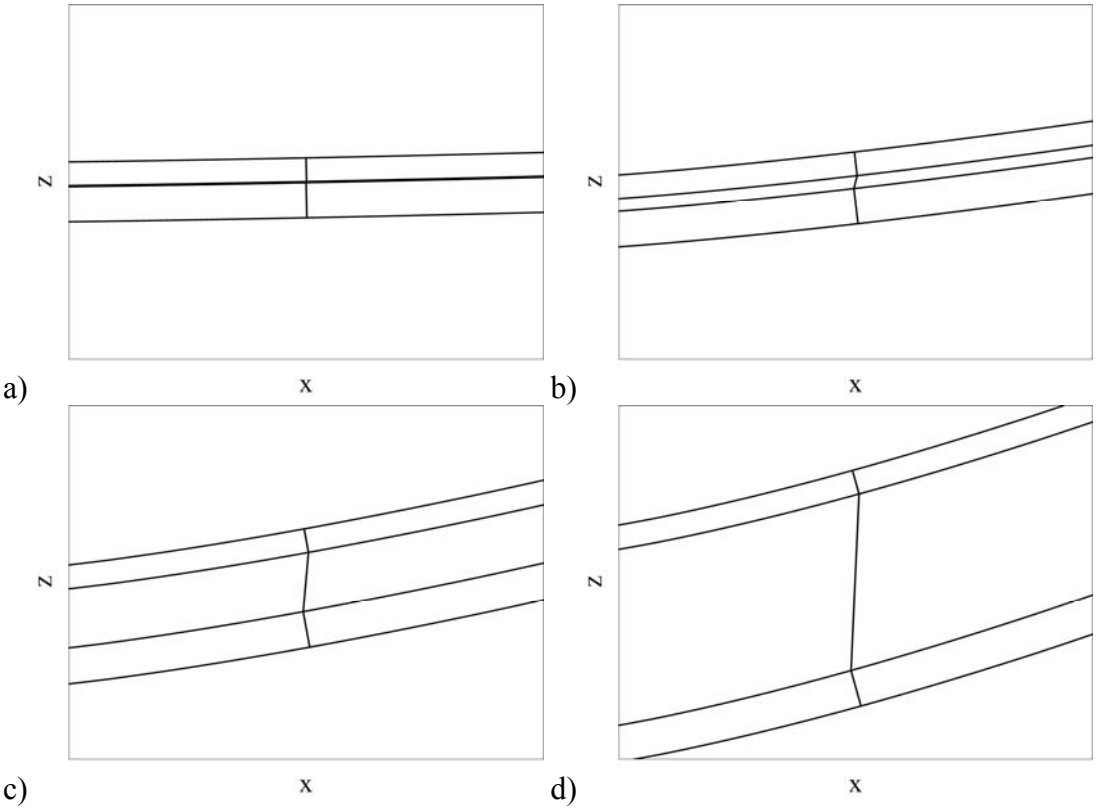

Figure 4.13: Deformed sections for the sandwich plate with soft EAR C-1002 core layer: a) h_2=0.1 mm; b) h_2=1.1 mm; c) h_2=5 mm; d) h_2=15 mm.

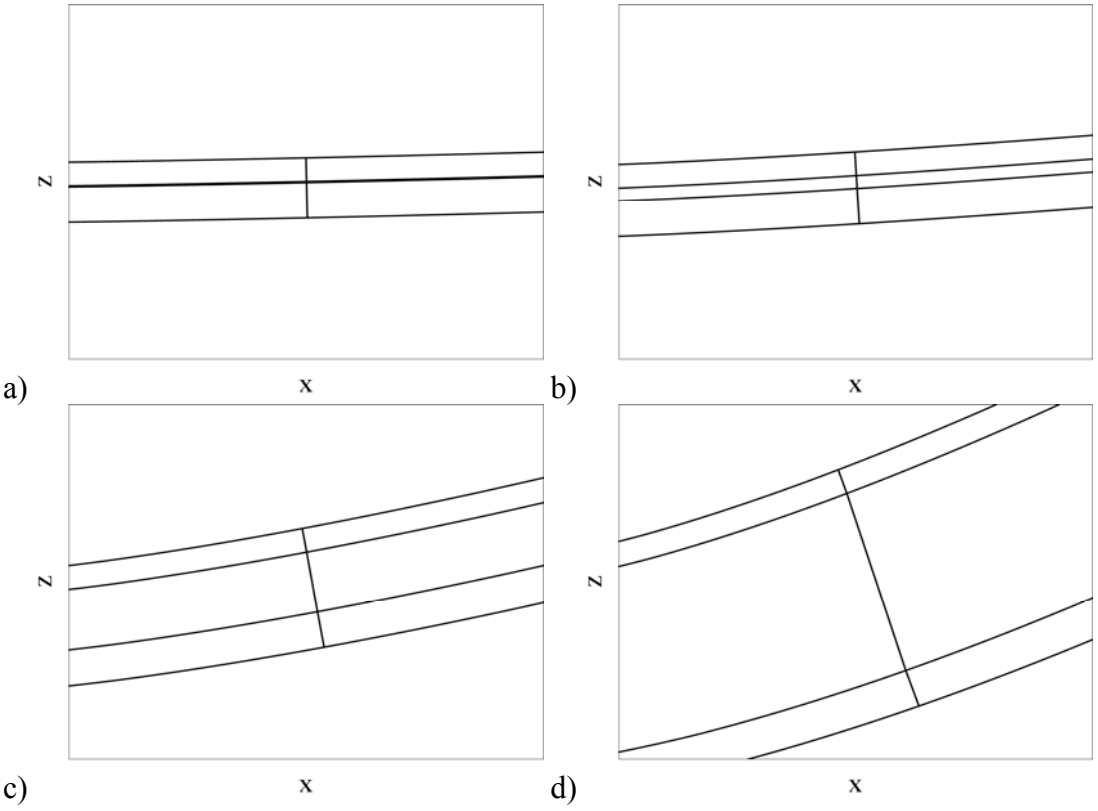

Figure 4.14: Deformed sections for the sandwich plates with stiff DYAD 609 core layer: a) h_2=0.1 mm; b) h_2=1.1 mm; c) h_2=5 mm; d) h_2=15 mm.

On the other hand, Figure 4.12 shows that the modal loss factor tends to increase with core thickness, as expected. As can be deduced from the figure, the best choices of core material in order to achieve better damping results are 3M ISD-110 and 3M 467, for smaller values of h_2. For thicker cores, GE.SMRD seems to be the best choice.

Lastly, the effect of the location of the viscoelastic core inside the plate is shown in Figure 4.15. The maximum values of the modal loss factor correspond to symmetrical configurations, where $h_1=h_3$, for all choices of the core material. This result was observed also for the sandwich beams in the previous section and it is expected since the core experiences the greatest magnitudes of shear stress for symmetrical configurations. On the other hand, this effect seems to be vice versa for the frequency for most of the core materials, i.e. the minimum value of the natural frequency corresponds to the symmetrical case and a deformation of symmetry increases the frequencies.

The best choice, in terms of vibration damping, seems to be 3M 467 for all possible variations of the location of viscoelastic core, for this specific configuration. The matching between the results obtained with FEM and GDQM is quite satisfactory for the loss factor; however, there is some discrepancy between the results obtained with these two methods for the frequency, especially for the stiff core materials and asymmetrical plate sections.

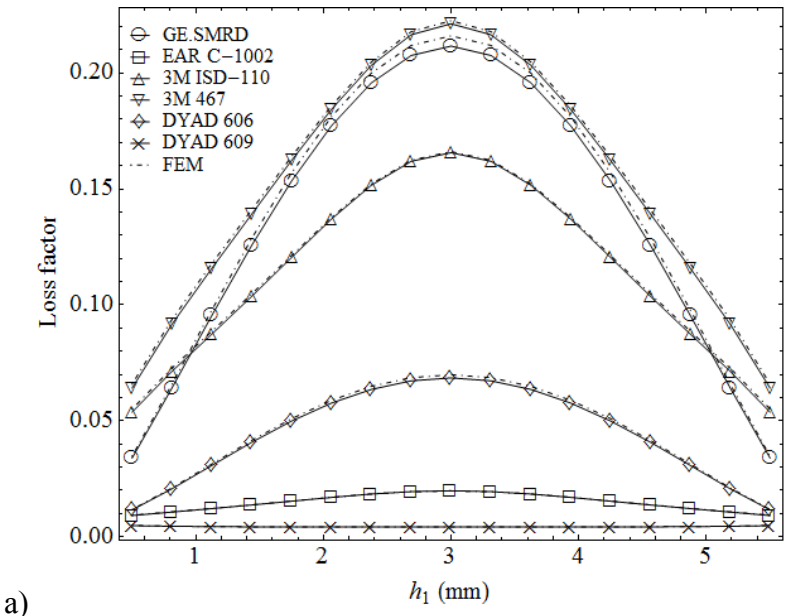

a)

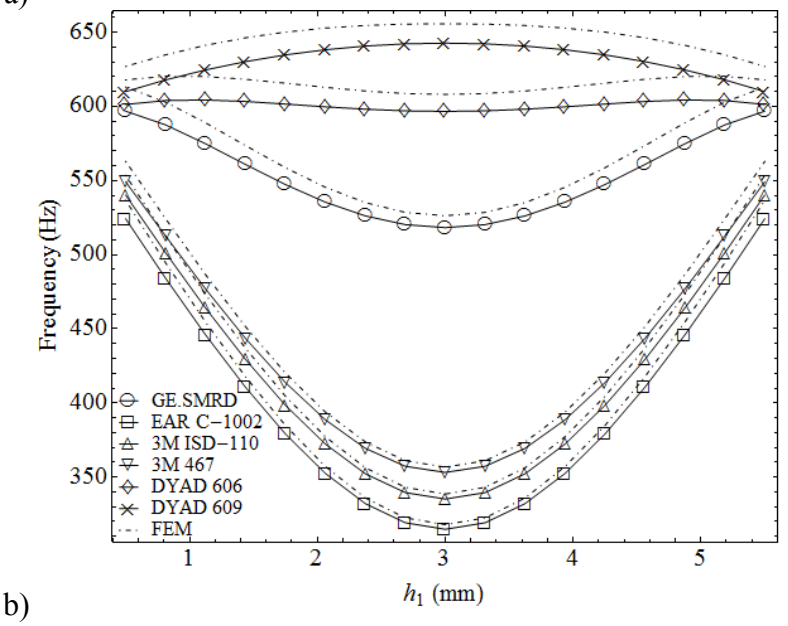

b)

Figure 4.15: Variation with the location of core (h_1+h_3=6mm, h_2=0.4mm, θ_1=0°, θ_3=0°): a) loss factor; b) frequency.

5. OPTIMIZATION VIA GENETIC ALGORITHMS

Genetic Algorithms (GAs) are heuristic search methods, firstly proposed by Holland in 1975 [71]. These methods are based on the principles that govern natural selection and genetics and they belong to the family of evolutionary algorithms (EAs).

Genetic algorithms have found great application due to their advantages over gradient-based methods. Firstly, they can be applied to any kind of optimization problem being discrete, continuous or a combination of both as long as they can be formulated into an objective function [72]. Another great advantage is that the GAs are highly suitable for parallel computations [72]. Due to this property of genetic algorithms, computation time can be substantially reduced if a grid of computers or a single computer with multiple CPU's is utilized.

5.1 Basic Principles of GAs

The solution of optimization problems by genetic algorithms holds a strong analogy to the basic principles of biological evolution [73]. Due to this property of GAs, Holland [71] chose to use the terminology of biology and described the basic structures that a GA manipulates as chromosomes. A chromosome, also called as a genome, is a structure that consists of a set of parameters, which define a proposed solution to the optimization problem:

$$\arg\max_{x \in X} f \tag{5.1}$$

with

$$f : X \to \mathbb{R} \tag{5.2}$$

Here, X is the search space, f is the objective function to be maximized and x is the vector of decision variables encoded into chromosomes. To be more specific, one can say that each chromosome is a solution candidate to the optimization problem defined by Eq. (5.1).

The chromosomes consist of genes, which are single bits or small blocks of neighboring bits that encode a particular element of the vector of decision variables *x*. The success of a chromosome is determined by the corresponding value of the objective function *f* and named as the fitness. A chromosome and the genes that it contains are presented in Figure 5.1 as an example:

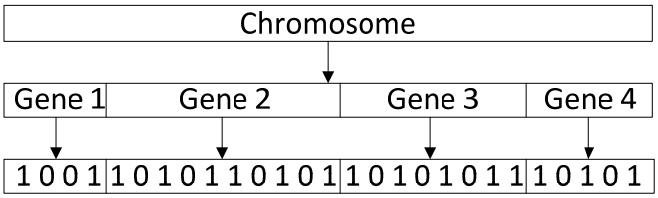

Figure 5.1: Representation of a chromosome.

A chromosome is a sequence of genes and the one presented in Figure 5.1 consists of four genes of different number of bits. The total length of the chromosome is named as the string length and the position of a gene in a string is called as the locus. The set of values that a gene can assume is named as alleles, which is an important term that will be used frequently. Also, the actual genetic structure that represents an individual is called as genotype and it's observed characteristics as an organism is called as phenotype.

The number of bits in a gene determines the number of intervals that the decision variable is to be divided into. If there are n number of bits in a gene, then the size of an interval would be:

$$\Delta = \frac{x_{\max} - x_{\min}}{2^n - 1} \tag{5.3}$$

where, x_{max} and x_{min} correspond to the upper and lower bounds of the actual decision variable respectively and Δ is the size of the interval.

Genetic algorithms are iterative procedures, which operate on a number of solution candidates encoded into chromosomes. Each of these chromosomes is named as an individual. The group of these individuals collectively comprises the population, which undergo a process called reproduction that transforms the current population into a new one.

This reproduction process is carried out with the elements of genetic algorithms, which are selection, crossover and mutation. A simple GA flowchart is presented in Figure 5.2, which summarizes the algorithm explained previously. The elements of GAs and the genetic operators are explained in the following text in detail.

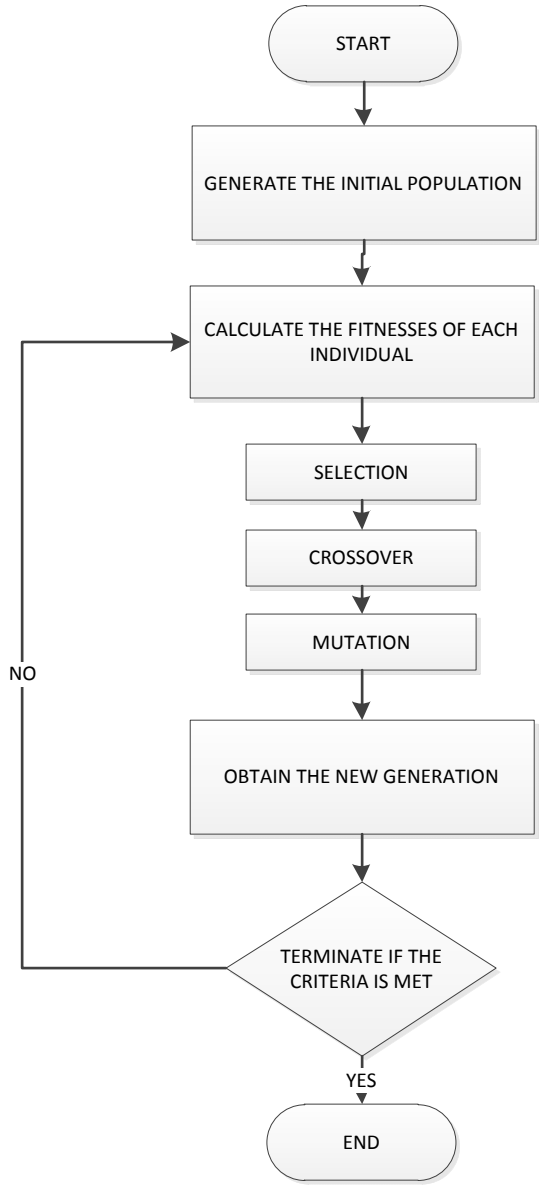

Figure 5.2: A simple genetic algorithm flowchart.

5.1.1 Encoding

Encoding is the process of representing individual genes in a chromosome, which strongly depends on the characteristics of the problem considered. Encoding can be performed in many different ways such as bits, numbers, arrays or any other object [72]. The possible encoding techniques are presented as follows:

- *Binary encoding*: This is the most commonly used encoding method, mainly because the pioneering works on GA used this type of encoding. The chromosomes consist of binary strings, where the genes can be either 1 or 0. The binary encoding has problems associated with the Hamming cliff [74], which describes the effect that some neighboring phenotypes are represented by completely different genotypes. As a result, a small disturbance in the chromosome results in a big variation on the decision variables, which is not a desired condition.

- *Gray encoding*: To overcome the drawbacks of the binary encoding, Gray encoding was proposed by Gray in 1953 [75]. With this technique, it is possible to encode every two neighboring phenotypes by neighboring genotypes. A comparison between the binary encoding and the Gray encoding for a four-bit string is presented in Table 5.1.

- *Permutation encoding*: In this technique, every chromosome is a string of numbers, which represents a sequence. This type of encoding is used in the ordering problems such as task ordering and the travelling salesman problem.

- *Value encoding*: Every chromosome is a string of values, which can be anything as long as connected with the optimization problem. The values can be real numbers, characters, objects etc. They can be quite useful where the decision variable cannot be formulated with binary form. This type of encoding often requires developing new types of mutation and crossover, which are problem-specific.

Table 5.1: Binary vs. Gray encoding.

Decimal	Binary	Gray	Decimal	Binary	Gray
0	0000	0000	8	1000	1100
1	0001	0001	9	1001	1101
2	0010	0011	10	1010	1111
3	0011	0010	11	1011	1110
4	0100	0110	12	1100	1010
5	0101	0111	13	1101	1011
6	0110	0101	14	1110	1001
7	0111	0100	15	1111	1000

5.1.2 Initial Population

First set of candidate solutions, namely individuals, are usually generated randomly and named as the initial population. A major problem is to determine the optimal population size, since a too small population would not allow sufficient room for exploring the search space effectively and a too large population would impair the efficiency of the method that no solution could be expected in a reasonable amount of time. The first attempt to determine a suitable population size was made by Goldberg using the idea of schemata [76]. This study revealed out that, the population size should increase as an exponential function of the string length.

It is necessary that the initial population should have a gene pool as large as possible, in order to be able to explore the search space efficiently. The problem of determining the minimum population size for a meaningful search to take place was solved by Reeves [77]. This principle is simply based on the idea that every point in the search space should be reachable from the initial population by crossover only. Assuming that the initial population is generated by a random sample with replacement (a member of the population can be picked up more than once) the probability that at least one allele is present at each locus can be derived for the binary strings as follows [78]:

$$P = (1-(1/2)^{N-1})^{l} \tag{5.4}$$

where, P is the probability, N is the number of individuals in the initial population and l is the string size. By using an exponential function approximation:

$$P \approx \exp\left(-l/2^{N-1}\right) \tag{5.5}$$

One can arrive at the following approximate solution [78]:

$$N \approx 1+\frac{\log\left(-l/\log(P)\right)}{\log\left(2\right)} \tag{5.6}$$

Also, note that, Eq. (5.4) has an exact solution that seems to be overlooked in Ref. [78]:

$$N = 1 - \frac{\log\left(1 - P^{1/l}\right)}{\log(2)} \tag{5.7}$$

As indicated by Reeves et al. [78], a population of size N=17 is sufficient to ensure that the required probability exceeds %99.9 for strings of length 50. However, it is important to note that, Eqs. (5.6) and (5.7) present a measure to determine the number of individuals a population should have for the search to be meaningful. As a result, it can be understood as a lower bound of the population size. On the other hand, an optimal number of individuals a population should contain is usually larger than this number in practical applications.

As mentioned before, it is easier to explore the search space with larger populations. Goldberg has shown that for a GA to reach the global optimum instead of local ones is mainly determined by the size of population [76]. A large population is quite useful however; it requires more CPU time and memory when compared to using a small population. This can be a major drawback for cases where it is expensive to evaluate an objective function. Also, it is important to note that the computation time required for a GA to converge is of order *O*(NlogN) function evaluations [72]. Therefore, determining an appropriate size for the initial population is very important in GAs.

5.1.3 Crossover (Recombination)

Crossover is the process of producing child solutions from the genotypes of two parent solutions. The chromosome strings of parents are cut at one or more randomly chosen positions and then swapped to produce two full-length chromosomes.

Crossover operator is applied to the individuals selected from the mating pool with the hope of creating better offsprings.

The crossover operator can be applied mainly in there ways:

- *Single point crossover*: The parent chromosomes are cut from a randomly chosen single point producing two head sections and two tail sections. Then the tails are swapped to produce two child solutions (See Figure 5.3).

- *Multiple-point crossover*: This technique is an extension and generalization of the single point crossover. Firstly, n points are determined randomly and then the substrings are swapped between these points. The case when n=2 is presented in Figure 5.4.
- *Uniform crossover*: In this method, each gene in the offspring is taken from one or the other parent. For this purpose, a binary crossover mask of the size of chromosome is generated randomly. If there is a 1 in the crossover mask, the gene is copied from the first parent and if there is a 0, it is copied from the second. The number of effective crossover point is not fixed in this method (See Figure 5.5).

There are also some problem-specific crossover techniques such as three parent crossover, crossover with reduced surrogate, shuffle crossover, precedence preservative crossover, ordered crossover and partially matched crossover etc. However, these are not commonly used ones and the details of these techniques are available in [72].

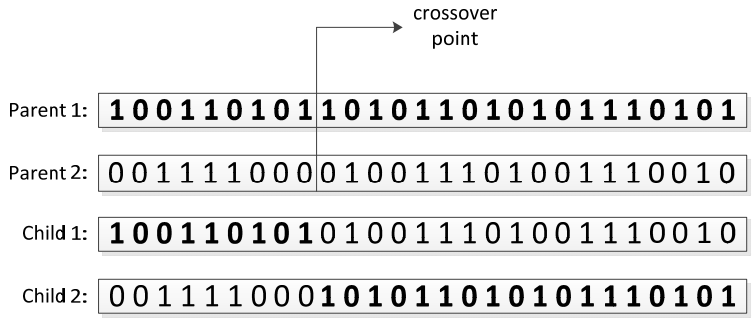

Figure 5.3: Representation of single point crossover operator.

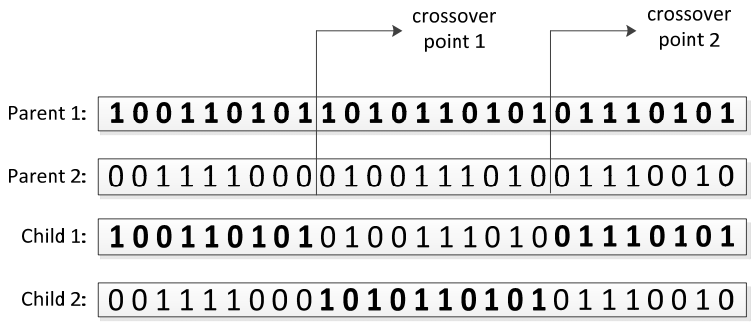

Figure 5.4: Representation of multi-point crossover operator.

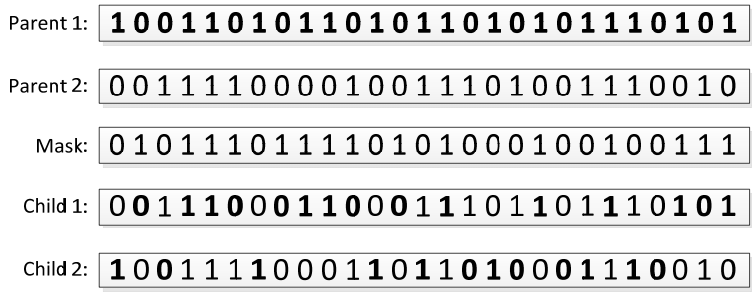

Figure 5.5: Representation of uniform crossover operator.

The traditional GA uses single point crossover. It should be noted that adding more crossover points reduces the performance of GAs [72] in terms of convergence speed. However, using a multiple point crossover or uniform crossover may have the benefit of exploring the search space more thoroughly. By this way, the algorithm to converge to a local extrema may also be avoided.

An important parameter in crossover is the crossover probability P_c. Having a crossover probability as $P_c=0$ means that this operator won't be used while producing the new population and the chromosomes will be exactly same with the old ones. On the other hand, $P_c=1$ corresponds to the case where all individuals of the new population are produced by crossover. Practical applications have shown that letting some individuals to survive in the next generation can slightly improve the convergence characteristics.

5.1.4 Mutation

This operator of GA is applied to the child chromosomes after the crossover and it is analogous to biological mutation. Mutation allows unguided jumps to different areas of the search space, therefore prevents the algorithm to be trapped in a local extrema. It randomly disturbs the genetic information and introduces new genetic structures by randomly modifying its building blocks. The primary objective of the mutation operator is to maintain genetic diversity in the population and help the algorithm to escape from sub-optimal regions of the solution space.

Mutation is applied to the genes of a chromosome with a possibility of P_m, which is usually chosen as a small number ($P_m<<1$). Moreover, this probability is usually taken as 1/(string length) so that only one bit of a chromosome is effected by mutation, averagely.

If there is no mutation (P_m=0), then the offsprings are created by crossover only and they are "genetically pure". If the mutation probability is taken as 1 (P_m=1), the chromosomes are inverted, which means that after an even number of steps in the algorithm, it is like no mutation has taken place at all. A high value for P_m also converts the algorithm to a random search method, which is not a desired condition.

There is no optimal value for the mutation probability and determination of a suitable value for P_m usually depends on the problem considered. There are mainly three ways of applying the mutation operator in GAs:

- *Flipping*: Mutation with flipping is simply changing the value of a bit from 1 to 0 and 0 to 1 based on the mutation mask created randomly (See Figure 5.6).
- *Interchanging*: Two positions in the chromosome is chosen randomly and the values corresponding to these positions are exchanged (See Figure 5.7).
- *Reversing*: A position on the chromosome is chosen randomly and then the values next to this position are reversed (See Figure 5.8).

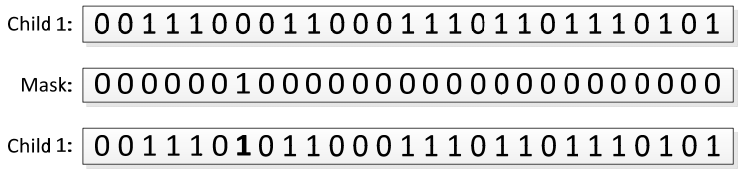

Figure 5.6: Representation of mutation flipping.

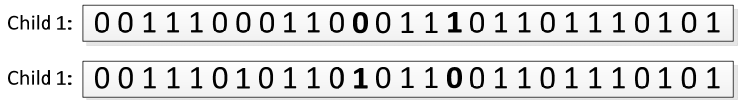

Figure 5.7: Representation of interchanging mutation.

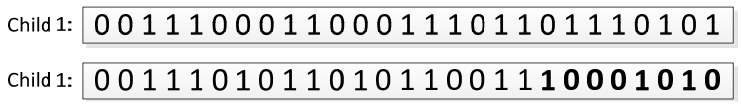

Figure 5.8: Representation of reversing mutation.

5.1.5 Selection

Selection is the process of choosing two parent solutions for crossing. In genetic algorithms, each individual solution is assigned a score, which depends on its fitness value. Naturally, the fitness value is closely related to the objective function to be maximized or minimized. Once a population is generated and the fitnesses are assigned to each candidate solution, the next step is to decide on how to select individuals that will create the next generation. The purpose of selection is to emphasize fitter individuals of the population in the hopes that their offsprings may have better fitness.

There are mainly three ways to accomplish the selection of these individuals, which can be summarized as follows:

- *Roulette-wheel selection (Proportional selection)*: The roulette wheel selection was firstly proposed in Holland's schema theorem. This type of selection uses a probability distribution, where the selection probability of an individual is directly proportional to its fitness. The selection probabilities of individuals are related to their fitnesses with the equation: $p_i = f_i / \sum_{j=1}^{N} f_j$.

  This equation implies that the greater fitness means greater possibility to be selected for crossing. Also, notice that the sum of probabilities is equal to 1. This is a moderately strong selection technique since the fitter individuals are not guaranteed to be selected but have a greater chance.

- *Rank selection*: In this technique, the individuals of the population are ordered according to their fitness. Every chromosome receives fitness from its rank i.e. the worst individual is assigned a fitness of 1 and the best is assigned a fitness of N. This approach results in slow convergence when compared to the roulette wheel selection. In addition, it keeps up the selection pressure when the variation of fitness among the population is low. This technique might be preferable to the classical roulette wheel selection when the fitness values of individuals differ too much. In fact, rank selection gives more chance to weak individuals than the proportional selection, which in turn provides better genetic diversity. A comparison between these two techniques is presented for a population of size N=5 in Figure 5.9.

- *Tournament selection*: This selection strategy depends on selecting *k* number of individuals from the population randomly and choosing the fittest one among them for reproduction. An advantage of this technique is that the selection pressure can be adjusted quite easily by choosing an appropriate value for *k*.

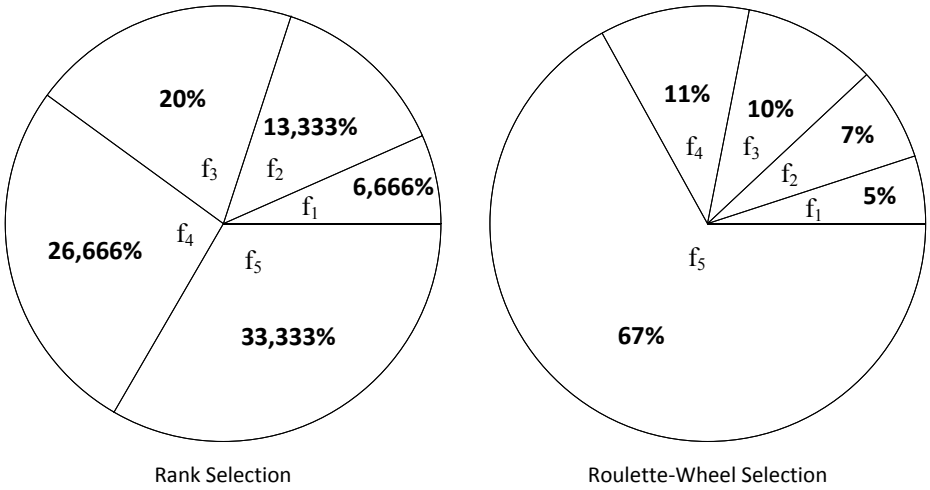

Figure 5.9: Rank selection vs. roulette-wheel selection.

5.1.6 Replacement

The last stage of the breeding cycle is the replacement of the old population with the newly created one. After producing the new population, which consists of child solutions created by mutation and crossover, it is necessary to figure out which of the new candidates should become members of the next generation. The method used for the replacement of old members with the new ones drastically affects the convergence characteristics of GAs. The possible replacement schemes for the GAs are as follows [73]:

- *Random replacement*: In this technique, a fraction of the old population that is chosen arbitrarily is replaced with the new individuals. This obviously decreases the convergence speed of the algorithm, however on the other hand helps to avoid premature convergence by increasing the diversity in the population and decreasing the selective pressure on the search.

- *Generational replacement*: This is the traditional replacement strategy that was proposed by Holland [71], which simply replaces the entire population by its descendants. This kind of selection implies that an individual can only reproduce with individuals from the same generation. From an optimization point of view, this is quite unfeasible since considerable effort might have been spent only to throw away a good solution obtained in the previous generation. In addition, it might happen that the fitness of the best individual decreases at some stage of the evolutionary computation. On the other hand, this strategy might help to avoid the convergence to a local extrema by putting into perspective the dominance of not only one individual but instead the dominance of a few individuals [73].

- *Elitism and population overlapping replacement*: To overcome the drawbacks of the generational replacement technique, De Jong introduced the concept of elitism and population overlaps [79]. In elitism strategy, the best individual of the previous population is not replaced but reserved and the remaining individuals are replaced by the newly produced ones. "Population overlaps" takes this concept one-step further by replacing only a fraction of the population at each generation. Both of these techniques increase the convergence speed of the GAs. However, it theoretically allows immortality of the retained best individuals of the previous generation, which might lead to a premature convergence. If mutation is applied also to the elite in order to prevent this premature convergence, then the replacement mechanism is named as "weak-elitism" [73].

- *Tournament replacement*: Similar to the tournament selection, tournament replacement depends on running competitions between sets of individuals from a pool that consists of the last and the actual generations, where the winners become part of the next generation.

5.1.7 Termination

Unlike the gradient-based optimization techniques, which terminate when a local optimum is reached, GAs are stochastic search methods that could in principle run forever. Therefore, it is necessary to define one or more criterions that terminate the iterative process when met. The commonly used ones are listed below:

- Number of generations run
- CPU time spent for the optimization
- Diversity of the population
    - Population convergence
    - Gene convergence

The convergence of a GA is determined by the likeliness of the individuals in a population. It is assumed that the population has converged, when the average fitness of the population is higher than a user-specified percentage away from the best fitness of the population. On the other hand, the gene convergence is assumed to be reached when a user-specified percentage of the genes that make up a chromosome are alike.

5.2 Optimization Problem

There are many studies devoted to the optimization of sandwich structures with a viscoelastic core, some of which are included in Refs. [32, 33, 68]. In these studies, the objective function is either the modal loss factor or the ratio of the shear strain energy stored in the viscoelastic core to the total stored strain energy, which in turn is related to the loss factor by the following relation [32]:

$$\eta = \sum_{i}^{N} \frac{\eta_i W_i}{W_t} \tag{5.8}$$

where, N is the number of viscoelastic elements, η_i is the material loss factor of the i'th element, W_i is the stored strain energy of i'th element and W_t is the total strain energy. Another approach exists in literature, where the objective function is defined so that an optimum is searched for the design parameters, which try to maximize the modal loss factor while minimizing the total mass of the structure [80].

Considering an objective function, which consists of the modal loss factor only, is somewhat incomplete since the loss factor itself does not give complete information about the response of the structure under a loading condition. In fact, it gives an idea about the resonance peak i.e. the higher the loss factor, the smaller the jump in the vibration amplitude at the resonant frequency.

Therefore, the objective function that is to be maximized is chosen in this work so that an optimum point is searched where the damping of sandwich structure is maximized while minimizing the displacement:

$$\max_{\mathbf{x}} \; f = \frac{1}{|H(0)|} \sum_{i=1}^{N} w_i \eta_i \tag{5.9}$$

subject to

$$\begin{aligned} & m \le m_{\max} \\ & x_i^l \le x_i \le x_i^u, \; i = 1, 2, ..., n \end{aligned} \tag{5.10}$$

where, |H(0)| is the receptance frequency response function (FRF) magnitude at ω=0, **x** is the vector of decision variables, w_i is the weighting coefficient, m_{max} is the maximum allowable mass, x_i^l is the lower bound and x_i^u the upper bound of the decision variable.

One could use the mass of the structure as a weighted variable of the objective function instead of a constraint, as in Ref. [80]. However, there is a trade-off between the mass and the structural rigidity of the sandwich structure and it may be pointless to decide on the priority of each variable. Therefore, it is found appropriate that the mass of the structure should be a design constraint.

The vector of decision variables for the optimization problem of sandwich beams and plates is as follows:

$$\mathbf{x} = \{M_1, M_2, M_3, \theta_1, \theta_3, h_1, h_2, h_3\} \tag{5.11}$$

where M_1, M_2 and M_3 are the material ID's of the constraining layer, core layer and the base layer respectively. The core layer is allowed to be one of the six viscoelastic materials in Table 2.1. On the other hand, the face layers can be assigned one of the following four composite materials; Carbon Fiber Reinforced Plastic (CFRP), Graphite-Epoxy (Gr-Ep), Glass-Epoxy (Gl-Ep) or Boron-Epoxy (Br-Ep), with the engineering constants presented in Table 5.2.

Table 5.2: Engineering constants of composite materials [81].

ID	Material	E_{11} (GPa)	E_{22} (GPa)	G_{13} (GPa)	G_{23} (GPa)	G_{12} (GPa)	ρ (kg/m^3)	ν_{12}
1	CFRP	138.6	8.27	4.96	4.96	4.12	1824	0.26
2	Gr-Ep (AS)	137.9	8.96	7.20	6.21	7.20	1450	0.30
3	Gl-Ep	53.78	17.93	8.96	3.45	8.96	1900	0.56
4	Br-Ep	206.9	20.69	6.9	4.14	6.9	1950	0.30

The upper bounds of the layer thicknesses are related to the maximum allowable weight of the structure m_{max} and the lower bound can be taken a small value. The angle of lamination of the face layers are considered between 0^0 and 90^0 due the geometrical symmetry of the structures. Then, the constraints in Eq. (5.10) become:

$$\begin{aligned} & m \le m_{\max} \\ & 0° \le \theta_i \le 90°,\ i = 1,3 \\ & 10^{-4} \le h_i \le \frac{m_{\max}}{\rho_{\min} A},\ i = 1,2,3 \\ & M_i = 1,2,3,4,\ i = 1,3 \\ & M_2 = 1,2,...,6 \end{aligned} \tag{5.12}$$

where, ρ_{min} is the density of the material that has the minimum value among the other materials and A is the surface area of the structure. Notice that any value of the thicknesses of the layers beyond this upper limit will automatically fail the first constraint in Eq. (5.12). It is observed in the computations that this approach dramatically decreases the computation time when compared to defining an arbitrary upper bound.

The main objective of this section is to find the set of eight parameters that maximizes the objective function in Eq. (5.9), subject to the constraints in Eq. (5.10). However, before going into the details of GA optimization, it is convenient to mention the frequency response functions that will be used to analyze and interpret the results.

5.2.1 Frequency Response Functions

Frequency response function (FRF) is an effective way of analyzing the vibration characteristics of a dynamical system. Considering the forced vibrations of a sandwich structure in frequency domain, the following equation can be written:

$$\left[\mathbf{K}(\omega)-\omega^2\mathbf{M}\right]\mathbf{u}(\omega)=\mathbf{F}(\omega) \tag{5.13}$$

where, **K**(ω) is the frequency dependent stiffness matrix, **M** is the mass matrix, **u**(ω) is the displacement vector and **F**(ω) is the Fourier transform of the time domain force history. The matrix [**K**(ω) - ω^2**M**] in Eq. (5.13) is known as the dynamic stiffness matrix of a multiple degree of freedom (MDoF) system [82], which is also denoted as **Z**(ω):

$$\mathbf{Z}(\omega)=\left[\mathbf{K}(\omega)-\omega^2\mathbf{M}\right] \tag{5.14}$$

Since this matrix is non-singular for the real values of the frequency ω, the amplitude responses of the system can be obtained as follows:

$$\mathbf{u}(\omega)=\left[\mathbf{Z}(\omega)\right]^{-1}\mathbf{F}(\omega) \tag{5.15}$$

The inverse of the dynamic stiffness matrix **Z**(ω) is defined as the receptance FRF matrix of the system [82]:

$$\mathbf{H}(\omega)=\left[\mathbf{Z}(\omega)\right]^{-1}=\left[\mathbf{K}(\omega)-\omega^2\mathbf{M}\right]^{-1} \tag{5.16}$$

As one can see from Eqs. (5.15) and (5.16), receptance is the displacement per unit force. Therefore, it is a good measure of how much a structure will resists translation when subjected to a given force. When the response and excitation points coincide, the FRF is referred to as a point FRF and when it does not, it is called a transfer FRF. Assuming that the MDoF system is of n dimensions, the receptance FRF at location *i* due to the force applied at location *j* can be written in the following general form:

$$\frac{u_i(\omega)}{F_j(\omega)}=\sum_{k=1}^{n}\frac{H_{ik}(\omega)F_k(\omega)}{F_j(\omega)} \tag{5.17}$$

For the specific case, where there is only one force applied to the system, we have [82]:

$$\frac{u_i(\omega)}{F_j(\omega)}=H_{ij}(\omega) \tag{5.18}$$

The receptance value is a complex quantity due to the complex stiffness matrix of the system. Therefore, it is necessary to separate this FRF into two parts, which are magnitude and phase:

Magnitude:

$$\left|\frac{u_i(\omega)}{F_j(\omega)}\right| = \sqrt{\mathrm{Re}\left[u_i(\omega)/F_j(\omega)\right]^2 + \mathrm{Im}\left[u_i(\omega)/F_j(\omega)\right]^2} \tag{5.19}$$

Phase angle:

$$\Phi = \tan^{-1}\frac{\mathrm{Im}\left[u_i(\omega)/F_j(\omega)\right]}{\mathrm{Re}\left[u_i(\omega)/F_j(\omega)\right]} \tag{5.20}$$

There are also other types of FRFs such as mobility FRF and accelerance FRF, which correspond to the vibration response of velocity and acceleration respectively. They are related to the receptance FRF with the following simple relations:

$$\text{Mobility FRF}: Y(\omega) = i\omega\frac{u_i(\omega)}{F_j(\omega)} \tag{5.21}$$

$$\text{Accelerance FRF}: A(\omega) = -\omega^2\frac{u_i(\omega)}{F_j(\omega)} \tag{5.22}$$

The half-power bandwidth method is explained in the following text, to give insight about the relation between the loss factor and the FRF of the structure.

Half-power bandwidth method: This method uses the receptance FRF data to determine the modal characteristics such as the natural frequency and the loss factor. The loss factor of a structure can be estimated by using the half-power bandwidth method from the width of the resonance peak as follows [82].

$$\eta = \frac{\omega_b^2 - \omega_a^2}{2\omega_r^2} \tag{5.23}$$

where, ω_r is the resonant frequency and ω_a, ω_b are the half power points, which are located at the right and left sides of the frequency peak with amplitude $|H(\omega_r)|/\sqrt{2}$, as presented in Figure 5.10. Assuming a symmetrical FRF peak, Eq. (5.23) can be simplified as follows:

$$\eta \approx \frac{\omega_b - \omega_a}{\omega_r} \tag{5.24}$$

This method is suitable for lightly damped FRF data with well-separated modes and good frequency resolution. It is usually utilized to extract the natural frequencies and loss factors from experimental data as in Ref. [83].

The comparison of results between the HPB method and the iterative technique introduced in Section 3.4.1 is presented in Table 5.3 for the clamped-free beams of length L=0.4m and the following set of parameters:

$$\mathbf{x} = \{2,\ 1,\ 2,\ 0,\ 0,\ 5,\ h_2,\ 5\} \tag{5.25}$$

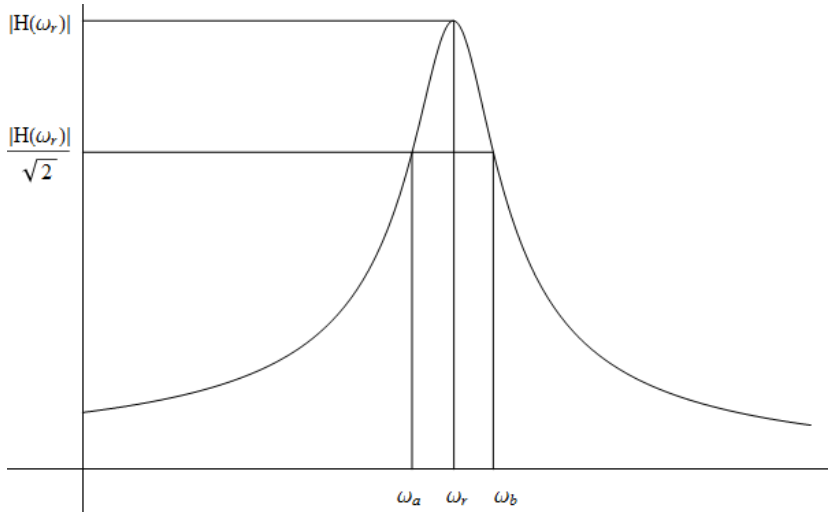

Figure 5.10: Graphical representation of the half-power bandwidth method.

One can realize that, this arbitrarily chosen vector of decision variables correspond to a symmetrical sectioned beam with Gr-Ep face layers and a 3M ISD-110 core (See Table 2.1, Table 5.2 and Eq. (5.11)). The face layer thicknesses are 5mm with 0^0 angle of lamination and the core layer thickness is variable.

Table 5.3: Comparison of results for the fundamental mode.

	Loss factor			Frequency, Hz		
h_2 (mm)	Direct M.	HPB	% Error	Direct M.	HPB	% Error
0.01	0.029819	0.030064	0.820859	97.3264	97.3131	0.013658
0.05	0.110733	0.114627	3.516896	92.0327	92.0832	0.054960
0.1	0.169586	0.179893	6.077547	86.7969	86.7894	0.008598
0.5	0.291962	0.335504	14.91361	67.9485	67.3084	0.941960

Results show good agreement between the iterative technique used in this work, which solves the eigenproblem defined by the dynamical stiffness matrix of the structure and the HPB method, which utilizes the FRF data. The frequency can be quite successfully obtained with either of these methods however; loss factors show some discrepancy especially for the thicker cores. This result is a consequence of the fact that the half-bandwidth method is valid only for lightly damped structures.

5.3 Optimization Parameters and Methodology

The first thing to make a decision on is the choosing of an appropriate encoding to represent the vector of decision variables. The first three parameters are the material ID's of the constraining layer, core layer and the base layer, as presented in Eq. (5.11). As mentioned before, the material ID's of the face layers can take values between 1 and 4, which can be represented successfully by two bits. However, the core layer ID can take values between 1 and 6, therefore it requires at least 3 bits to represent this gene. As a result, two of the possible alleles will not be used since 8 different alleles can be represented by 3 bits, which may affect the convergence speed of the algorithm.

To avoid this possible inefficiency, it is decided that the value encoding would be most suitable for the first three parameters. For the remaining five parameters, Gray encoding is used with a string size of 10 bits for each gene. The chromosome that encodes the vector of decision variables is presented in Figure 5.11.

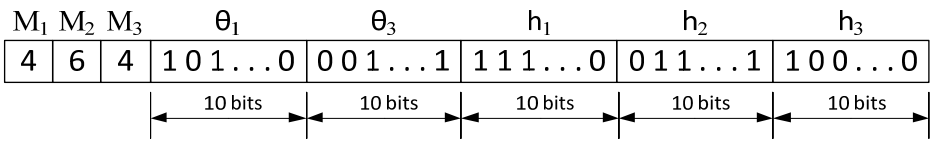

Figure 5.11: Encoding of the optimization parameters.

The total string length of the chromosome presented in Figure 5.11 is 53. By representing each real variable with 10 bits provide a sufficiently small interval size, as can be seen from Eq. (5.3). The GA parameters and the evolutionary strategy that is used in the optimization are summarized as follows:

- The algorithm starts with a large initial population with N=300 individuals to guarantee the required diversity. Then, to speed up the algorithm, the population size is reduced by removing the worst two individuals at each generation until N=60.
- Single point crossover is utilized with a crossover probability P_c=1.
- Flipping mutation is applied for the binary parts of the chromosome (last 50 bits). For the value encoded part (first three genes), the material ID is changed to one of the others randomly, if one of these genes is to be mutated. The mutation probability is not taken as a constant value but it is assigned values linearly changing between 3/(string length) and 0.1/(string length). This approach is also supported by Pham et al.; since it is likely there are few good solutions in the population in first generations, it is preferable to start with a high mutation probability to accelerate the search [84].
- The classical roulette-wheel is used as the selection method.
- The replacement of the old population with the new one is carried out by means of weak elitism.
- The algorithm termination is carried out after 400 generations, G=G_{max}=400.

A detailed flowchart of the optimization algorithm is presented in Figure 5.12.

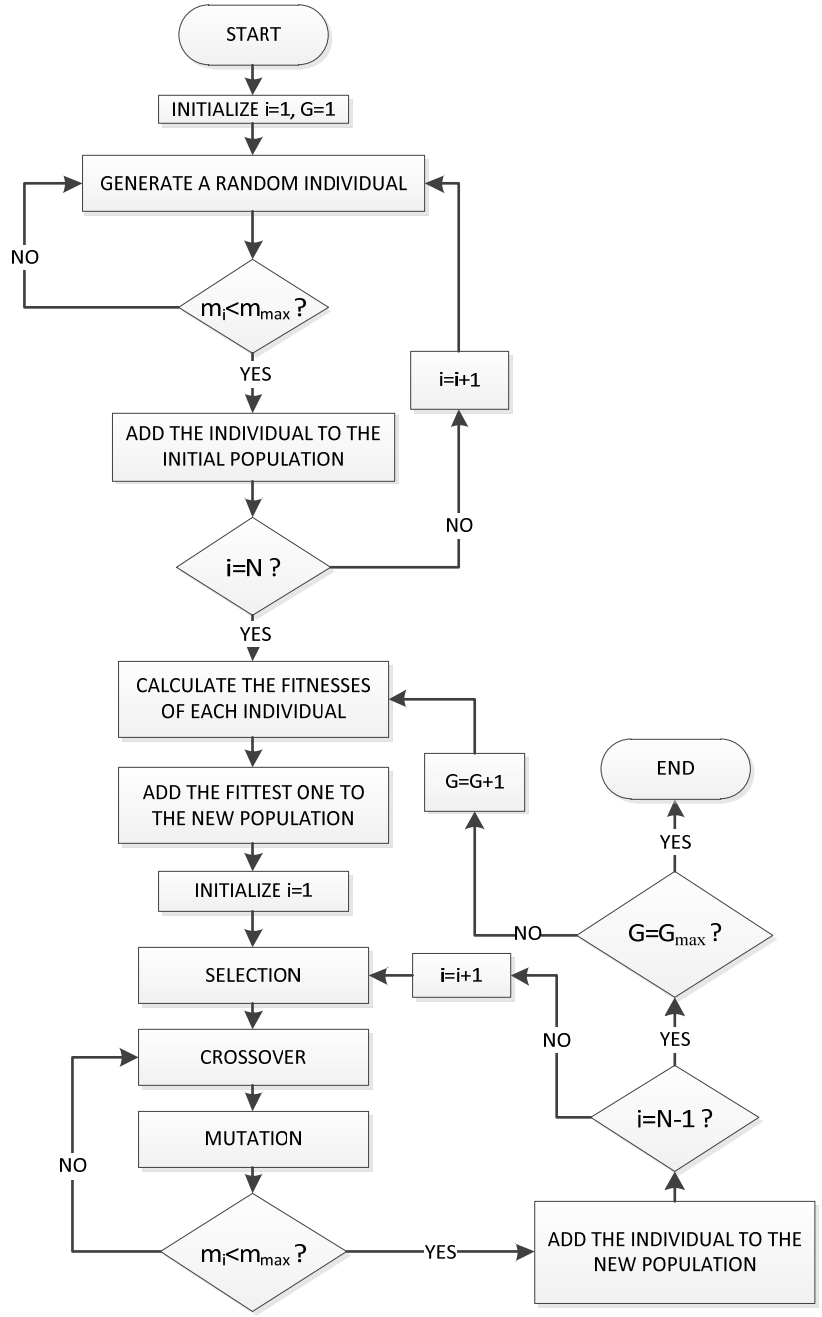

Figure 5.12: Optimization algorithm.

5.4 Optimization Results

5.4.1 Results for the Sandwich Beams

In this section, the vector of decision variables that maximize the objective function in Eq. (5.9), for a three-layered sandwich beam with clamped free boundary conditions will be searched by the genetic algorithm method. The finite element model presented in Section 3.3 with a mesh of 10 elements is utilized.

In the computations, it is observed that taking into account only the fundamental loss factor in the objective function is sufficient. The beam length is taken as L=0.4 m and assumed to have unit width. Then, the optimization problem and constraints can be summarized as follows:

$$\max_{\mathbf{x}} \; f = \frac{1}{|H(0)|}\eta_1 \text{, where } \mathbf{x} = \{M_1,\, M_2,\, M_3,\, \theta_1,\, \theta_3,\, h_1,\, h_2,\, h_3\} \tag{5.26}$$

subject to:

$$\begin{aligned} & m \le m_{\max} \\ & 0° \le \theta_i \le 90°,\; i = 1,3 \\ & 10^{-4} \le h_i \le \frac{m_{\max}}{1450 \times 0.4},\; i = 1,3 \\ & 10^{-4} \le h_2 \le \frac{m_{\max}}{709 \times 0.4} \\ & M_i = 1,2,3,4,\; i = 1,3 \\ & M_2 = 1,2,...,6 \end{aligned} \tag{5.27}$$

The receptance FRF |H(0)| is obtained at the free end of the beam with a point load applied to this location. The optimization results for different values of the allowable mass are presented in Table 5.4.

Table 5.4: Optimization results for the clamped-free sandwich beam.

	m_{max} = 1 kg									
	M_1	M_2	M_3	θ_1	θ_3	h_1,mm	h_2,mm	h_3,mm	m,kg	OBJ: f
Initial 1	4	6	4	45.924	36.686	0.101	0.169	0.460	0.526	0.0282
Initial 2	1	5	4	20.147	88.241	0.216	0.872	0.177	0.543	0.7021
Initial 3	4	3	1	67.478	65.015	0.551	0.617	0.148	0.776	0.3676
Optimal	2	1	2	0	0	0.373	1.486	0.361	1.000	1035.33
	m_{max} = 2 kg									
	M_1	M_2	M_3	θ_1	θ_3	h_1,mm	h_2,mm	h_3,mm	m,kg	OBJ: f
Initial 1	3	6	4	60.528	27.889	0.870	1.451	0.209	1.579	15.207
Initial 2	2	2	3	82.874	42.229	1.402	0.603	0.773	1.661	115.253
Initial 3	1	1	4	50.850	81.994	0.284	2.968	0.105	1.435	143.174
Optimal	4	5	4	0	0	0.562	3.995	0.549	2.000	8650.48
	m_{max} = 3 kg									
	M_1	M_2	M_3	θ_1	θ_3	h_1,mm	h_2,mm	h_3,mm	m,kg	OBJ: f
Initial 1	4	5	4	76.188	33.607	1.330	2.747	0.153	1.936	214.44
Initial 2	2	6	2	59.824	36.686	1.437	2.716	0.207	2.366	47.732
Initial 3	3	6	4	67.214	67.654	0.802	0.338	1.060	1.612	1.6023
Optimal	4	5	4	0	0	0.763	6.284	0.797	3.000	38884

The initial designs presented in Table 5.4 correspond to the randomly selected individuals of the initial population. The optimal designs for all values of the allowable mass correspond to symmetrical or near-symmetrical configurations, where $M_1=M_3$, $\theta_1=\theta_3$ and $h_1=h_3$, which is consistent with the parametric analyses carried out in Section 3.4.2 . Another important point is that the objective function has its greatest values at $\theta_1=\theta_3=0$ degrees for all variations of m_{max}. Receptance FRFs and the variation of average and optimal objective functions with respect to the generation number are presented in Figures 5.13-5.15 for different vales of the m_{max}.

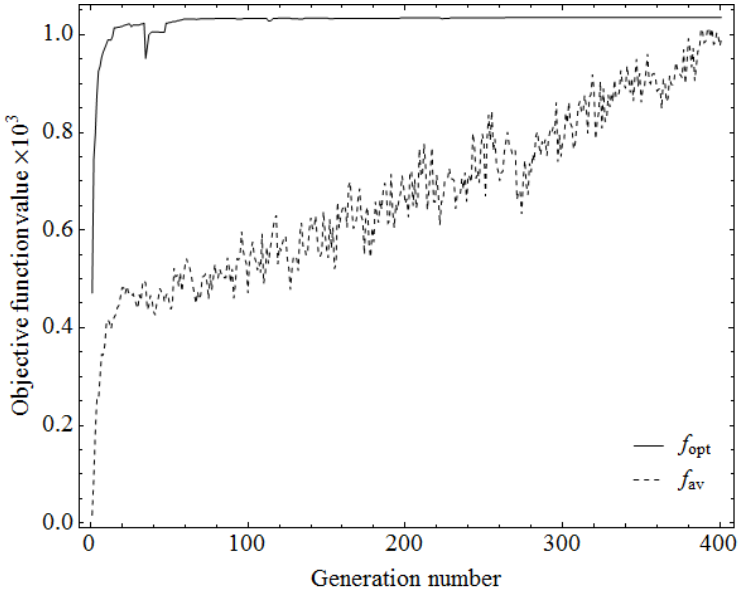

a)

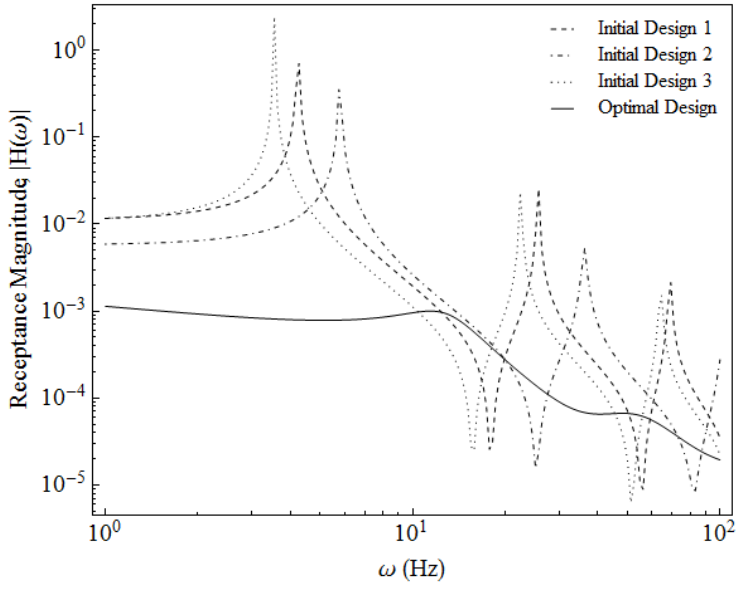

b)

Figure 5.13: Optimization results for sandwich beams, m_{max}=1 kg: a) variation of average and optimal objective functions with generation number; b) receptance magnitude for the initial and final designs.

Figures show fast convergence of the GA approach used in this work i.e.; it is usually sufficient to continue the iteration up to 100-200 generations for at least a near-optimal solution. One can observe from Table 5.4 that there are great differences between the objective functions of the initial and the optimal designs. The outcomes of these differences on the frequency response of the sandwich beams can be clearly observed from Figure 5.13, Figure 5.14 and Figure 5.15. The initial designs have sharp peaks at the resonant frequencies; moreover, displacements at low frequencies are much greater, when compared with the optimal designs.

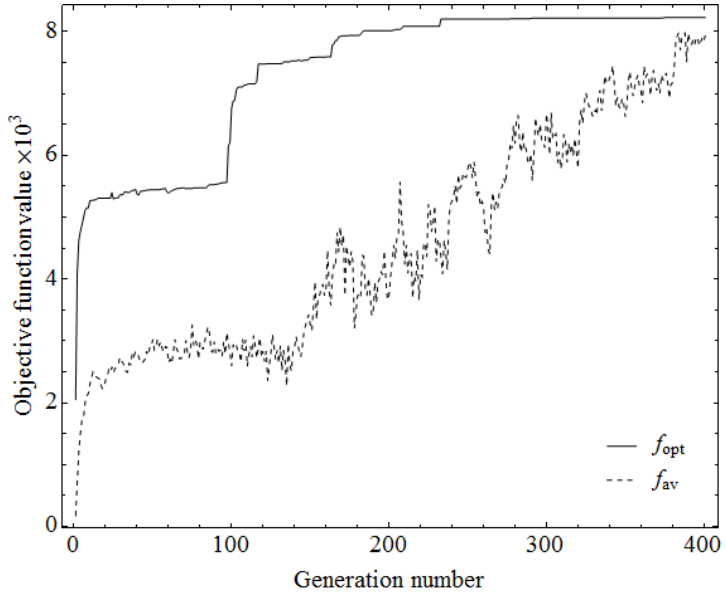

a)

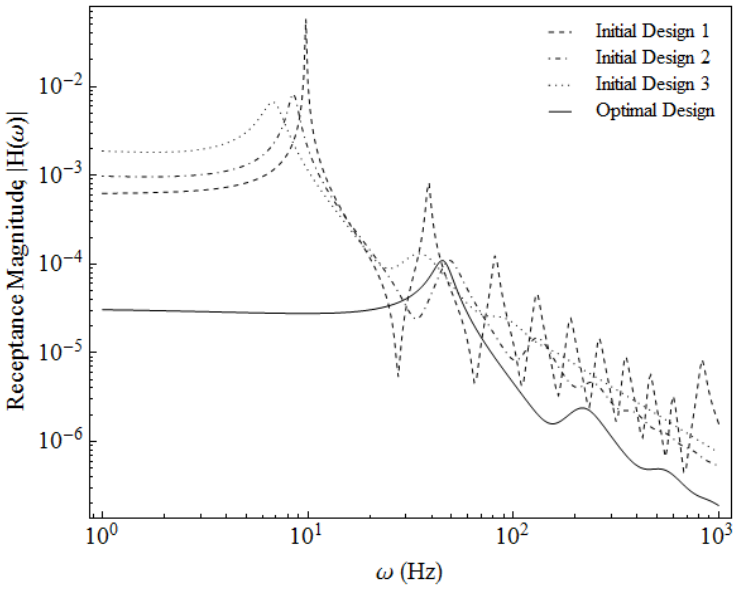

b)

Figure 5.14: Optimization results for sandwich beams, m_{max}=2 kg a) variation of average and optimal objective functions with generation number; b) receptance magnitude for the initial and final designs.

Another interesting result that can be observed from Table 5.4 is that the core layer is much thicker than the face layers for the optimal designs and the ratio between thicknesses of these layers increase with the allowable mass. In the computations, it is observed that optimal designs always have the maximum allowable mass because of the obvious trade-off between the mass and the maximum displacement of the structure.

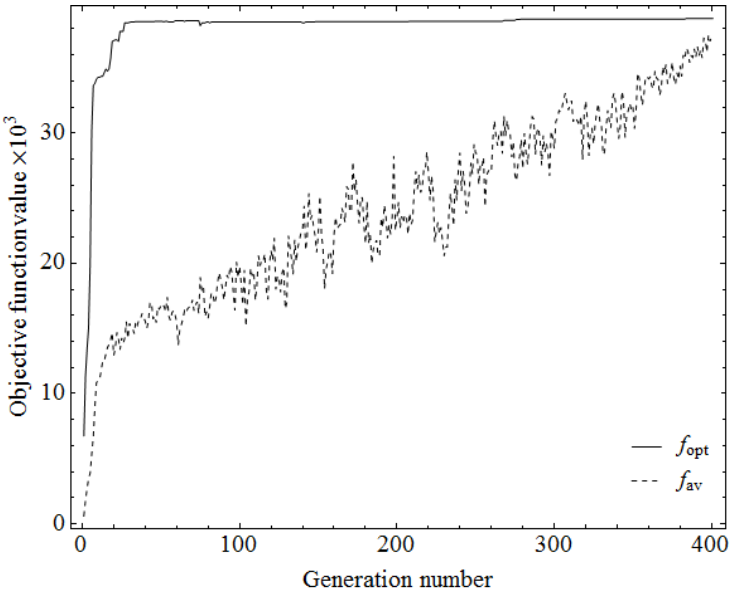

a)

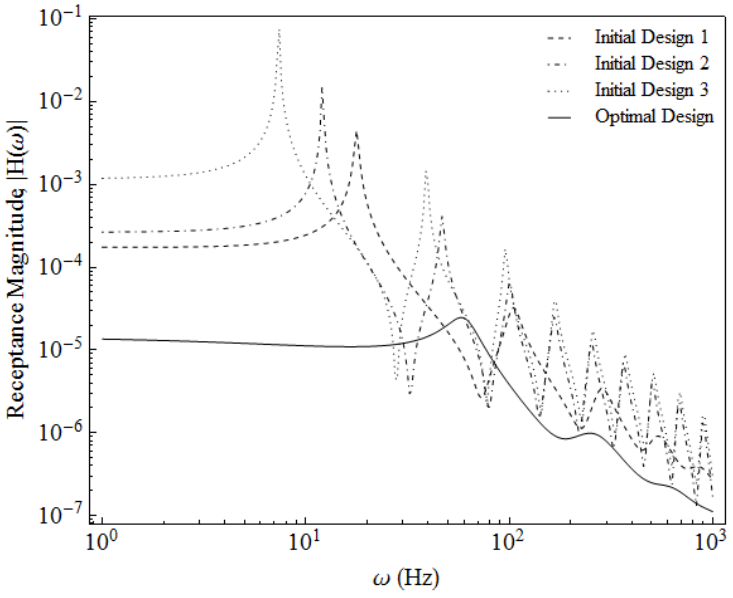

b)

Figure 5.15: Optimization results for sandwich beams, m_{max}=3 kg: a) variation of average and optimal objective functions with generation number; b) receptance magnitude for the initial and final designs.

5.4.2 Results for the Sandwich Plates

In the light of the previous section and the computations carried out, it is found reasonable to consider only the symmetrical configurations, in order to decrease the computational cost. In this case, the chromosome that encodes the decision variables becomes:

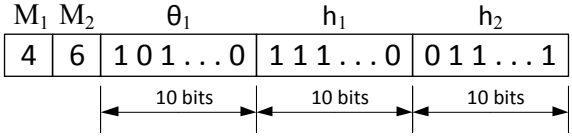

Figure 5.16: Encoding of the optimization parameters for three-layered symmetrical-sectioned plates.

Since the string length of the chromosome decreases to 32 bits for the symmetrical sections, the mutation rate should be increased accordingly i.e., it should change linearly between 3/32 and 0.1/32. For a symmetrical-sectioned plate with dimensions a=0.3m and b=0.4m, the optimization problem and constraints can be summarized as follows:

$$\max_{\mathbf{x}} \; f = \frac{1}{|H(0)|}\eta_1 \text{, where } \mathbf{x} = \{M_1,\, M_2,\, \theta_1,\, h_1,\, h_2\} \tag{5.28}$$

subject to:

$$\begin{aligned} & m \le m_{\max} \\ & 0° \le \theta_1 \le 90° \\ & 10^{-4} \le h_1 \le \frac{m_{\max}}{2\times 1450\times 0.3\times 0.4} \\ & 10^{-4} \le h_2 \le \frac{m_{\max}}{709\times 0.3\times 0.4} \\ & M_1 = 1,2,3,4 \\ & M_2 = 1,2,...,6 \end{aligned} \tag{5.29}$$

with:

$$M_3 = M_1,\; h_3 = h_1 \text{ and } \theta_3 = \theta_1 \tag{5.30}$$

Notice that, only the loss factor at the fundamental frequency is taken into consideration, as it was done in the previous section.

The solutions are carried out by using GDQM with a 7x9 grid distribution. The receptance point FRF |H(0)| is obtained at the center of the sandwich plate and the optimization results are presented in Table 5.5.

Table 5.5: Optimization results for the clamped sandwich plates.

				m_{max} = 0.5 kg			
	$M_{1,3}$	M_2	$\theta_{1,3}$	$h_{1,3}$, mm	h_2 ,mm	m, kg	OBJ: f
Initial 1	2	4	30.176	0.198	0.738	0.167	52.8305
Initial 2	1	4	34.839	0.157	0.761	0.170	64.2018
Initial 3	3	2	52.346	0.418	0.950	0.314	505.535
Optimal	4	5	0	0.369	3.846	0.500	28233.2
				m_{max} = 1 kg			
	$M_{1,3}$	M_2	$\theta_{1,3}$	$h_{1,3}$, mm	h_2 ,mm	m, kg	OBJ: f
Initial 1	1	4	67.126	0.480	1.594	0.339	378.584
Initial 2	4	5	28.416	0.154	1.686	0.433	2839.77
Initial 3	4	2	35.191	1.789	0.203	0.468	34812.5
Optimal	2	5	0	2.635	0.973	1.000	146680
				m_{max} = 2 kg			
	$M_{1,3}$	M_2	$\theta_{1,3}$	$h_{1,3}$, mm	h_2 ,mm	m, kg	OBJ: f
Initial 1	4	6	8.798	3.854	0.996	1.081	12158.4
Initial 2	4	3	38.710	1.044	4.742	0.818	11841.5
Initial 3	2	5	31.584	0.652	1.709	1.002	11184.0
Optimal	2	5	0	5.598	0.606	2.000	891271

The optimal configurations for sandwich plates have the maximum allowable mass, $m=m_{max}$, as it was observed for the optimization results of sandwich beams. Again, the optimal solutions have zero angle of lamination i.e. the fibers are oriented in x direction. This is quite natural since in this case, the sides of the plate with smaller distance between each other are connected with fibers, which in turn increases the rigidity of the structure. The optimal solution has a thicker core compared to its face layers for m_{max} = 0.5 kg and for the other two cases this is vice versa. In addition, one can realize from Table 5.5 that, the difference between the thicknesses of core and face layers increase with the value of m_{max}.

The variation of optimal and average solutions and the receptance FRF of initial and final designs are presented in Figure 5.17, Figure 5.18 and Figure 5.19.

The figures show rapid fluctuations especially for the first generations due to weak-elitism used in the algorithm to maintain the genetic diversity. Nevertheless, the convergence is attained before the maximum number of generations is reached, partly with the help of linearly decreasing mutation rate.

The FRF data in these figures show a great difference between initial and optimal solutions proving that the optimization algorithm is successful. In previous sections, it was claimed that an objective function that consists of the modal loss factor only was not a proper choice, since the loss factor does not give complete information about the dynamical response of the structure. Figure 5.17b verifies this claim since the initial design 3 and the optimal solution have similar loss factors, which are 0.483 and 0.499 respectively; however, there is a great difference between the frequency responses.

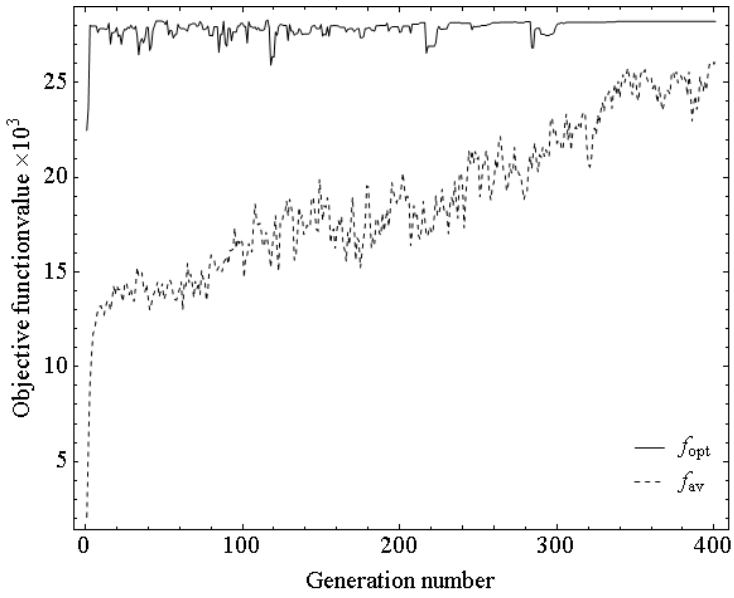

a)

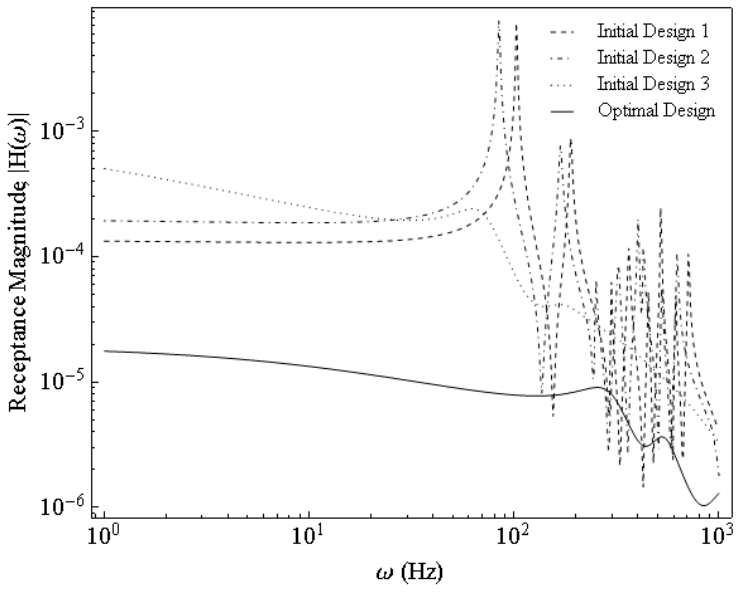

b)

Figure 5.17: Optimization results for sandwich plates, m_{max}=0.5 kg: a) variation of average and optimal objective functions with generation number; b) receptance magnitude for the initial and final designs.

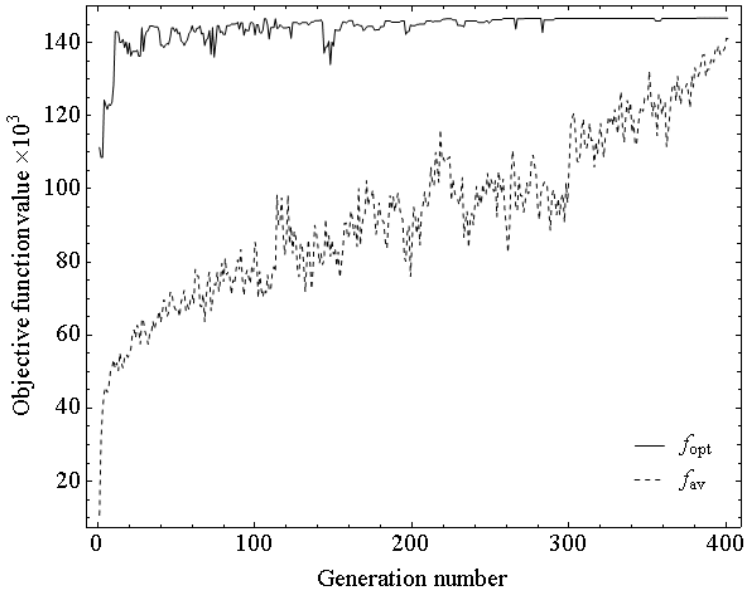

a)

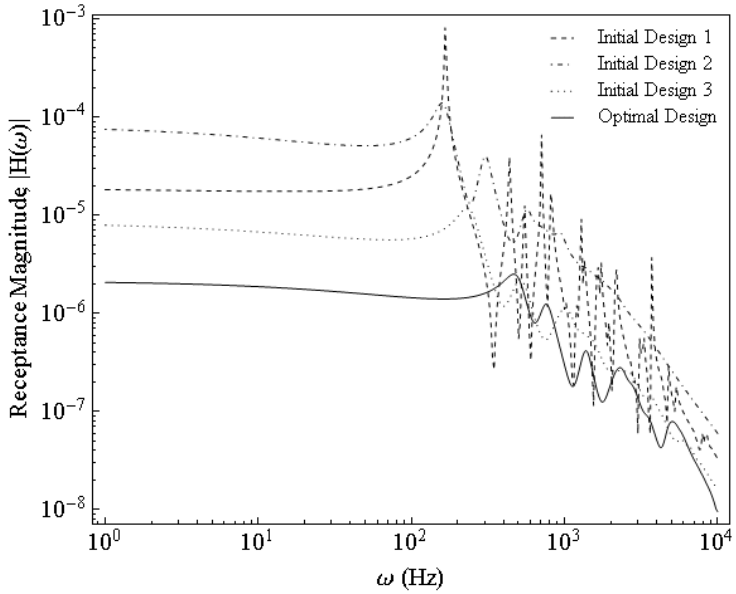

b)

Figure 5.18: Optimization results for sandwich plates, m_{max}=1 kg: a) variation of average and optimal objective functions with generation number; b) receptance magnitude for the initial and final designs.

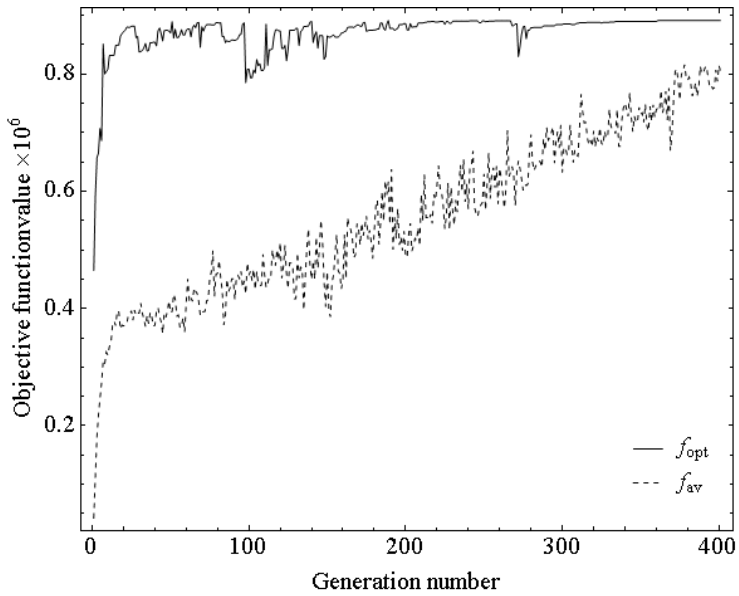

a)

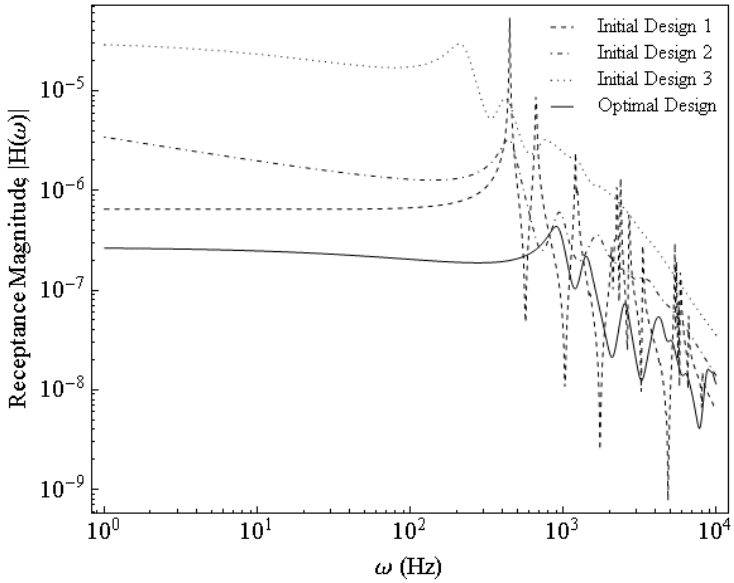

b)

Figure 5.19: Optimization results for sandwich plates, m_{max}=2 kg: a) variation of average and optimal objective functions with generation number; b) receptance magnitude for the initial and final designs.

6. CONCLUSION

This thesis presents the multi-parameter damping optimization of composite sandwich beams and plates with a frequency dependent viscoelastic core. The core layer is modeled with the five-parameter Zener model and the master curves for four commercial damping polymers are obtained by using the experimental data that exist in literature. The governing equations and boundary conditions of sandwich beams and plates are obtained by using the principle of virtual work. Then, the eigenvalue problems defined by these equations are solved by using DTM and GDQM for the first time. Effect of system parameters i.e., the layer thicknesses, materials used in the layers and the lamination angle of the face layers, on the loss factor and frequency are thoroughly studied. Results are validated against the ones that exist in literature when possible. For other cases, the validation is carried out against the currently developed FEM models. Lastly, the optimal configurations that provide the best damping are determined by using the genetic algorithms. The following conclusions can be drawn from the present study:

- Five-parameter Zener model can quite successfully capture the viscoelastic behavior.
- Numerical results show that DTM and GDQM can be successfully used in the vibration analysis of sandwich structures, as robust and accurate alternatives to FEM.
- The results of parametric analyses and optimization show that the configurations that provide the best vibration damping correspond to symmetrical sections.
- The face layers of optimal configurations always have 0° angle of lamination for clamped-free sandwich beams. For the clamped rectangular plates, it is either 0° or 90° depending on the dimensions.

- The optimal configurations for beams have thicker cores when compared with their face layers. For the plates, the ratio between the core layer thickness and the face layer thicknesses varies with the maximum allowable mass.
- The materials of layers that provide the best damping also vary with the maximum allowable mass. There is not a single configuration of the layer materials, which provide the best damping for all cases. The best choices for the face layers are either Gr-Ep or Br-Ep and for the core layer either 3M ISD-110 or GE.SMRD.

The future studies that can be carried out, by following the analyses presented in this thesis, can be listed as follows:

- The effect of temperature can be investigated; the optimal configurations can be searched for different operating temperatures.
- Vibration analysis and optimization can be carried out for multi-layered beams and plates with multiple viscoelastic cores.
- The method presented here can be extended for the analysis of sandwich shells.

REFERENCES

[1] **Golla, D. F., and Hughes, P. C.** (1985). Dynamics of Viscoelastic Structures - a Time-Domain, Finite-Element Formulation. *Journal of Applied Mechanics-Transactions of the Asme*. Vol. **52**, no. 4, pp. 897-906.

[2] **Mctavish, D. J., and Hughes, P. C.** (1993). Modeling of Linear Viscoelastic Space Structures. *Journal of Vibration and Acoustics-Transactions of the Asme*. Vol. **115**, no. 1, pp. 103-110.

[3] **Lesieutre, G. A., and Bianchini, E.** (1995). Time Domain Modeling of Linear Viscoelasticity Using Anelastic Displacement Fields. *Journal of Vibration and Acoustics-Transactions of the Asme*. Vol. **117**, no. 4, pp. 424-430.

[4] **Galucio, A. C., Deu, J. F., and Ohayon, R.** (2004). Finite Element Formulation of Viscoelastic Sandwich Beams Using Fractional Derivative Operators. *Computational Mechanics*. Vol. **33**, no. 4, pp. 282-291.

[5] **Pritz, T.** (2003). Five-Parameter Fractional Derivative Model for Polymeric Damping Materials. *Journal of Sound and Vibration*. Vol. **265**, no. 5, pp. 935-952.

[6] **Zhou, J. K.** (1986). Differential Transformation and Its Application for Electrical Circuit. Huazhong University Press, Wuhan.

[7] **Arikoglu, A., and Ozkol, I.** (2005). Solution of Boundary Value Problems for Integro-Differential Equations by Using Differential Transform Method. *Applied Mathematics and Computation*. Vol. **168**, no. 2, pp. 1145-1158.

[8] **Arikoglu, A., and Ozkol, I.** (2008). Solutions of Integral and Integro-Differential Equation Systems by Using Differential Transform Method. *Computers & Mathematics with Applications*. Vol. **56**, no. 9, pp. 2411-2417.

[9] **Arikoglu, A., and Ozkol, I.** (2006). Solution of Differential-Difference Equations by Using Differential Transform Method. *Applied Mathematics and Computation*. Vol. **181**, no. 1, pp. 153-162.

[10] **Arikoglu, A., and Ozkol, I.** (2006). Solution of Difference Equations by Using Differential Transform Method. *Applied Mathematics and Computation*. Vol. **174**, no. 2, pp. 1216-1228.

[11] **Arikoglu, A., and Ozkol, I.** (2007). Solution of Fractional Differential Equations by Using Differential Transform Method. *Chaos Solitons & Fractals*. Vol. **34**, no. 5, pp. 1473-1481.

[12] **Arikoglu, A., and Ozkol, I.** (2009). Solution of Fractional Integro-Differential Equations by Using Fractional Differential Transform Method. *Chaos Solitons & Fractals*. Vol. **40**, no. 2, pp. 521-529.

[13] **Bellman, R., Casti, J., and Kashef, B. G.** (1972). Differential Quadrature - Technique for Rapid Solution of Nonlinear Partial Differential Equations. *Journal of Computational Physics*. Vol. **10**, no. 1, pp. 40-52.

[14] **Shu, C., and Richards, B. E.** (1992). Application of Generalized Differential Quadrature to Solve 2-Dimensional Incompressible Navier-Stokes Equations. *International Journal for Numerical Methods in Fluids*. Vol. **15**, no. 7, pp. 791-798.

[15] **Ross, D., Ungar, E. E., and Kerwin, E. M.** (1959). "Damping of Plate Flexural Vibrations by Means of Viscoelastic Laminae", Structural Damping; Papers Presented at a Colloquium on Structural Damping Held at the Asme Annual Meeting in Atlantic City, N.J., in December 1959. American Society of Mechanical Engineers, New York,.

[16] **Kerwin, E. M.** (1959). Damping of Flexural Waves by a Constrained Viscoelastic Layer. *Journal of the Acoustical Society of America*. Vol. **31**, no. 7, pp. 952-962.

[17] **Ditaranto R. A.** (1965). Theory of Vibratory Bending for Elastic and Viscoelastic Layered Finite-Length Beams. *Journal of Applied Mechanics*. Vol. **32**, no. 4, pp. 881-886.

[18] **Mead, D. J., and Markus, S.** (1969). Forced Vibration of a 3-Layer, Damped Sandwich Beam with Arbitrary Boundary Conditions. *Journal of Sound and Vibration*. Vol. **10**, no. 2, pp. 163-175.

[19] **Mead, D. J., and Markus, S.** (1970). Loss Factors and Resonant Frequencies of Encastre Damped Sandwich Beams. *Journal of Sound and Vibration*. Vol. **12**, no. 1, pp. 99-112.

[20] **Sadasiva. Y. V., and Nakra, B. C.** (1974). Vibrations of Unsymmetrical Sandwich Beams and Plates with Viscoelastic Cores. *Journal of Sound and Vibration*. Vol. **34**, no. 3, pp. 309-326.

[21] **Lu, Y. P., Killian, J. W., and Everstine, G. C.** (1979). Vibrations of 3 Layered Damped Sandwich Plate Composites. *Journal of Sound and Vibration*. Vol. **64**, no. 1, pp. 63-71.

[22] **Johnson, C. D., and Kienholz, D. A.** (1982). Finite-Element Prediction of Damping in Structures with Constrained Viscoelastic Layers. *AIAA Journal*. Vol. **20**, no. 9, pp. 1284-1290.

[23] **Lall, A. K., Asnani, N. T., and Nakra, B. C.** (1988). Damping Analysis of Partially Covered Sandwich Beams. *Journal of Sound and Vibration*. Vol. **123**, no. 2, pp. 247-259.

[24] **Cupial, P., and Niziol, J.** (1995). Vibration and Damping Analysis of a 3-Layered Composite Plate with a Viscoelastic Mid-Layer. *Journal of Sound and Vibration*. Vol. **183**, no. 1, pp. 99-114.

[25] **Kung, S. W., and Singh, R.** (1998). Complex Eigensolutions of Rectangular Plates with Damping Patches. *Journal of Sound and Vibration*. Vol. **216**, no. 1, pp. 1-28.

[26] **Wang, G., Veeramani, S., and Wereley, N. M.** (2000). Analysis of Sandwich Plates with Isotropic Face Plates and a Viscoelastic Core. *Journal of Vibration and Acoustics-Transactions of the Asme*. Vol. **122**, no. 3, pp. 305-312.

[27] **Fasana, A., and Marchesiello, S.** (2001). Rayleigh-Ritz Analysis of Sandwich Beams. *Journal of Sound and Vibration*. Vol. **241**, no. 4, pp. 643-652.

[28] **Ganesan, N., and Bhangale, R. K.** (2006). Thermoelastic Buckling and Vibration Behavior of a Functionally Graded Sandwich Beam with Constrained Viscoelastic Core. *Journal of Sound and Vibration*. Vol. **295**, no. 1-2, pp. 294-316.

[29] **Ganesan, N., Pradeep, V., and Bhaskar, K.** (2007). Vibration and Thermal Buckling of Composite Sandwich Beams with Viscoelastic Core. *Composite Structures*. Vol. **81**, no. 1, pp. 60-69.

[30] **Tang, S. J., and Lumsdaine, A.** (2008). Analysis of Constrained Damping Layers, Including Normal-Strain Effects. *AIAA Journal*. Vol. **46**, no. 12, pp. 2998-3011.

[31] **Yeh, J. Y., and Chen, L. W.** (2004). Vibration of a Sandwich Plate with a Constrained Layer and Electrorheological Fluid Core. *Composite Structures*. Vol. **65**, no. 2, pp. 251-258.

[32] **Mantena, P. R., Gibson, R. F., and Hwang, S. J.** (1991). Optimal Constrained Viscoelastic Tape Lengths for Maximizing Damping in Laminated Composites. *AIAA Journal*. Vol. **29**, no. 10, pp. 1678-1685.

[33] **Lee, D. H., and Hwang, W. S.** (2004). Layout Optimization of Unconstrained Viscoelastic Layer on Beams Using Fractional Derivative Model. *AIAA Journal*. Vol. **42**, no. 10, pp. 2167-2170.

[34] **Jung, B. C., Lee, D. H., and Youn, B. D.** (2009). Optimal Design of Constrained-Layer Damping Structures Considering Material and Operational Condition Variability. *AIAA Journal*. Vol. **47**, no. 12, pp. 2985-2995.

[35] **Araujo, A. L., Martins, P., Soares, C. M. M., Soares, C. A. M., and Herskovits, J.** (2009). Damping Optimization of Viscoelastic Laminated Sandwich Composite Structures. *Structural and Multidisciplinary Optimization*. Vol. **39**, no. 6, pp. 569-579.

[36] **Jones, D. I. G.** (2001). Handbook of Viscoelastic Vibration Damping. J. Wiley, Chichester ; New York.

[37] **Nutting, P. G.** (1921). A New General Law of Deformation. *Journal of the Franklin Institute*. Vol. **191**, pp. 0679-0685.

[38] **Gemant, A.** (1936). A Method of Analyzing Experimental Results Obtained from Elasto-Viscous Bodies. *Physics-a Journal of General and Applied Physics*. Vol. **7**, no. 1, pp. 311-317.

[39] **Blair, G. W. S., and Caffyn, J. E.** (1949). An Application of the Theory of Quasi-Properties to the Treatment of Anomalous Strain-Stress Relations. *Philosophical Magazine*. Vol. **40**, no. 300, pp. 80-94.

[40] **Blair, G. W. S., Veinoglou, B. C., and Caffyn, J. E.** (1947). Limitations of the Newtonian Time Scale in Relation to Non-Equilibrium Rheological States and a Theory of Quasi-Properties. *Proceedings of the Royal Society of London Series a-Mathematical and Physical Sciences*. Vol. **189**, no. 1016, pp. 69-87.

[41] **Caputo, M., and Mainardi, F.** (1971). A New Dissipation Model Based on Memory Mechanism. *Pure and Applied Geophysics*. Vol. **91**, no. 8, pp. 134-147.

[42] **Bagley, R. L., and Torvik, P. J.** (1983). A Theoretical Basis for the Application of Fractional Calculus to Viscoelasticity. *Journal of Rheology*. Vol. **27**, no. 3, pp. 201-210.

[43] **Bagley, R. L., and Torvik, P. J.** (1983). Fractional Calculus - a Different Approach to the Analysis of Viscoelastically Damped Structures. *AIAA Journal*. Vol. **21**, no. 5, pp. 741-748.

[44] **Bagley, R. L., and Torvik, P. J.** (1985). Fractional Calculus in the Transient Analysis of Viscoelastically Damped Structures. *AIAA Journal*. Vol. **23**, no. 6, pp. 918-925.

[45] **Bagley, R. L., and Torvik, P. J.** (1986). On the Fractional Calculus Model of Viscoelastic Behavior. *Journal of Rheology*. Vol. **30**, no. 1, pp. 133-155.

[46] **Torvik, P. J., and Bagley, R. L.** (1984). On the Appearance of the Fractional Derivative in the Behavior of Real Materials. *Journal of Applied Mechanics-Transactions of the Asme*. Vol. **51**, no. 2, pp. 294-298.

[47] **Drozdov, A. D.** (1998). Viscoelastic Structures : Mechanics of Growth and Aging. Academic Press, San Diego, Calif. ; London.

[48] **Shahsavari, R., and Ulm, F. J.** (2009). Indentation Analysis of Fractional Viscoelastic Solids. *Journal of Mechanics of Materials and Structures*. Vol. **4**, no. 3, pp. 523-550.

[49] **Podlubny, I.** (1999). Fractional Differential Equations : An Introduction to Fractional Derivatives, Fractional Differential Equations, to Methods of Their Solution and Some of Their Applications. Academic Press, San Diego.

[50] **Friedrich, C., and Braun, H.** (1992). Generalized Cole-Cole Behavior and Its Rheological Relevance. *Rheologica Acta*. Vol. **31**, no. 4, pp. 309-322.

[51] **Drake, M. L.** (1988). Damping Properties of Various Materials. AFWAL-TR-88-4248

[52] **Yang, W. P., Chen, L. W., and Wang, C. C.** (2005). Vibration and Dynamic Stability of a Traveling Sandwich Beam. *Journal of Sound and Vibration*. Vol. **285**, no. 3, pp. 597-614.

[53] **Shi, Y. M., Sol, H., and Hua, H. X.** (2006). Material Parameter Identification of Sandwich Beams by an Inverse Method. *Journal of Sound and Vibration*. Vol. **290**, no. 3-5, pp. 1234-1255.

[54] **Mace, M.** (1994). Damping of Beam Vibrations by Means of a Thin Constrained Viscoelastic Layer - Evaluation of a New Theory. *Journal of Sound and Vibration*. Vol. **172**, no. 5, pp. 577-591.

[55] **Johnson, C. D., Kienholz, D. A., and Rogers, L. C.** (1981). Finite Element Prediction of Damping in Structures with Constrained Viscoelastic Layers. *Shock and Vibration Bulletin*. Vol. **51**, no. 1, pp. 71-81.

[56] **Kung, S. W., and Singh, R.** (1998). Vibration Analysis of Beams with Multiple Constrained Layer Damping Patches. *Journal of Sound and Vibration*. Vol. **212**, no. 5, pp. 781-805.

[57] **Gao, J. X., and Liao, W. H.** (2005). Vibration Analysis of Simply Supported Beams with Enhanced Self-Sensing Active Constrained Layer Damping Treatments. *Journal of Sound and Vibration*. Vol. **280**, no. 1-2, pp. 329-357.

[58] **Tanimoto, T.** (2002). Carbon-Fiber Reinforced Plastic Passive Composite Damper by Use of Piezoelectric Polymer/Ceramic. *Japanese Journal of Applied Physics Part 1-Regular Papers Short Notes & Review Papers*. Vol. **41**, no. 11B, pp. 7166-7169.

[59] **Arikoglu, A., and Ozkol, I.** (2010). Vibration Analysis of Composite Sandwich Beams with Viscoelastic Core by Using Differential Transform Method. *Composite Structures*. Vol. **92**, no. 12, pp. 3031-3039.

[60] **Arikoglu, A., and Ozkol, I.** (2012). Vibration Analysis of Composite Sandwich Plates by the Generalized Differential Quadrature Method. *AIAA Journal*. Vol. 50, no. 3, pp. 620-630.

[61] **Lall, A. K., Asnani, N. T., and Nakra, B. C.** (1987). Vibration and Damping Analysis of Rectangular Plate with Partially Covered Constrained Viscoelastic Layer. *Journal of Vibration Acoustics Stress and Reliability in Design-Transactions of the Asme*. Vol. **109**, no. 3, pp. 241-247.

[62] **Lin, R. M., Lim, M. K., and Du, H.** (1994). Deflection of Plates with Nonlinear Boundary Supports Using Generalized Differential Quadrature. *Computers & Structures*. Vol. **53**, no. 4, pp. 993-999.

[63] **Tornabene, F., and Viola, E.** (2007). Vibration Analysis of Spherical Structural Elements Using the Gdq Method. *Computers & Mathematics with Applications*. Vol. **53**, no. 10, pp. 1538-1560.

[64] **Zienkiewicz, O. C., and Taylor, R. L.** (2005). The Finite Element Method for Solid and Structural Mechanics. Elsevier Butterworth-Heinemann, Amsterdam ; Boston.

[65] **Gao, J. X., and Shen, Y. P.** (1999). Vibration and Damping Analysis of a Composite Plate with Active and Passive Damping Layer. *Applied Mathematics and Mechanics-English Edition*. Vol. **20**, no. 10, pp. 1075-1086.

[66] **Hu, M. Y., and Wang, A. W.** (2009). Free Vibration and Transverse Stresses of Viscoelastic Laminated Plates. *Applied Mathematics and Mechanics-English Edition*. Vol. **30**, no. 1, pp. 101-108.

[67] **Jeung, Y. S., and Shen, I. Y.** (2001). Development of Isoparametric, Degenerate Constrained Layer Element for Plate and Shell Structures. *AIAA Journal*. Vol. **39**, no. 10, pp. 1997-2005.

[68] **Araujo, A. L., Soares, C. M. M., Soares, C. A. M., and Herskovits, J.** (2010). Optimal Design and Parameter Estimation of Frequency Dependent Viscoelastic Laminated Sandwich Composite Plates. *Composite Structures*. Vol. **92**, no. 9, pp. 2321-2327.

[69] **Araujo, A. L., Soares, C. M. M., Soares, C. A. M., and Herskovits, J.** (2010). Characterisation by Inverse Techniques of Elastic, Viscoelastic and Piezoelectric Properties of Anisotropic Sandwich Adaptive Structures. *Applied Composite Materials*. Vol. **17**, no. 5, pp. 543-556.

[70] **Tornabene, F., and Viola, E.** (2008). 2-D Solution for Free Vibrations of Parabolic Shells Using Generalized Differential Quadrature Method. *European Journal of Mechanics a-Solids*. Vol. **27**, no. 6, pp. 1001-1025.

[71] **Holland, J. H.** (1975). Adaptation in Natural and Artificial Systems : An Introductory Analysis with Applications to Biology, Control, and Artificial Intelligence. University of Michigan Press, Ann Arbor.

[72] **Sivanandam, S. N., and Deepa, S. N.** (2007). Introduction to Genetic Algorithms. Springer, Berlin ; New York.

[73] **Affenzeller, M.** (2009). Genetic Algorithms and Genetic Programming : Modern Concepts and Practical Applications. CRC Press, Boca Raton.

[74] **Schaffer, J. D., Caruana, R. A., Eshelman, L. J., and Das, R.** (1989). A Study of Control Parameters Affecting Online Performance of Genetic Algorithms for Function Optimization. Morgan Kaufmann Pub Inc, San Mateo.

[75] **Gray, F.** (1953). Pulse Code Communications. U.S. Patent 2632058

[76] **Goldberg, D. E.** (1985). Optimal Initial Population Size for Binary-Coded Genetic Algorithms. TCGA Report 85001

[77] **Reeves, C. R.** (1993). Modern Heuristic Techniques for Combinatorial Problems. Halsted Press, New York.

[78] **Reeves, C. R., and Rowe, J. E.** (2003). Genetic Algorithms : Principles and Perspectives : A Guide to Ga Theory. Kluwer Academic Publishers, Boston.

[79] **De Jong, K. A.** (1975). An Analysis of the Behavior of a Class of Genetic Adaptive Systems.

[80] **Hao, M., Rao, M. D., and Schabus, M. H.** (2004). Optimum Design of Multiple-Constraint-Layered Systems for Vibration Control. *AIAA Journal*. Vol. **42**, no. 12, pp. 2448-2461.

[81] **Pradhan, S. C., Ng, T. Y., Lam, K. Y., and Reddy, J. N.** (2001). Control of Laminated Composite Plates Using Magnetostrictive Layers. *Smart Materials & Structures*. Vol. **10**, no. 4, pp. 657-667.

[82] **He, J., and Fu, Z.-F.** (2001). Modal Analysis. Butterworth-Heinemann, Oxford ; Boston.

[83] **Mandal, N. K., Abd Rahman, R., and Leong, M. S.** (2004). Experimental Study on Loss Factor for Corrugated Plates by Bandwidth Method. *Ocean Engineering*. Vol. **31**, no. 10, pp. 1313-1323.

[84] **Pham, D. T., and Karaboga, D.** (1997). Genetic Algorithms with Variable Mutation Rates: Application to Fuzzy Logic Controller Design. *Proceedings of the Institution of Mechanical Engineers Part I-Journal of Systems and Control Engineering*. Vol. **211**, no. 2, pp. 157-167.

CURRICULUM VITAE

Name Surname: Aytaç ARIKOĞLU

Place and Date of Birth: Kayseri, 27/11/1978

E-Mail: arikoglu@itu.edu.tr

B.Sc.: 2002, ITU Aeronautical Engineering

M.Sc.: 2004, ITU Aeronautical and Astronautics Engineering

List of Publications:

- Senalp, A. D., **Arikoglu, A.**, Ozkol, I., and Dogan, V. Z. (2010). Dynamic Response of a Finite Length Euler-Bernoulli Beam on Linear and Nonlinear Viscoelastic Foundations to a Concentrated Moving Force. *Journal of Mechanical Science and Technology*. Vol. 24, no. 10, pp. 1957-1961.

- Komurgoz, G., **Arikoglu, A.**, Turker, E., and Ozkol, I. (2010). Second-Law Analysis for an Inclined Channel Containing Porous-Clear Fluid Layers by Using the Differential Transform Method. *Numerical Heat Transfer Part A-Applications*. Vol. 57, no. 8, pp. 603-623.

- **Arikoglu, A.**, Komurgoz, G., Ozkol, I., and Gunes, A. Y. (2010). Combined Effects of Temperature and Velocity Jump on the Heat Transfer, Fluid Flow, and Entropy Generation over a Single Rotating Disk. *Journal of Heat Transfer-Transactions of the ASME*. Vol. 132, no. 11.

- Yalcin, H. S., **Arikoglu, A.**, and Ozkol, I. (2009). Free Vibration Analysis of Circular Plates by Differential Transformation Method. *Applied Mathematics and Computation*. Vol. 212, no. 2, pp. 377-386.

- **Arikoglu, A.**, and Ozkol, I. (2009). Solution of Fractional Integro-Differential Equations by Using Fractional Differential Transform Method. *Chaos, Solitons & Fractals*. Vol. 40, no. 2, pp. 521-529.

- Havzali, M., **Arikoglu, A.**, Komurgoz, G., Keser, H. I., and Ozkol, I. (2008). Analytical-Numerical Analysis of Entropy Generation for Gravity-Driven Inclined Channel Flow with Initial Transition and Entrance Effects. *Physica Scripta*. Vol. 78, no. 4.

- **Arikoglu, A.**, Ozkol, I., and Komurgoz, G. (2008). Effect of Slip on Entropy Generation in a Single Rotating Disk in MHD Flow. *Applied Energy*. Vol. 85, no. 12, pp. 1225-1236.

▪ **Arikoglu, A.**, and Ozkol, I. (2008). Solutions of Integral and Integro-Differential Equation Systems by Using Differential Transform Method. *Computers & Mathematics with Applications*. Vol. 56, no. 9, pp. 2411-2417.

▪ **Arikoglu, A.**, Komurgoz, G., and Ozkol, I. (2008). Effect of Slip on the Entropy Generation from a Single Rotating Disk. *Journal of Fluids Engineering-Transactions of the ASME*. Vol. 130, no. 10.

▪ Ozkol, I., Komurgoz, G., and **Arikoglu, A.** (2007). Entropy Generation in Laminar Natural Convection from a Constant Temperature Vertical Plate in an Infinite Fluid. *Proceedings of the Institution of Mechanical Engineers Part a-Journal of Power and Energy*. Vol. 221, no. A5, pp. 609-616.

▪ **Arikoglu, A.**, and Ozkol, I. (2007). Solution of Fractional Differential Equations by Using Differential Transform Method. *Chaos, Solitons & Fractals*. Vol. 34, no. 5, pp. 1473-1481.

▪ **Arikoglu, A.**, and Ozkol, I. (2006). Solution of Difference Equations by Using Differential Transform Method. *Applied Mathematics and Computation*. Vol. 174, no. 2, pp. 1216-1228.

▪ **Arikoglu, A.**, and Ozkol, I. (2006). On the MHD and Slip Flow over a Rotating Disk with Heat Transfer. *International Journal of Numerical Methods for Heat & Fluid Flow*. Vol. 16, no. 2-3, pp. 172-184.

▪ **Arikoglu, A.**, and Ozkol, I. (2006). Solution of Differential-Difference Equations by Using Differential Transform Method. *Applied Mathematics and Computation*. Vol. 181, no. 1, pp. 153-162.

▪ **Arikoglu, A.**, and Ozkol, I. (2005). Analysis for Slip Flow over a Single Free Disk with Heat Transfer. *Journal of Fluids Engineering-Transactions of the ASME*. Vol. 127, no. 3, pp. 624-627.

▪ **Arikoglu, A.**, and Ozkol, I. (2005). Inner-Outer Matching Solution of Blasius Equation by DTM. *Aircraft Engineering and Aerospace Technology*. Vol. 77, no. 4, pp. 298-301.

▪ **Arikoglu, A.**, and Ozkol, I. (2005). Solution of Boundary Value Problems for Integro-Differential Equations by Using Differential Transform Method. *Applied Mathematics and Computation*. Vol. 168, no. 2, pp. 1145-1158.

PUBLICATIONS ON THE THESIS

▪ **Arikoglu, A.**, and Ozkol, I. (2012). Vibration Analysis of Composite Sandwich Plates by the Generalized Differential Quadrature Method. *AIAA Journal*. Vol. 50, no. 3, pp. 620-630.

▪ **Arikoglu, A.**, and Ozkol, I. (2010). Vibration Analysis of Composite Sandwich Beams with Viscoelastic Core by Using Differential Transform Method. *Composite Structures*. Vol. 92, no. 12, pp. 3031-3039.